# INVESTIGATING THE DOMINANT FACTORS REGARDING IGNITION TRANSIENT IN THE DESIGN PROCEDURE OF THE NOZZLE OF A PYROGEN IGNITER

A THESIS SUBMITTED TO
THE GRADUATE SCHOOL OF NATURAL AND APPLIED SCIENCES
OF
MIDDLE EAST TECHNICAL UNIVERSITY

BY

YAVUZ YEŞİLYURT

IN PARTIAL FULFILLMENT OF THE REQUIREMENTS
FOR
THE DEGREE OF MASTER OF SCIENCE
IN
MECHANICAL ENGINEERING

SEPTEMBER 2019

Approval of the thesis:

**INVESTIGATING THE DOMINANT FACTORS REGARDING IGNITION TRANSIENT IN THE DESIGN PROCEDURE OF THE NOZZLE OF A PYROGEN IGNITER**

submitted by **YAVUZ YEŞİLYURT** in partial fulfillment of the requirements for the degree of **Master of Science in Mechanical Engineering Department, Middle East Technical University** by,

Prof. Dr. Halil Kalıpçılar
Dean, Graduate School of **Natural and Applied Sciences** ________________

Prof. Dr. Sahir Arıkan
Head of Department, **Mechanical Engineering** ________________

Prof. Dr. Almıla Güvenç Yazıcıoğlu
Supervisor, **Mechanical Engineering, METU** ________________

**Examining Committee Members:**

Prof. Dr. Tuba Okutucu Özyurt
Mechanical Engineering, METU ________________

Prof. Dr. Almıla Güvenç Yazıcıoğlu
Mechanical Engineering, METU ________________

Assoc. Prof. Dr. Cüneyt Sert
Mechanical Engineering, METU ________________

Assist. Prof. Dr. Feyza Kazanç Özerinç
Mechanical Engineering, METU ________________

Assist. Prof. Dr. Sıtkı Uslu
Mechanical Engineering, TOBB ETÜ ________________

Date: 17.09.2019

**I hereby declare that all information in this document has been obtained and presented in accordance with academic rules and ethical conduct. I also declare that, as required by these rules and conduct, I have fully cited and referenced all material and results that are not original to this work.**

Name, Surname: Yavuz Yeşilyurt

Signature:

# ABSTRACT

## INVESTIGATING THE DOMINANT FACTORS REGARDING IGNITION TRANSIENT IN THE DESIGN PROCEDURE OF THE NOZZLE OF A PYROGEN IGNITER


Yeşilyurt, Yavuz
Master of Science, Mechanical Engineering
Supervisor: Prof. Dr. Almıla Güvenç Yazıcıoğlu



September 2019, 134 pages



In a standard solid rocket motor (SRM) system, the propellant of the SRM is generally ignited by a pyrotechnic device (which is much smaller in size compared to SRM itself). However, grand systems like solid propellant Space Propulsion Systems need more mass flow rate in a very short time duration to be ignited, which is not easy task for a pyrotechnic igniter. The solution for this issue is utilizing pyrogen igniter in the SRM system, which is both a small-scale SRM and an igniter. Here ignition transient becomes a very important design subject, because an extra element is added to the ignition train of the SRM system when a pyrogen igniter is used. In this thesis work, the nozzle design of pyrogen igniters is investigated and the most dominant factors that pressurize (therefore, accelerate ignition) the grand SRM propellant empty volume and shorten the ignition transient duration are determined by a design of experiment (DOE) procedure. The series of test case simulations is made by a "Fully Coupled Compressible Solver for Turbulent Perfect Gas Flows", which is designed to solve closed volume problems like shock tube interactions, in a systematic and comparable manner. Before starting DOE procedure, the solver is validated by a test case having an exact solution. The importance and junction of parameters that should

be considered in nozzle design of pyrogen igniters are discussed in the end of the thesis work.

Keywords: Pyrogen, Igniter, Solid Propellant Rocket Motor, Propulsion Systems

# ÖZ

## PİROJEN ATEŞLEYİCİ NOZULU TASARIMI SÜRECİNDE ATEŞLEME GEÇİŞİ AÇISINDAN BASKIN OLAN ETMENLERİN ARAŞTIRILMASI

Yeşilyurt, Yavuz
Yüksek Lisans, Makina Mühendisliği
Tez Danışmanı: Prof. Dr. Almıla Güvenç Yazıcıoğlu

Eylül 2019, 134 sayfa

Standart katı yakıtlı roket motorlarında (KYRM), motor yakıtı genellikle motorun kendisine göre çok küçük boyutta olan piroteknik aygıtlar tarafından ateşlenir. Katı yakıtlı Uzay Sevk Sistemleri gibi büyük sistemlerinin ateşlenebilmesi için ise çok kısa süre içinde piroteknik ateşleyicinin sağlayabileceğinden çok daha fazla kütle debisine ihtiyaç bulunmaktadır. Bu problemin çözüm için KYRM sistemlerinde hem küçük boyutlu bir motor hem de ateşleyici görevi gören Pirojen Ateşleyici kullanılır. Bu noktada ateşleme geçişi çok önemli bir tasarım konusu haline gelir çünkü KYRM sisteminde pirojen ateşleyici kullanıldığı zaman ateşleme zinicirine ek bir eleman eklenmiş olur. Bu tez çalışması kapsamında, pirojen ateşleyicilerin nozul tasarımları üzerinde durulmuş olup, büyük KYRM yakıt boş iç hacmini basınçlandırmada (ve sonucunda ateşlemeyi hızlandırmada) ve ateşleme geçişi süresini azaltmada en etkin olan etmenler, deney tasarımı metoduyla belirlenmiştir. Kapalı hacimlerde oluşan şok tüpü etkileşimleri gibi problemlerin çözümüne yönelik tasarlanan "Fully Coupled Compressible Solver for Turbulent Perfect Gas Flows" çözücüsü ile sistematik ve karşılaştırılabilir bir şekilde bir dizi test simülasyonu çözülmüştür. Deney tasarımı süreci öncesinde çözücü, kesin çözümü olan bir test örneği ile doğrulanmıştır. Nozul tasarımında önemli olan parametreler ve bu parametrelerin tasarıma katılması, tez çalışmasının sonucunda ele alınmıştır.

Anahtar Kelimeler: Pirojen, Ateşleyici, Katı Yakıtlı Roket Motoru, Sevk Sistemleri

To my mother…

## ACKNOWLEDGEMENTS

First of all, I would like to express my gratitude to Prof. Dr. Almıla GÜVENÇ YAZICIOĞLU for her great help with my work.

I also would like to thank ROKETSAN A.Ş. for supplying both material and moral infrastructure for the development of this work. I thank my mentors and colleagues, Mr. Osman YÜCEL, Mrs. Funda EROĞUL KÖMBE, Mr. Mustafa AKDEMİR, Mr. Bora KALPAKLI, Mr. Yusuf ATA, Mrs. Tuğba SÜER and Mr. Ömer Uğur ARKUN for their keen support and guidance.

I especially thank my dear friends; Mr. Özgür HARPUTLU, Mr. Oğuz Kaan ONAY, Ms. Cansu ÇAYLAN, Mr. Yakup ERTURAN, Mrs. Berna BAŞDOĞAN BOZKIR, Mr. Irmak Taylan Karpuzcu, Mr. Şahin ONGÜN, Mr. Umut ÇAKIR, Mr. Mesut KOÇ, Mr. Nail Etkin Can AKKAYA and Mr. Emir Bediğ ACAR for always supporting me.

Furthermore, I would like to offer my sincere gratitude to my father Mr. İdris YEŞİLYURT, my brother Mr. Oğuz YEŞİLYURT, my aunt-in-law Mrs. Seda Hikmet YEŞİLYURT, my uncle Mr. Fatih SAYIN, my beautiful nephew Ms. Ela YEŞİLYURT and my little (and extremely mischievous) niece Mr. Kuzey YEŞİLYURT.

The last gratitude is to my aunt Mrs. Meral SAYIN and my mother Mrs. Fatma YEŞİLYURT; for this work could not be completed without your loadstar from the beginning.

# TABLE OF CONTENTS

# LIST OF TABLES

TABLES

# LIST OF FIGURES

FIGURES

## LIST OF ABBREVIATIONS

ABBREVIATIONS

| | |
|---|---|
| 3D | Three Dimensional |
| Al | Aluminum |
| $Al_2O_3$ | Alumina |
| AP | Ammonium Perchloride |
| AVUM | Attitude Vernier Upper Module |
| BPN | Boron Potassium Nitrate |
| CEA | Chemical Equilibrium with Applications |
| CFD | Computational Fluid Dynamics |
| CTPB | Carbon -Terminated PolyButadiene |
| DOE | Design of Experiment |
| EPDM | Ethylene Propylene Diene Monomer |
| HTPB | Hydroxyl-Terminated PolyButadiene |
| L/D | Length to Diameter Ratio |
| MEOP | Maximum Expected Operating Pressure |
| MTV | Magnesium Teflon Viton |
| NASA | National Aeronautics and Space Administration |
| PAP | Propulseur d'Appoint à Poudre |
| PBAN | Polybutadiene acrylonitrile |
| RSRM | Reusable Solid Rocket Motor |

| | |
|---|---|
| SRM | Solid Rocket Motor |
| S&A | Safe and Arm |
| USA | United States of America |
| Z9 | Zefiro 9 |
| Z16 | Zefiro 16 |
| Z23 | Zefiro 23 |

## LIST OF SYMBOLS

SYMBOLS

| | |
|---|---|
| A | Area, [m$^2$] |
| $\Delta h_f^0$ | Enthalpy of Formation at Reference State Temperature, [J] |
| $c_{p,k}$ | Constant Pressure Specific Heat [J/kgK] |
| $c_{v,k}$ | Constant Volume Specific Heat [J/kgK] |
| $CS$ | Control Surface |
| $CV$ | Control Volume |
| dA | Area Element, [m$^2$] |
| dV | Volume Element, [m$^3$] |
| $e$ | Thermal Energy [J/kg] |
| $e_k$ | Mass Specific Energy [J/kg] |
| E | Energy, [J] |
| $\sum$ | Total |
| F | Body Forces, [N] |
| $h$ | Enthalpy, [J/kg] |
| $h_k$ | Mass Specific Enthalpy, [J/kg] |
| k | Thermal Conductivity, [W/mK] |
| $\dot{m}$ | Mass Flow Rate, [kg/s] |
| $\boldsymbol{n}$ | Unit Vector |

| | |
|---|---|
| P | Pressure [Pa] |
| $p$ | Partial Pressure [Pa] |
| $\rho$ | Density [kg/m$^3$] |
| R | Universal Gas Constant [J/moleK] |
| $R_k$ | Gas Constant |
| $\dot{Q}$ | Volumetric Heat Generation [W] |
| $s$ | Entropy [J/kgK] |
| $s_k$ | Mass Specific Entropy [J/kgK] |
| $s_{k,0}$ | Reference State Entropy [J/kgK] |
| T | Temperature [K] |
| $T_0$ | Reference State Temperature [K] |
| $v$ | Velocity [m/s] |
| V | Volume [m$^3$] |
| W | Molecular Weight [g/mole] |
| $\dot{W}$ | Work [Watt] |
| $Y$ | Mass Fraction |

## CHAPTER 1

## INTRODUCTION AND RESEARCH BACKGROUND

### 1.1. Solid Rocket Motors

Solid rocket motors (SRM) are basically energy conversion systems that convert the chemical energy stored within their propellant into thermal energy by means of combustion and then convert thermal energy into kinetic energy by accelerating hot combustion products via their nozzle openings. Typically, a SRM consists of a motor case to hold SRM together and endure the combustion pressure, a propellant grain which is going to be combusted, an igniter to initiate the ignition, an insulation to protect motor case from hot combustion products and a nozzle to exhaust the combustion products and produce thrust in the opposite direction (see Figure 1).

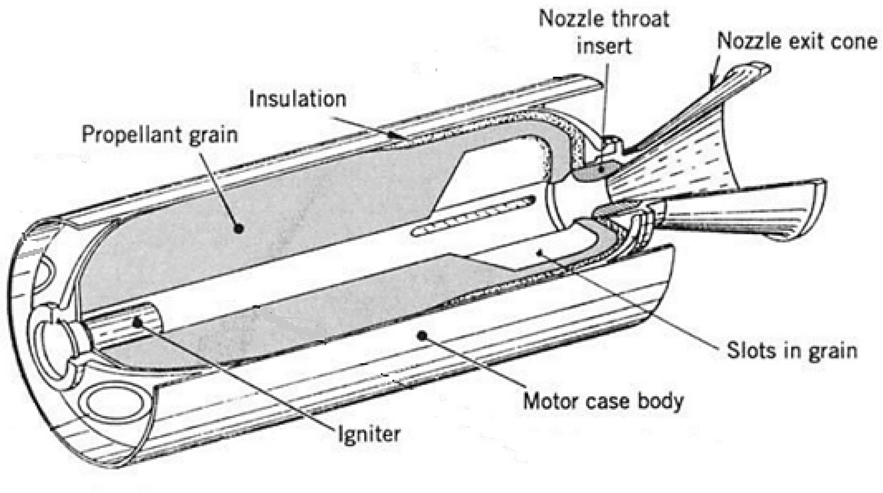


*Figure 1.1.* Schematics of a typical solid rocket motor [1]

There exist a large variety designs of solid rocket motors for various purposes. Depending on their objective and system requirements, a solid rocket motor might have one or multiple nozzles, pyrotechnic or bagged igniter initiators, steel or composite material motor case, composite or double-based propellant, bulk or slotted propellant grain geometry, fixed or moving nozzle exit cone etc. In this thesis work, solid rocket motors which also behave as igniters and their nozzle configurations will be investigated and optimized.

### 1.2. Pyrogen Igniters and Ignition Transient

Pyrotechnic igniters are mostly used in small and medium sized Solid Rocket Motors (SRM). In these igniters, pyrotechnic materials such as Boron Potassium Nitrate (BPN), Magnesium Teflon Viton (MTV) or black powder are used as propellants. If the inner port volume (volume that the igniter pressurizes in an SRM) and the dimensions of an SRM (diameter and length) increase, the dimensions of its igniter and the amount of the pyrotechnic materials used in that igniter also increases in a directly proportional manner. This is due to the fact that the high temperature mass flow rate and increased working duration is expected from the igniter in order to ignite the large-scale propellant of the SRM. However, packaging of large amounts of pyrotechnic materials can be dangerous during transportation and assembly of the SRM or before static firing test/flying mission of the SRM, because these materials are very sensitive to vibrations and ambient conditions. Also, if used, packaging space used for a pyrotechnic igniter could be very broad and idle in the front part of the large-scale SRM systems. Therefore, in order to ignite the propellant of the SRM with high mass flow rate, increased working duration, a more compact space use and without pyrotechnic explosion jeopardy, pyrogen igniters are used in large-scale SRM. Essentially, a pyrogen igniter is a small-sized SRM, which is mounted to the front of a larger SRM. A pyrogen igniter also possesses a pyrotechnic igniter, which starts the firing chain system in the rocket motor. In summary, the main purpose of the pyrogen igniter/motor is not to produce thrust or momentum as most of the time rocket motors do, but to pressurize the combustion chamber of the main SRM and ignite its propellant. The schematics of a SRM, which includes a pyrogen igniter can be seen in Figure 1.2.

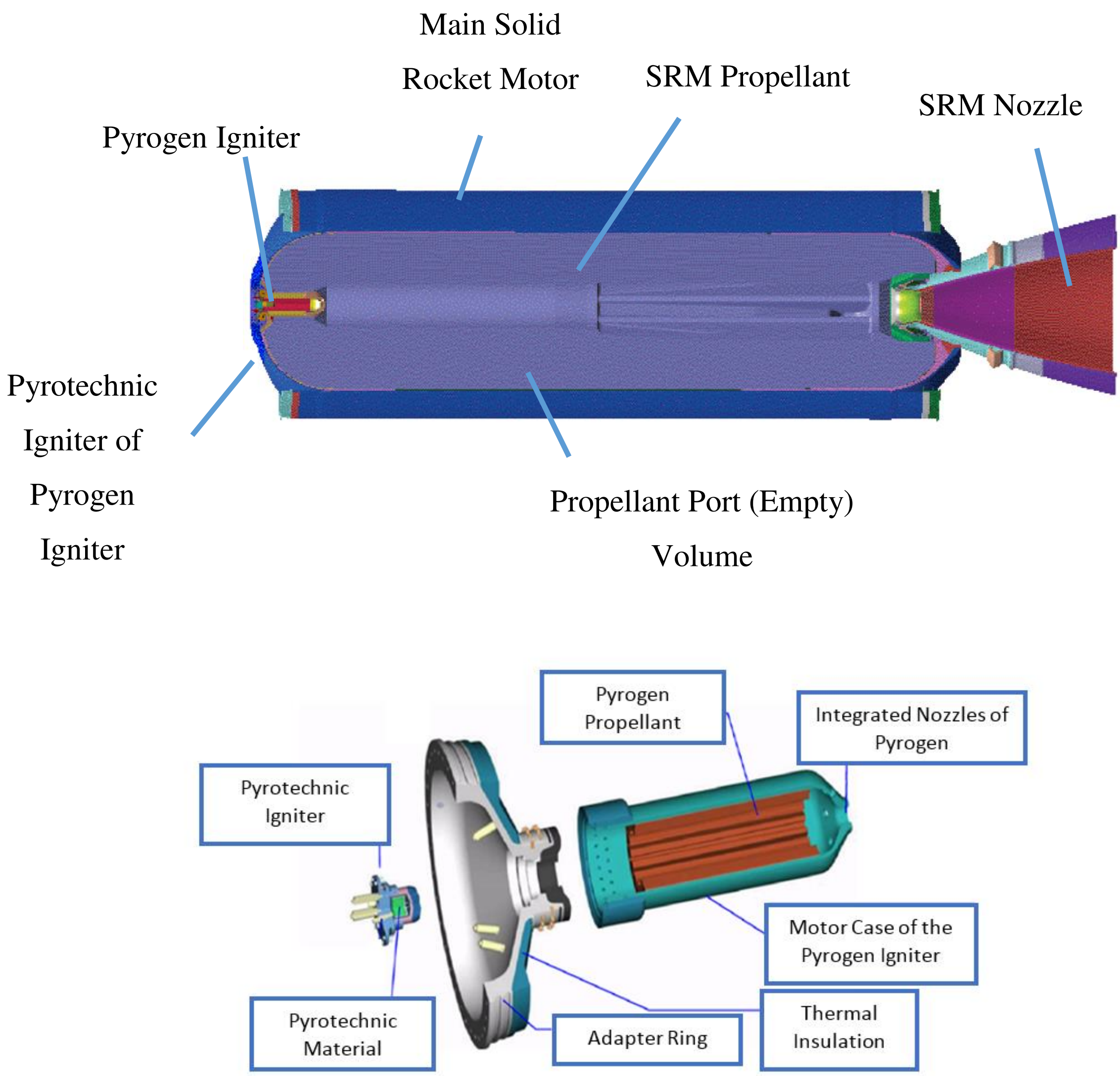


*Figure 1.2.* Schematics of main solid rocket motor and its pyrogen igniter [2]

The propellant used in pyrogen igniters can be cast inside the motor (which, in this case the rocket motor is the pyrogen igniter itself) or can be cast outside and inserted as a cartridge structure. The mixture of the propellant can be either composite propellant having a high burning rate or extruded double based propellant. In addition to these, there are some other necessary features that are expected from a pyrogen igniter as follows:

- Pyrogen igniter itself should ignite fast and the ignition transient phase duration should not be too long.
- Pyrogen igniter should discharge high temperature gas with a high mass flow rate in a short time duration.
- Pyrogen igniter should provide sustainable operation between large pressure and temperature ranges, in which the large SRM could possibly be conditioned to before static firing test or flight mission. Therefore, the temperature sensitivity of burning rate and the sensitivity of pressure exponent values should be as low as possible.
- The burn rate of the propellant of the pyrogen igniter should have high values like 20-30 mm/s.
- The hot jet flow ($\sim 3000 - 3500$ K) blowing out of the nozzles of the pyrogen igniter should not damage or crumble the propellant of the SRM in order not to increase the burning area of the propellant in an uncontrolled way; and therefore, rapidly increase the inner pressure of the SRM to an unanticipated degree in a very short time duration.
- The production, transportation and storage of the pyrogen igniter should be safe and secure. During storing, the igniter should not be exposed to high degrees of humidity.
- If its core structure is not consumable, the pyrogen igniter should maintain its integrity during SRM firing and operation in order not to damage propellant, insulation, and/or nozzle of the SRM.

The firing sequence and ignition transient of an SRM propellant which possesses a pyrogen igniter can be described as follows, after the pyrotechnics ignited the pyrogen propellant (see Figure 1.3):

1. With the ignition of the pyrogen igniter, the hot jet flows coming from pyrogen blows into the surface of main SRM's propellant, which is inside the combustion chamber of the SRM.
2. Convection heat transfer occurs between the hot gases flowing outside of the pyrogen and the colder main SRM propellant surface. The temperature of the main SRM propellant increases because of the heat transfer until its self-ignition begins (locally). This phase is called "induction" of the burning. Also, pressure waves originated from igniter jets propagate forwards and reflect backwards inside the closed main SRM port empty volume. This phenomenon, occurring merely in milliseconds, increases the pressure in the main SRM which in turn favors the self-ignition and flame propagation.
3. The hot gases coming out of both pyrogen igniter and the newly ignited parts of main propellant warm up the unignited part of the main propellant via conduction, convection, and radiation heat transfer modes. Radiation is mostly dominant in areas which are behind the pyrogen igniter, conduction is dominant in areas near the newly ignited main propellant and convection is dominant in areas that are close to the nozzle part of main SRM. All these heat transfer phenomena spread the burning process through all the surfaces of the main propellant and this phase is called "flame spreading".
4. The gaseous burning products of main SRM propellant start to fill the combustion chamber, which is also known as the port/empty volume of the main SRM; thus, increasing the inside pressure of the motor. When the pressure difference between the combustion chamber and the outer environment reaches a critical value, the nozzle plug bursts due to the pressure waves similar to a shock tube configuration.
5. After the nozzle plug bursts, the pressurized hot gases that are accumulated inside the combustion chamber start to accelerate towards the nozzle throat of the main SRM because the pressure is lower outside of the motor. In a very short time, nozzle condition becomes chocked.

6. Through all the ignition steps explained above, due to inclusion of gases into the system and the increase of the amount of the gas inside the combustion chamber, dynamic pressure waves start to originate between the front and the aft part of the chamber. The tide motion of these waves increases the inner pressure of the SRM.
7. When all of the propellant of the pyrogen igniter is consumed and burned, the main propellant of the SRM is already ignited. After this phase, the pressure waves originated during ignition transient are absorbed in the combustion chamber and the motor reaches to quasi-steady operation conditions in a short time.

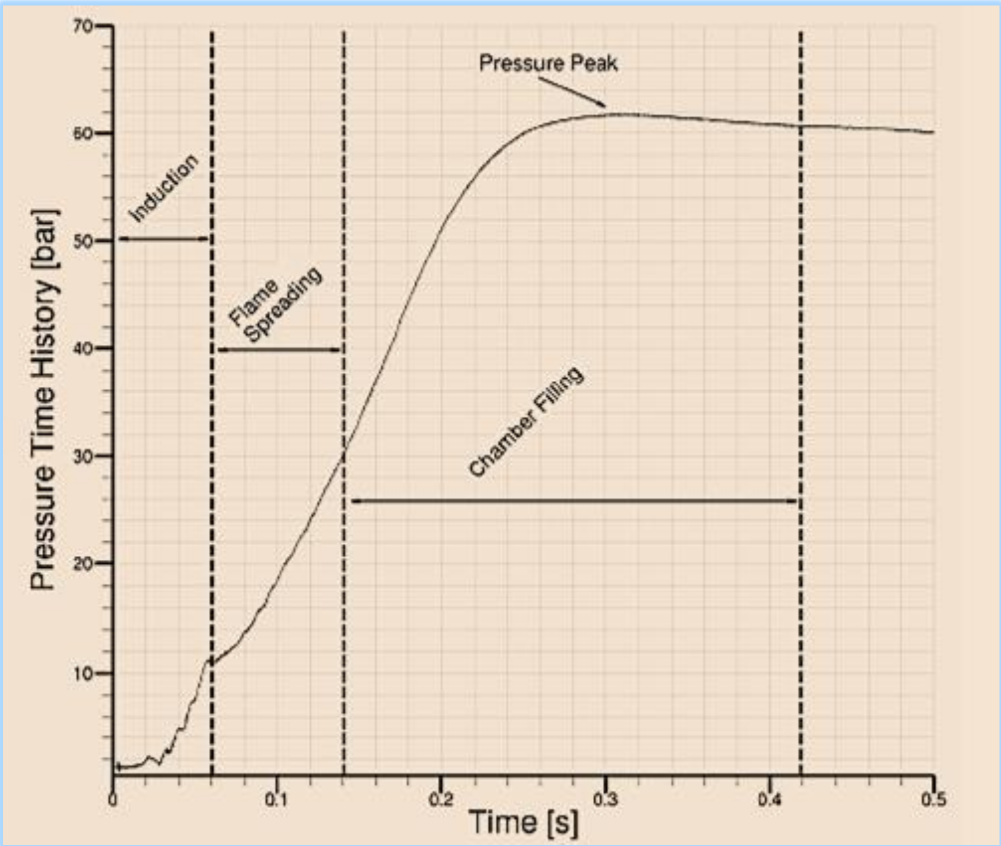


*Figure 1.3.* Common pressure vs. time graph of ignition transient in a SRM [3]

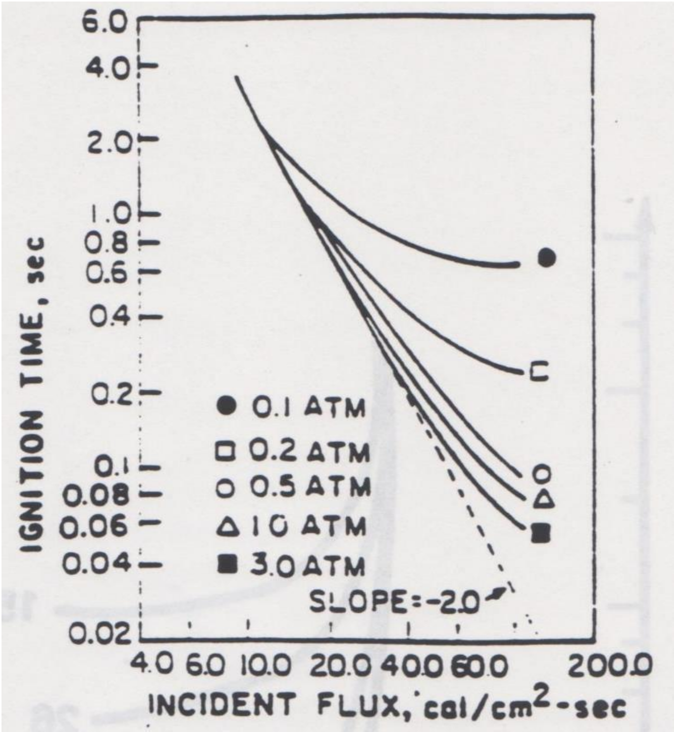


*Figure 1.4.* Measured effect of radiant flux at different pressures on ignition delay for PBAN/AP composite propellant [4]

In the Figure 1.4, the basic relationship between the pressurization of a propellant (energetic material) and the ignition time can be observed. In order to obtain the experimental plots in the Figure 1.4, PBAN/AP composite propellant samples, in which Polybutadiene acrylonitrile (PBAN) acts as a polymer binder and Ammonium Perchlorate acts as an oxidizer, are ignited under different pressures via varying heat fluxes applied on them. As it can be clearly observed, when the same heat is applied on the propellant sample, the ignition time decreases with the increasing surrounding pressure value. Thus, ignition time and pressure applied on the propellant are inversely proportional. The faster a propellant desired to be ignited, the more it should be pressurized. Therefore, since the ignition -in the induction phase (see Figure 1.3)- is a part of the ignition transient phenomena, in order to shorten the ignition transient time duration of a SRM, its inner environment should be pressurized faster and higher in value.

### 1.3. Comparison of Large-Scale Rocket Motors and Their Pyrogen Igniters

The main space propulsion systems which utilize pyrogen igniters are listed below and their comparison can be seen in Table 1.1.

Table 1.1. *Comparison of large-scale rocket motors which are utilizing a pyrogen igniter*

| Rocket Motor/ Features | Grand System | Country | Motor Length [m] | Motor Diameter [m] | Motor L/D | Burn Time [s] | Motor Port Volume [$m^3$] |
|---|---|---|---|---|---|---|---|
| **RSRM** | SPACE SHUTTLE | USA | 38.5 | 3.7 | 10 | 124 | UD[2] |
| **ANTARES III** | SCOUT | USA | 2.87 | 0.77 | 3.73 | 48 | UD |
| **PAP** | ARIANE IV | EUROPE | 8.5 | 1.07 | 7.94 | 41 | UD |
| **P230** | ARIANE V | EUROPE | 24 | 3.1 | 8 | 130 | UD |
| **Z16[1]** | VEGA | EUROPE | 3.83 | 1.9 | 2.02 | 80 | 0.9 |
| **Z9** | VEGA | EUROPE | 7.5 | 1.9 | 3.95 | 111 | 0.66 |
| **Z23** | VEGA | EUROPE | 3.85 | 1.9 | 2.03 | 71.6 | UD |
| **P80** | VEGA | EUROPE | 10.5 | 3 | 3.5 | 107 | UD |
| **S200** | GSLV MK III | INDIA | 22 | 3.2 | 6.88 | 128 | UD |

[1]Zefiro 16 (Z16) SRM is not used in VEGA Space Propulsion System (see Figure 1.5). It is a motor that is manufactured and fired in order to develop and demonstrate the technologies and processes that will be used in sub-solid rocket motors of VEGA system, namely Zefiro 9, 23 and P80.

[2]Undefined

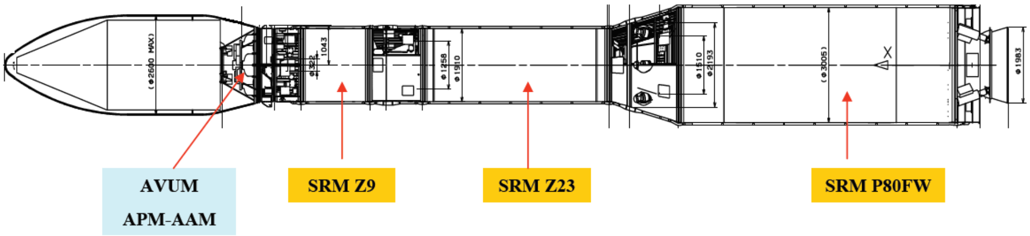


*Figure 1.5.* Vega Launch Vehicle configuration [2]

When the propellant geometries of pyrogen igniters of relatively small sized PAP, Zefiro 9, 16, and 23 are investigated, it is seen that these propellants have low web thickness (smaller than 10 mm) and contain high number of slots (minimum 13). The main objective here is to decrease the total mass of the propellant while increasing its burn area, in order to increase the ejection mass flow rate during the operation of the pyrogen igniter. Increasing burn area, which is achieved by increasing the number of slots in the propellant geometry, increases the mass flow rate in a directly proportional manner (Ejected mass flow rate = Density of the propellant * Burn rate of the propellant * Burn area of the propellant). However, manufacturing and process conditions allows to this increase in a fragile geometry up to only some degree; otherwise, the propellant (which is a viscoelastic and composite material in most cases) might not retain its structural integrity. As seen in Figure 1.6, the propellant geometry of the PAP pyrogen igniter (ARIANE IV) represents an example to this kind of ballistic design.

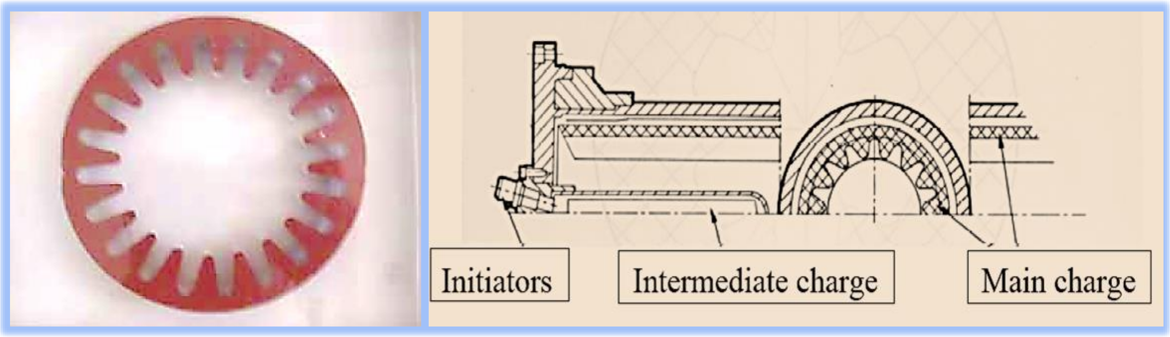


*Figure 1.6.* Propellant geometry of pyrogen igniter of PAP SRM (ARIANE IV) [5]

The main characteristics of the pyrogen igniters used in motors shown in Table 1.1 are presented in Table 1.2.When these characteristic parameters are investigated, it can be concluded that the igniters have operation times lower than 500 milliseconds. The reason for this phenomenon is that, these igniters, which have less than 10 kg of propellant, are fired under high pressure (1500-2000 psi) conditions; thus, they blow hot ignited product gases with mass flow rates greater than 10 kg/s into the main SRM propellant surface in order to achieve fast ignition. The main reason of keeping the propellant of the pyrogen in low amounts can be based on two facts. The first one is, if the pyrogen igniter blows more hot gases into the main SRM propellant surface than needed for ignition, it may deform or break up the main SRM propellant which in turn increases the burn area of that propellant at an instant. This undesired situation increases the inner pressure of the main motor in an uncontrolled and unpredictable way, which in turn might force the motor case too much or burst it. The second reason why the pyrogen propellant is kept in low amounts is that, if the nozzle plug of the main motor does not burst for some unpredictable or unknown reason, the pressure level inside the combustion chamber should not damage the motor and this level should be kept as low as possible. The two-aforementioned pressure level increase phenomena may lead to combustion instabilities in main SRM or motor failures during static firings or flight missions.

Table 1.2. *Main characteristic of pyrogen igniters*

| Reference Motor / Pyrogen Igniter Features | RSRM (Main Pyrogen Igniter) | ANTARES | PAP | P230 (Main Pyrogen Igniter) | Z16 | Z9 | Z23 | P80 | S200 |
|---|---|---|---|---|---|---|---|---|---|
| Diameter (mm) | 430 | 138 | 180 | 470 | 200 | 260 | 362 | 830 | - |
| Length (mm) | 1200 | 356 | 550 | 1180 | 500 | 556 | 720 | 1160 | - |
| L/D | 2.8 | 2.6 | 3 | 2.5 | 2.75 | 2.1 | 2 | 1.4 | - |
| Propellant Mass (kg) | 60 | 0.55 | 2.05 | 65 | 4 | 3.3 | 9.4 | 22 | - |
| Number of Slots in Propellant Geometry | 30 | - | 20 | 30 | 13-16 (Star Geometry) | | | | 24 |
| Max. Mass Flow Rate (kg/s) | 113.4 | - | 15 | 140 | 15-16 | 12 | - | - | - |
| Burn Time (s) | 0.7 | - | 0.2 - 0.4 | 0.3 – 0.5 | 0.4 - 0.5 | 0.25 - 0.5 | 0.2 | 0.4 | 1 |
| Operation Pressure (Psi) | 1600 | - | - | 1100 | - | 1950 | 1630 | 2175 | - |
| Number of Nozzles / Orientation | 1 Axial | 6 Radial | 6 Radial - 1 Axial | 5 Radial | 3 Radial | 6 Radial - 1 Axial | | | 5 Radial |
| Motor Case Material | Steel | Steel | Composite | Steel | Steel | Composite | | | Steel |

In this part of the thesis study, the pyrogen igniters of large scale solid rocket motors will be analyzed in detail, which will give informative input to Section 1.4.

### 1.3.1. RSRM and its Pyrogen Igniter

Solid Rocket Motor of the Space Shuttle (RSRM), which has a diameter of 3.7 m and length of 38.5 m, burns for approximately 125 seconds. In Figure 1.7, time variation of pressure behavior of this SRM can be seen. The ignition transient phase of the Shuttle lasts between 150 and 450 milliseconds and the propellant used in the SRM is a composite type propellant embedded with Aluminum particles [6].

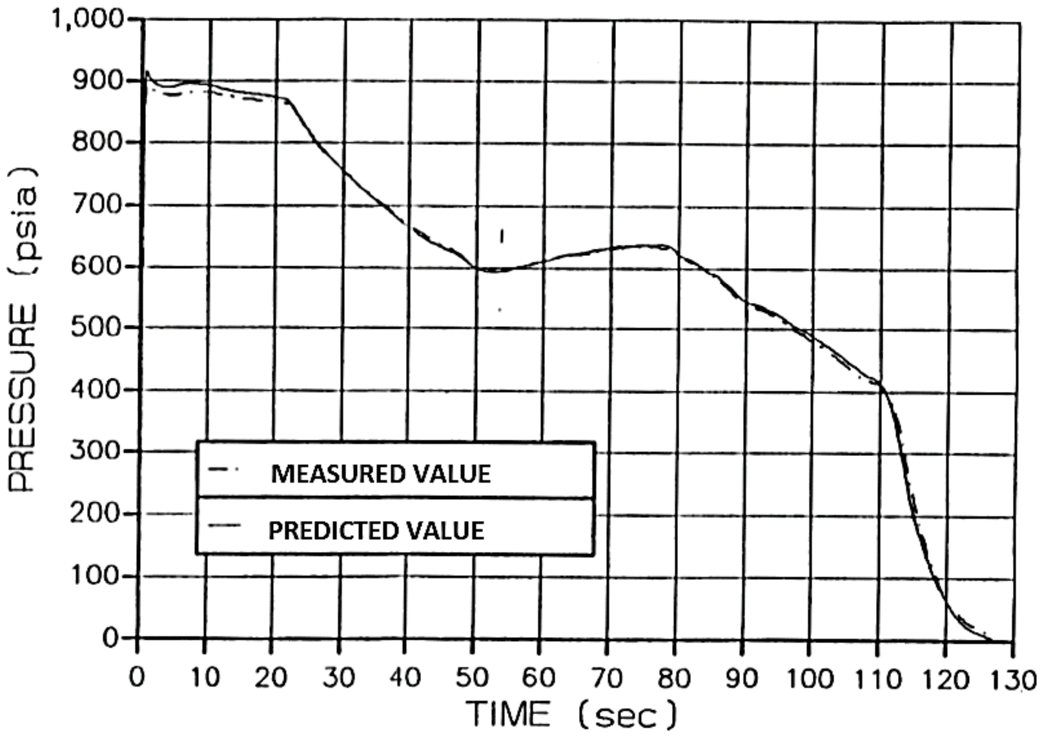


*Figure 1.7.* Time variation of pressure behavior of RSRM [7]

The pyrogen igniter of RSRM consists of 3 main parts. The first part is the Safe and Arm (S&A) Device, which contains two Standard NASA Initiator and pyrotechnic booster charge, BPN. The second part is called ''Primer Igniter'' which is a small sized pyrogen igniter and the third part is called ''The Main Igniter" which is a bigger sized pyrogen igniter, respectively. As it can be seen, there are two pyrogen igniters in RSRM, a pyrogen within a pyrogen, of which both have solid propellant in order to ignite their grand system. The firing sequence is initiated when the ignition signal sent and the pyrotechnic charge (B-$KNO_3$) and initiators are activated, after the S&A device is set in ''ARM'' position. This pyrotechnically activated items fire the Primer Igniter which in turn, fires the Main Igniter.

The solid propellant of the Primer Igniter, TP-H1178, weights 680 grams and its casted grain geometry involves 30-star shaped slots (see Figure 1.8). This tiny solid rocket motor operates under approximately 11.72 MPa (~1700 psi) for 80 milliseconds and produces mass flow rate of 5 kg/s in this short time duration, thanks to its high burn area originated from 30 slots in its propellant grain geometry. The steel case of this motor has six integrated nozzles at the aft part, whose throat inserts are made carbon-phenolic material. In order to secure the contained S&A device and adaptors from being exposed to high temperature and prevent melting of its own steel motor case, the Primer Igniter is insulated externally with approximately 10 mm of NBR filled with silica and asbestos. This pyrogen ignitor can be used in only one mission, either static firing or flight, and will be substituted in the next one [6].

As it can be seen in Figure 1.9 the Main Igniter has a D6AC steel motor case which is insulated both internally and externally because it is exposed to high temperature gas flow from both sides. It contains only one nozzle, which has silica-phenolic throat insert. The solid propellant of the Main Igniter weights 42.6 kg of TP-H1178, its casted grain geometry includes 40-star shaped slots and it burns for 300 milliseconds producing approximately 100 kg/s of mass flow rate on its peak value [5]. 100 kg/s produced in 300 ms is an extreme value of mass flow rate but it is necessary to fill empty volume of RSRM and in order to ignite this vast space propulsion system. This pyrogen ignitor can be used in more than one mission on the contrary to its primer counterpart. Both aforementioned pyrogen igniters had been ballistically and mechanically designed with a safety factor greater than two.

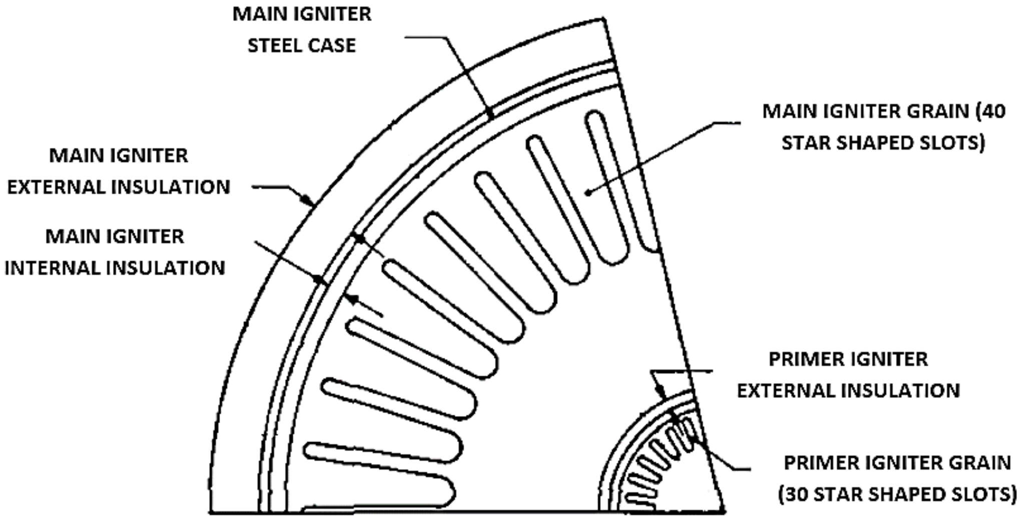


*Figure 1.8.* Propellant geometries of RSRM pyrogen igniters [6]

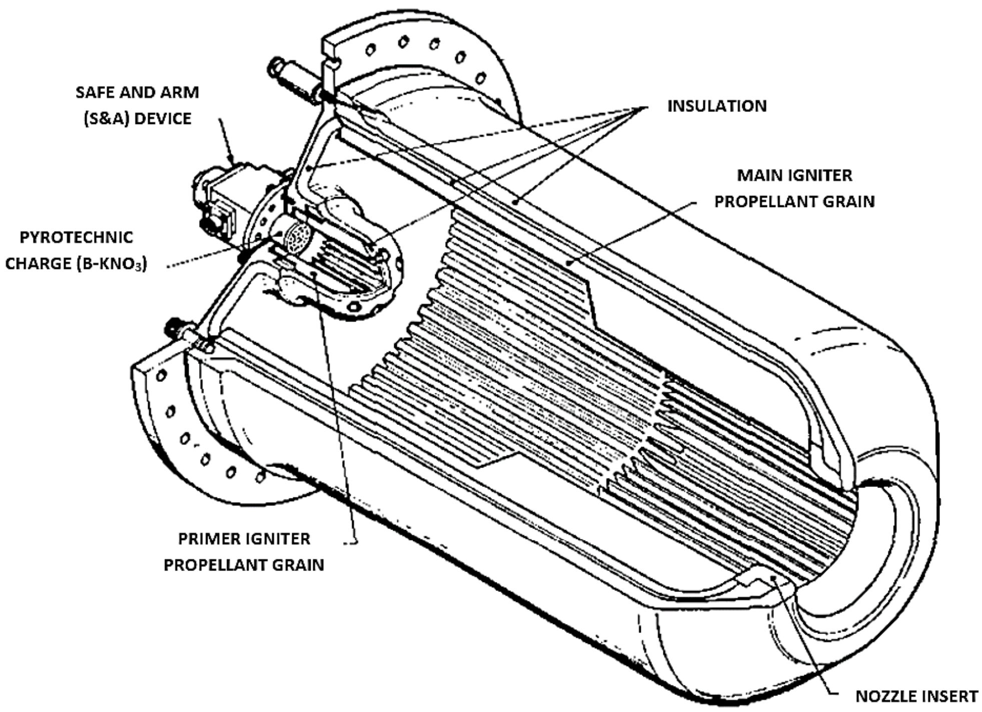


*Figure 1.9.* Pyrogen igniter of RSRM [6]

Pressure trace of the Main Igniter with respect to time can be seen in Figure 1.10. The pressure inside the combustion chamber of the Main Igniter reaches to approximately 1400 psi (~9.65 MPa) in a time shorter than 0.1 seconds.

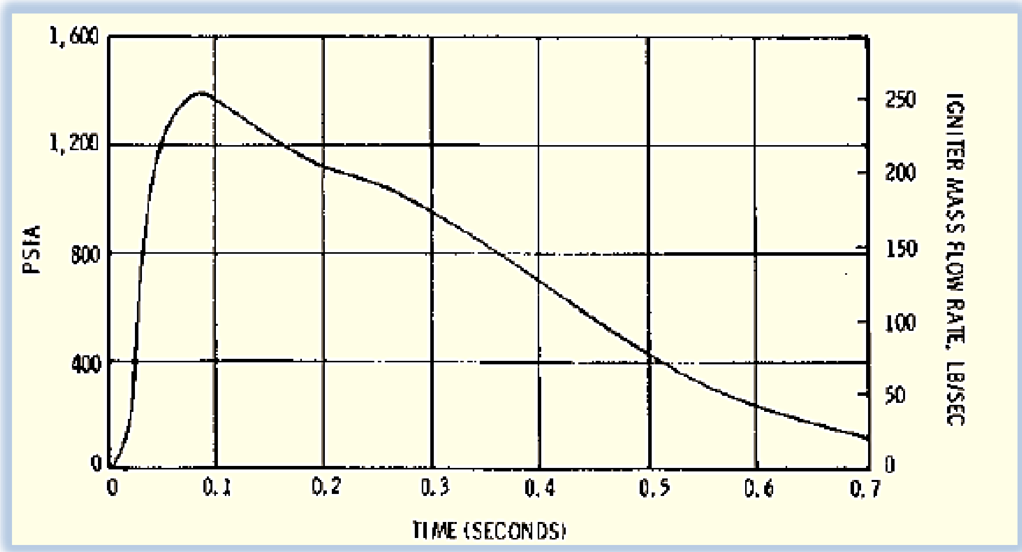


Figure 1.10. Pressure variation of RSRM main igniter with time [6]

The propellant used in both pyrogen igniters of RSRM, TP-H1178, has high burning rate as well as high flame temperature characteristics. In order to suppress instable burning phenomena, it includes Aluminum particles. The characteristic properties of TP-H1178 propellant is shown in Table 1.3 [6].

Table 1.3. *Characteristic properties of TP-H1178 propellant used in pyrogen igniters of RSRM [5]*

| | |
|---|---|
| **Propellant** | TP - H1178 |
| **Composition** | HB Polymer and Epoxy Resin (% 18)<br>Ammonium Perchlorate - AP (%69)<br>Aluminum - Al (%10)<br>Ferric Oxide - $Fe_2O_3$ (%3) |
| **Ballistic Properties** | Burn Rate ($r_b$) => 24.46 mm/s (at 2000 psi)<br>Char. Nozzle Exit Velocity (C*) => 1510 m/s<br>Burn Rate Pressure Exponent (n) => 0.38<br>Density of the Propellant ($\rho$) => 1.71 g/cm$^3$ |

### 1.3.2. Antares III and its Pyrogen Igniter

Antares III is the third stage solid rocket motor of Scout Launch Vehicle. The SRM consist of a Kevlar filament case, an EPDM insulation, a pyrogen igniter, an HTPB propellant and a nozzle with Titanium housing, Carbon-Carbon material nozzle throat and Carbon-Phenolic material exit cone (see Figure 1.11). Antares III operates approximately 47-48 seconds with a maximum expected pressure of roughly 1000 psi (Figure 1.12) [8].

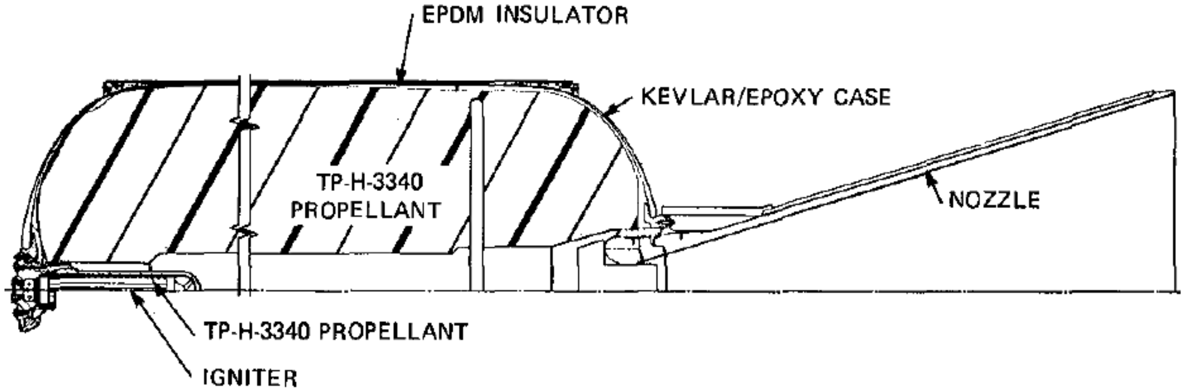


*Figure 1.11.* Antares III SRM and its components [8]

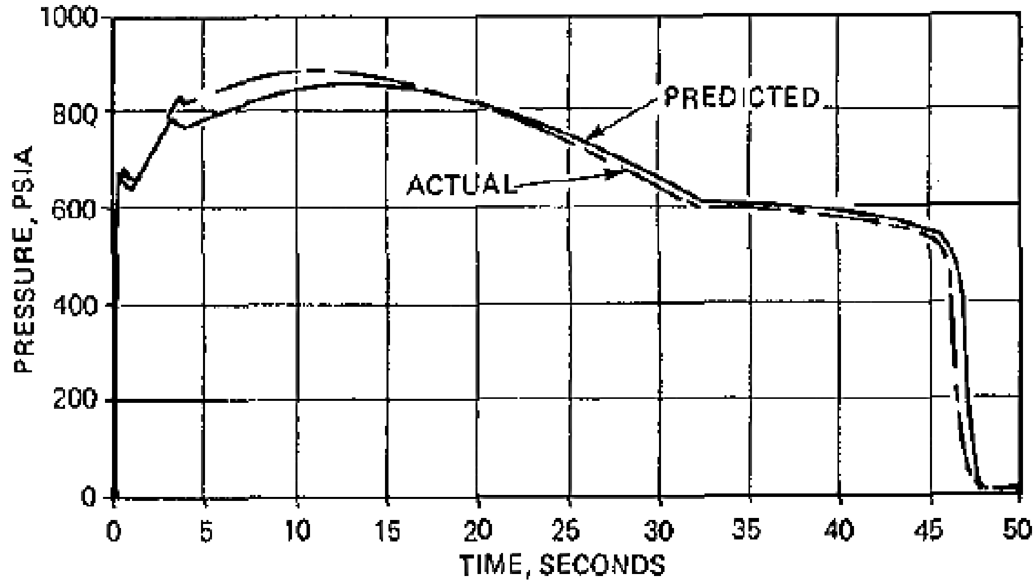


*Figure 1.12.* Pressure vs. time trace of the Antares III SRM [8]

The interest of this work, pyrogen igniter of Antares III (see Figure 1.13), consists of a pyrotechnic igniter which incapsulates boron pellets, a Titanium motor case which is insulated by EPDM insulation on the outer side, a cartridge type propellant (which is loaded inside the Titanium case) and a Silica-Phenolic material nozzle with six exhaust ports. The propellant of Antares III pyrogen igniter consists of 14% CTPB

(Carbon-Terminated Poly Butadiene), 16 % Al particles and 70% AP (Ammonium Perchloride) [8]. The nozzle design of Antares III pyrogen igniter is very uncomplicated, by means of manufacturing, and will be mentioned in Chapter 1.4 explicitly.

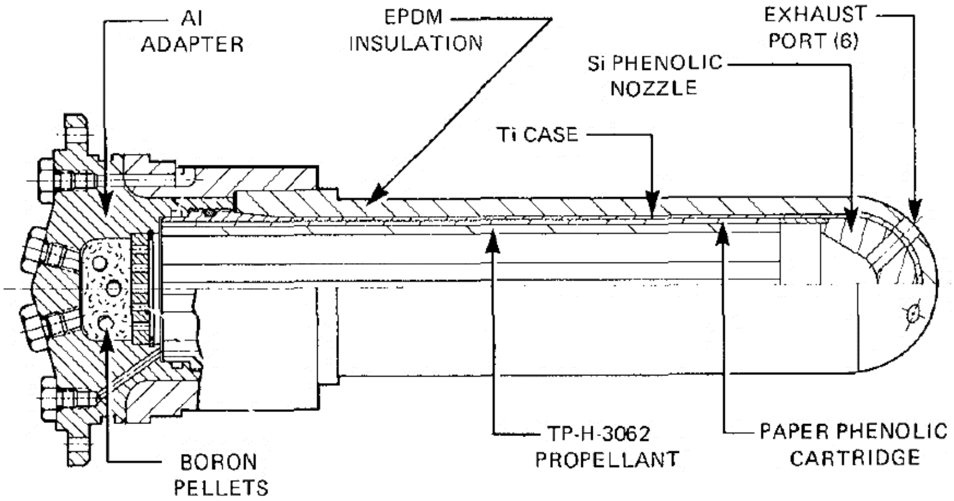


*Figure 1.13.* Pyrogen igniter of Antares III SRM and its components [8]

### 1.3.3. P230 and its Pyrogen Igniter

Solid Rocket Motor of the Ariane V Space Propulsion System (P230), which has a diameter of 3.1 m and length of 24 m, burns for approximately 130 seconds. The ignition subsystem of P230 (see Figure 1.14) is composed of 4 parts, namely main pyrogen igniter (in a main charge chase), primer pyrogen igniter (in an intermediate case), pyrotechnic igniter (containing initiators and pyrotechnics) and basket & the igniter flange. The total length of the ignition subsystem is 1180 mm whereas, its diameter is 470 mm. Very much like RSRM (Space Shuttle), P230 utilizes a pyrogen within a pyrogen and a pyrotechnic igniter in it. [9].

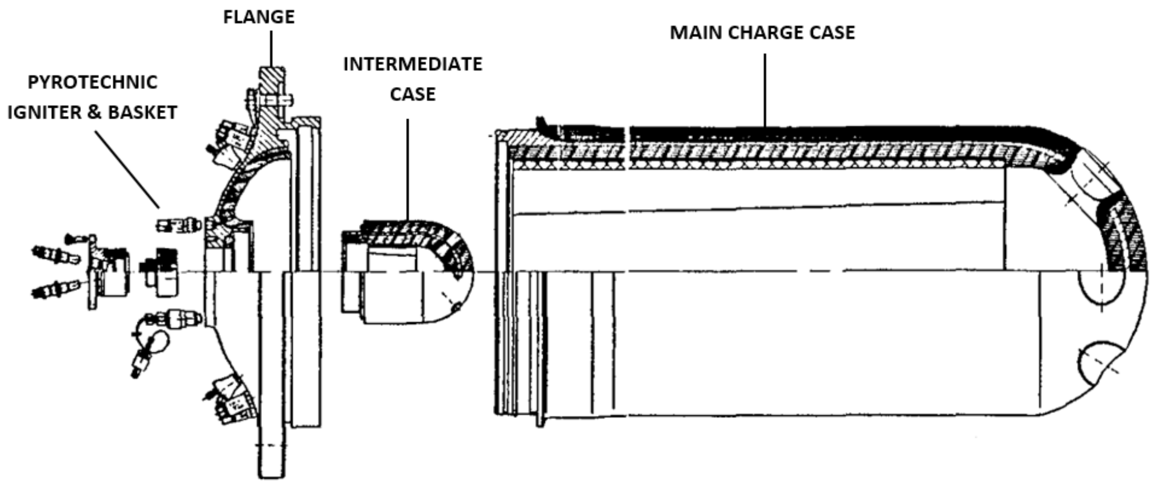


*Figure 1.14.* Configuration of P230 igniter system [9]

The igniter charge of the pyrotechnic igniter is made of granule formed BPN ($BKNO_3$) pellets put in polyethylene bags inside a basket. Nozzle inserts of the pyrotechnic igniter, which direct the flow of burning products into the primer pyrogen igniter, are made of graphite in order to ensure steady flow conditions [9].

The propellant geometries of the primer and the main pyrogen igniters are produced by casting process and involve 25 and 30-star shaped slots, respectively. The propellant involves of Hydroxyl Terminated Polybutadiene (HTPB) as polymer binder and Ammonium Perchloride (AP) as oxidizer. It also contains high percentage of Aluminum (Al) inside its composition. The two pyrogen igniters and their propellants are designed in a such manner that [9]:

- They can produce the required mass flow rate in order to ignite their main SRM,
- They have least amount of undesired tail-off phase at the end of their burning in their ballistic design,
- They keep operating and endure the selected operation pressure, structurally,

- They can operate in various environmental conditions.

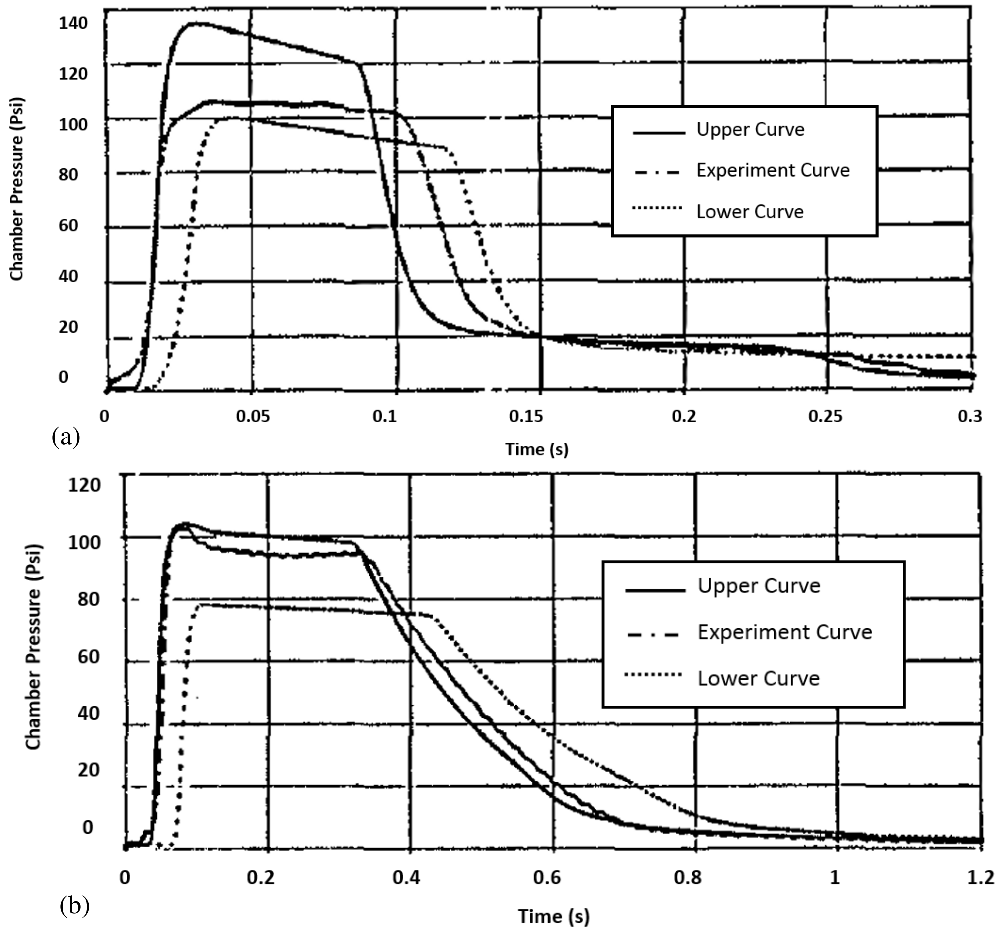


*Figure 1.15.* Mass flow rate vs. time traces of the primer (a) and the main (b) pyrogen igniters of P230 SRM [9]

As can be seen in Figure 1.15, the primer and main pyrogen igniters in the systems, which have star shaped propellant geometry, possess similar natural pressure profiles. The primer igniter operating pressure reaches to 110-140 bars in 30-40 milliseconds whereas, the main igniter pressure reaches to 85-110 bars in 90-110 milliseconds. After reaching their peak values, the pressure values became stable and burn-out phase is observed between 85-120 milliseconds in the primer igniter and 330-430 milliseconds in the main one, respectively. The maximum value of the inner pressure (the curve in the middle in both figures) obtained from test results remain inside the theoretical maximum (upper curves) and minimum (lower curves); therefore, it can be concluded that, the ballistic design and modelling is viable and acceptable.

### 1.3.4. Pyrogen Igniters of Subsystem Solid Rocket Motors of VEGA Space Propulsion System

Vega Space Propulsion System (Launcher), developed by AVIO, is composed of three solid rocket motor stages (namely P80, Zefiro 23 & Zefiro 9), a liquid propulsion module (namely AVUM) and a fairing (see Figure 1.16). Inside the fairing, there exist 1500 kilograms of payload to be transported into the low earth orbit [10]. In most cases, for space propulsion systems, payload consist of satellites, auxiliary equipment etc. whereas for defensive/military purposes, it is generally warheads, weapons etc. The total Vega Launcher configuration heights approximately 30 meters and weighs 140 tons [11].

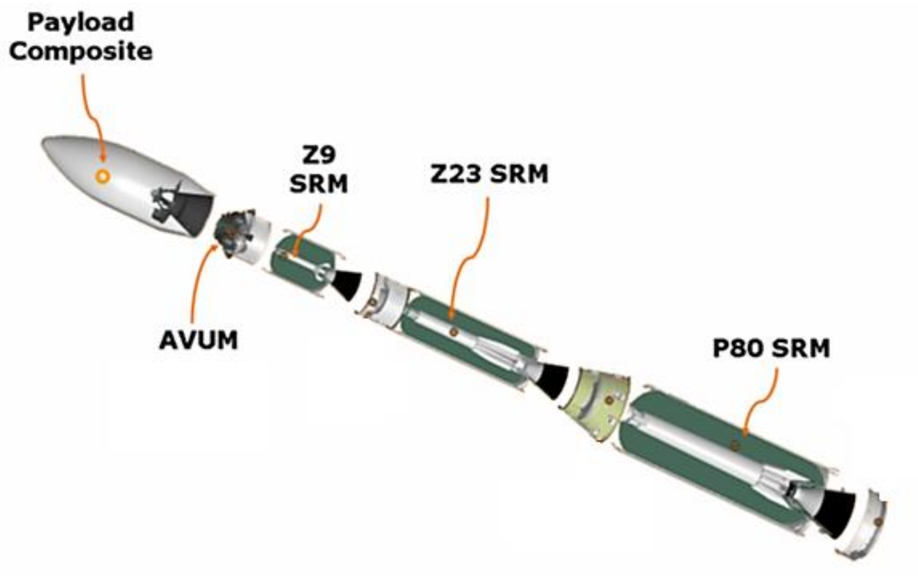


*Figure 1.16.* Vega Launcher and its components [10]

All of the solid rocket motor stages of Vega Launcher possess a pyrogen igniter. The characteristic of these solid rocket motors (length, diameter, burn time, operating pressure etc.) are different from each other; which means, the internal empty (port) volumes and surface areas - to be ignited - are all different from each other. Thus, each individual solid rocket motor has its own individual pyrogen igniter. Also, Vega family has another rocket motor which possesses its own pyrogen igniter, Zefiro 16 (Z16), which is produced and tested in order to develop and demonstrate the technological background that will be used in P80, Zefiro 23 (Z23) & Zefiro 9 (Z9). To sum up, during development, qualification and operation phases, four different pyrogen igniters are developed for Vega Space Propulsion System.

The characteristic properties of P80, Z23, Z9 and Z16 solid rocket motors are shown in Table 1.1. These properties include overall motor length, diameter, L/D ratio, burn time and motor port volume parameters. P80 is the first stage and the largest solid rocket motor of Vega Space Propulsion system. 87733 kilograms of aluminized propellant inside P80 burns in 110 seconds within maximum expected operating pressure (MEOP) 9.5 MPa. Z23, which is the intermediate stage of Vega Space Propulsion system, possesses approximately 24000 kilograms of aluminized propellant and its burn time is 72 seconds. MEOP value of Z23 10.6 MPa, which is higher than P80. It can be noticed that, Z23 operates in tougher pressure condition than P80, but in a shorter range of time. Z9 is the third and the last stage solid rocket motor of Vega Space Propulsion system (see Figure 1.17). 9935 kilograms of aluminized propellant inside Z9 burns in 111 seconds within MEOP value of 8.6 MPa. The motor cases of all Vega subsystem solid rocket motors are manufactured from composite filament winding, not steel, in order to carry that much amount of propellant with these operating and structural characteristics [11].

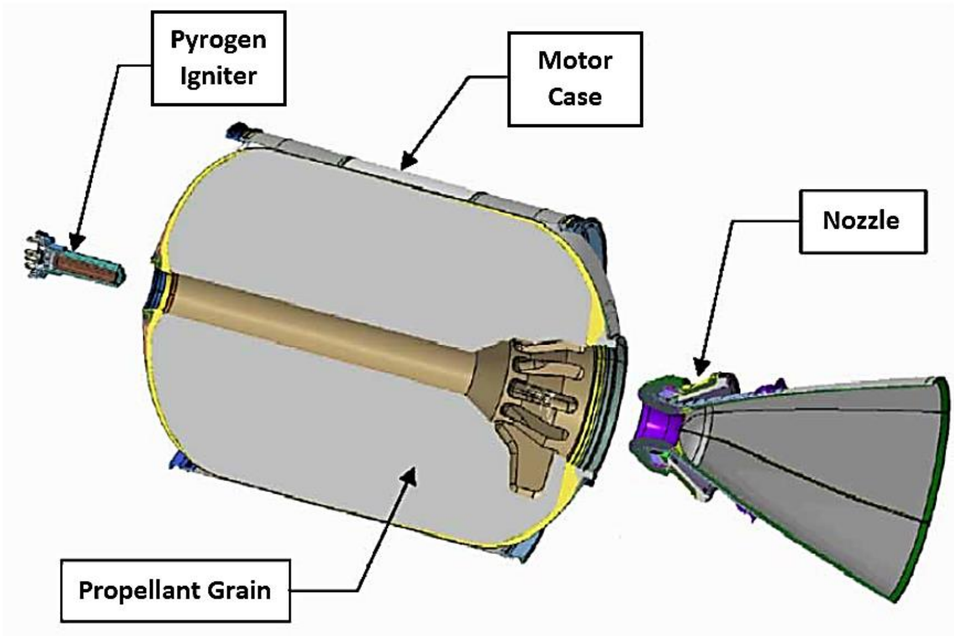


*Figure 1.17.* Zefiro 9 SRM and its components [10]

The pyrogen igniter of P80 solid rocket motor has a cartridge type installed propellant grain. In this type of production, the propellant is casted outside somewhere and then put into the rocket motor, unlike case bonded propellants which are directly casted into the rocket motor case. Propellant grains of Z23, Z9 & Z16 pyrogen igniters are also cartridge type. These propellants all involve Hydroxyl Terminated Polybutadiene (HTPB) as polymer binder and Ammonium Perchloride (AP) as oxidizer. They also contain high percentage of Aluminum (Al) inside the composition. The propellant grains of these pyrogen igniters have 13 to 16-star shaped slots in their geometry (Similar to Figure 1.6, grain geometry of PAP pyrogen but with less number of slots).

The characteristic properties of pyrogen igniters of Vega Launcher sub-solid rocket motors are represented in Table 1.2. Pyrogen igniter of P80, which has the largest pyrogen igniter in Vega system as expected, weights approximately 130 kilograms, with having 22 kilograms of propellant inside. Burn time of P80 pyrogen is 0.4 seconds within maximum expected operating pressure (MEOP) of 15 MPa. Notice that the pressure inside pyrogen igniter is greater than the pressure inside P80 SRM. As a matter of fact, the pressure inside the pyrotechnic igniter is greater than the pressure inside the pyrogen igniter of P80. In most cases, the igniter of a SRM endures much more inside pressure compared to its grand system, but for a very small amount of time (again compared to the grand system). By having 9.4 kilograms of propellant inside, Z23 pyrogen weights approximately 34 kilograms. Burn time of Z23 pyrogen is between 0.2 seconds within maximum expected operating pressure (MEOP) of 11 MPa. Z9 pyrogen igniter weights approximately 15 kilograms, with having 3.3 kilograms of propellant inside. Z9 pyrogen igniter burns in approximately 0.35 seconds and its MEOP value is 13.5 MPa.

The structural composition of Vega Launcher pyrogen igniters all consist of an insulated adapter ring, a pyrotechnic igniter, a filament wound case and integrated nozzle in addition to the propellant grain (Please refer Figure 1.19). Adapter grain, which is made of high strength aluminum alloy acts as an interference between the SRM and its pyrogen igniter. It seals the clearance between the SRM and pyrogen when the SRM is pressurized. Pyrotechnic igniter, which is both insulated with EPDM from inside and outside, contains B-$KNO_3$ pellets as igniter charge inside the steel basket. The filament winding material for the motor case is carbon epoxy. During SRM operation time, carbon epoxy endures the harsh pressure and temperature conditions occurring inside the SRM, holds the integrity of the pyrogen and restrains the rupture of the case. The erosion rate and performance of carbon epoxy is so low that there is no need for putting nozzle inserts (generally graphite, tungsten or carbon/carbon materials are used as nozzle inserts in solid rocket motors) to the nozzle throats of integrated nozzles of these pyrogen igniters (see Figure 1.18 and Figure 1.19) [12].


(a) (b)

*Figure 1.18.* Pyrogen igniters of P80 (a) and Zefiro 9 (b) SRMs [13]

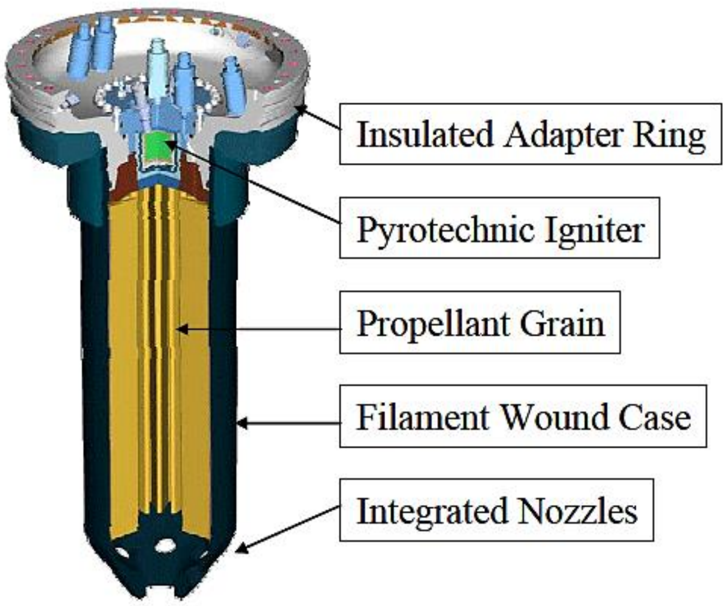


*Figure 1.19.* Schematic view of Zefiro 23 pyrogen igniter and its parts [12]

Zefiro 16 is a special prototype solid rocket motor which is not used in VEGA Space Propulsion System. It is manufactured and fired (statically tested) in order to innovate and demonstrate the technologies and processes that will be used in other solid rocket motors of VEGA system (P80, Z23 & Z9). Manufacturing the motor case with a composite filament winding material and the nozzle with a composite material and also using star shaped finocyl geometry in the SRM propellant (see Figure 1.20 and Figure 1.21) are some of these technologies in order to achieve a high performance solid rocket motor [3]. Detailed 3D CFD simulations containing investigation of ignition transient and tail-off phenomenon, pressure oscillations and combustion instability, effects of using different pressurizing gases in the motor start-up etc. are also performed during the development stage of this SRM and the outcomes of the studies are compared with actual test results after static firings in qualification stage. Zefiro 16 is a fully qualified SRM today [2] [14] [15].

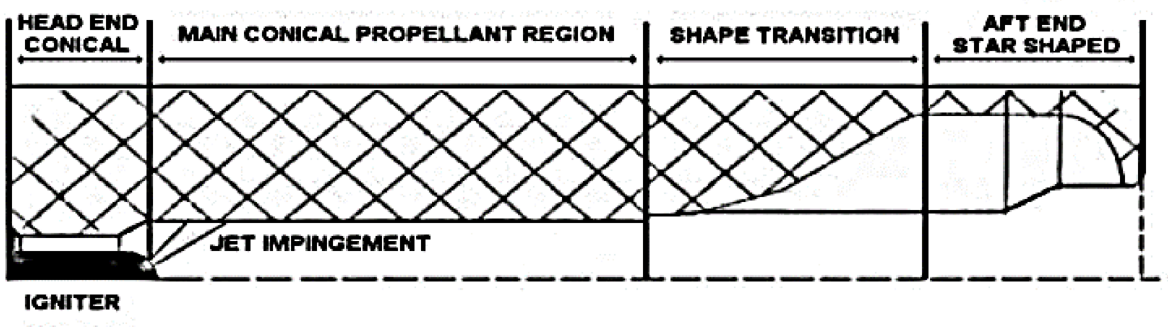


*Figure 1.20.* Zefiro 16 SRM chamber port section (finocyl geometry at the aft part) [14]

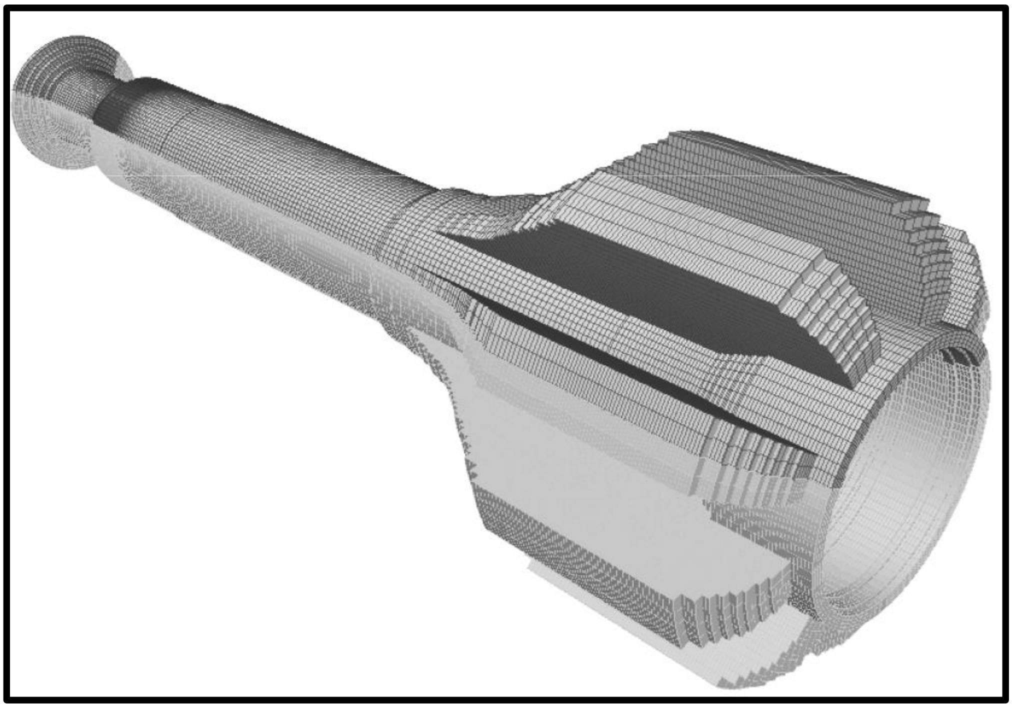

*Figure 1.21.* Constructed mesh geometry of port volume of Zefiro 16 SRM [15]

The characteristic properties of Z16 SRM and its pyrogen igniter can be seen in Table 1.1 and Table 1.2, respectively. The motor case material and production technique, propellant grain design and the propellant composition of other Vega sub-system solid rocket motors are similar to Zefiro 16. Approximately 16 tons of highly aluminized propellant in the motor burns approximately in 80 seconds with producing 8.3 MPa of maximum expected operating pressure (MEOP). 4 kilograms of propellant (which has similar composition with the SRM propellant) in its pyrogen igniter burns between 0.4 and 0.5 second, producing maximum amount of 15 kg/s mass flow rate (into the SRM port volume). The pressurization trend of the igniter is similar to other Vega sub-system SRMs and the pressure vs. time trace of Zefiro 16 SRM can be seen in Figure 1.22 with a boost (up to 20 seconds) and a sustain (from 20 to 80 seconds) phases, again in similar fashion with other Vega sub-system SRMs [15].

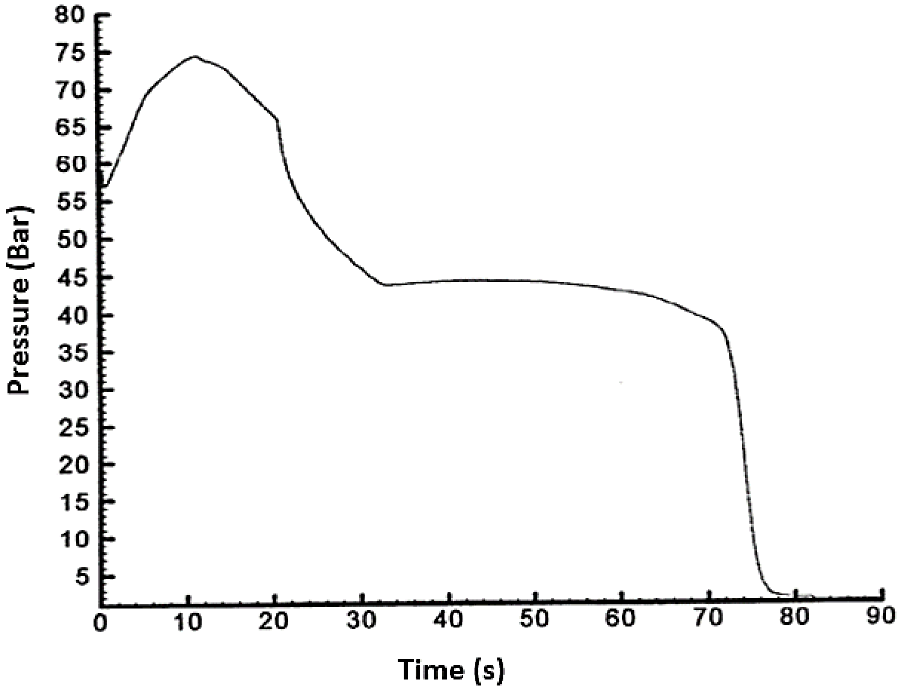


*Figure 1.22.* Pressure vs. time trace of the Zefiro 16 SRM [15]

### 1.3.5. Patents Related to Pyrogen Igniters

There exist many patents related to pyrogen igniters having various design approaches in the literature. A fully consumable pyrogen igniter during main SRM burn time (which will be ejected from main SRM nozzle after burning) is one of the examples that can be pointed out [16]. An igniter having a molded plastic motor case instead of a steel or composite material winding case or an igniter having dual propellant inside the motor case (combustion chamber) for boost and sustain purposes (see Figure 1.23) are another two examples found in the literature [17] [18]. However, most of these patents are somewhat outdated and taken between years 1960s and 90s (generally in United States). In those years, which we can call the beginning, footsteps era of the space age, igniting the propellant of a large SRM with a smaller one was a novel or developing technology. Today, pyrogen igniters are comprehensively known and qualified technologic subsystems. Therefore, instead of a whole pyrogen igniter configuration, patents related to innovative manufacturing techniques or material related researches have been published in the last decade. Vega sub-system solid rocket motors and their modern approach during in both material selection and production (Please refer section 1.3.4) constitute an appropriate example for this situation [12] [13].

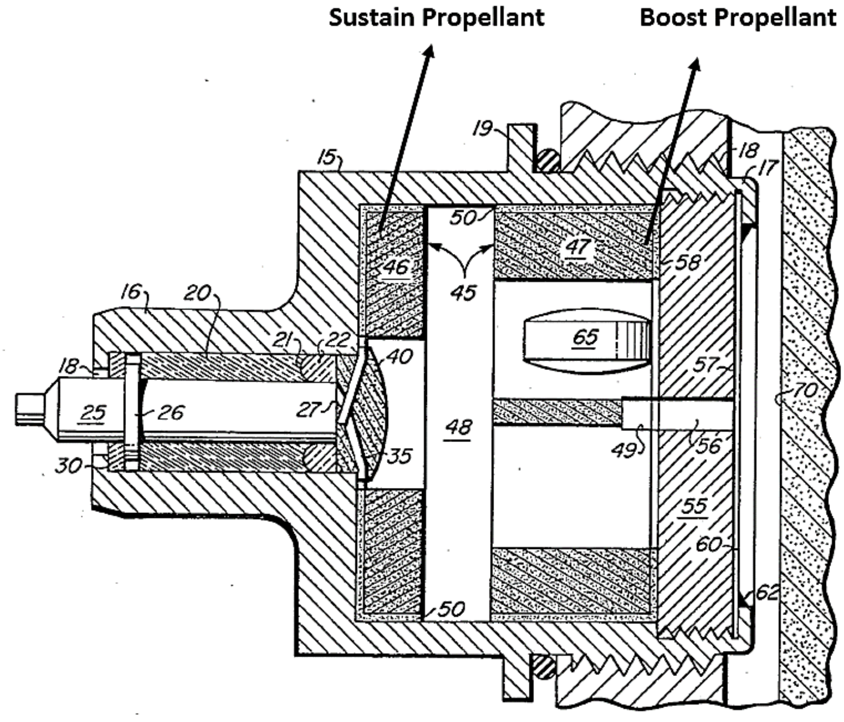


*Figure 1.23.* Pyrogen igniter patent having dual propellant configuration inside combustion chamber (1985) [17]

## 1.4. Nozzle Configurations of Pyrogen Igniters

In this part of the work, nozzle configurations of pyrogen igniters of grand solid rocket motor systems explained in Section 1.3. are analyzed, in detail. A major objective of this thesis work is to identify the dominant factors in pyrogen nozzle design and to optimize them in order to achieve a shorter and effective ignition transient for a well-defined SRM system (with pre-determined pyrogen and grand SRM ballistic designs). Therefore, the first step is to analyze the nozzle structure of those pyrogen igniters.

### 1.4.1. Space Shuttle - RSRM Pyrogen Nozzle Configurations

RSRM has two pyrogen igniters inside its ignition system: a small primer igniter and a large main igniter whose propellant is ignited by the primer igniter in the ignition sequence. As can be seen in Figure 1.9, the primer igniter has total of six radial nozzles at its aft section. All of these nozzles have carbon-phenolic material nozzle inserts in their throat section in order to prevent the nozzle throats from erosion. The main igniter, on the other hand, has one large nozzle opening which is insulated by silica-phenolic material from both inside and outside [6].

The selection of configuration of nozzles of these pyrogen igniters, whether they are axial or radial, is totally related to ballistic reasons and requirements. Radial nozzles produce both axial and radial mass flow; whereas, axial nozzles produces only axial mass flow in the earlier stages of ignition. Therefore, the axial-to-radial nozzle ratio should be determined by the ignition transient and pressurization requirements for each rocket motor, individually.

### 1.4.2. Scout - Antares III Pyrogen Nozzle Configuration

Antares III utilizes six radial nozzles within its pyrogen igniter with 60° intervals. As it can be seen in Figure 1.13, an individual radial nozzle is divided into three parts. The first part, which is the entrance of the nozzle and located inside the pyrogen is made of silica phenolic material. It acts both like a nozzle port and an inner insulation for the nozzle. The second part, in which the jet flow passes through, is made of titanium and has no insulation. The last part is the vent in the outer insulation of the pyrogen igniter, which is manufactured from EPDM material. This part is where the jet flow leaves the pyrogen igniter and starts to travel towards Antares III SRM propellant and for that reason it is called ''Exhaust Port'' in the reference document [8].

### 1.4.3. Ariane V - P230 Pyrogen Nozzle Configurations

Much like RSRM, P230 also owns two pyrogen igniters in its igniter mechanism: again, a small primer igniter and a large main igniter. In this igniter system both primer and main igniter have got five equally spaced nozzle ports in their own dome(aft) section. Nozzles of the main igniter are positioned 45° above the longitudinal axis of the main igniter itself (see Figure 1.24). Both primer and main igniter have carbon-phenolic material nozzle inserts in their nozzle throats in order to withstand erosion and shear effects of jet flow which has high temperature and velocity [9].

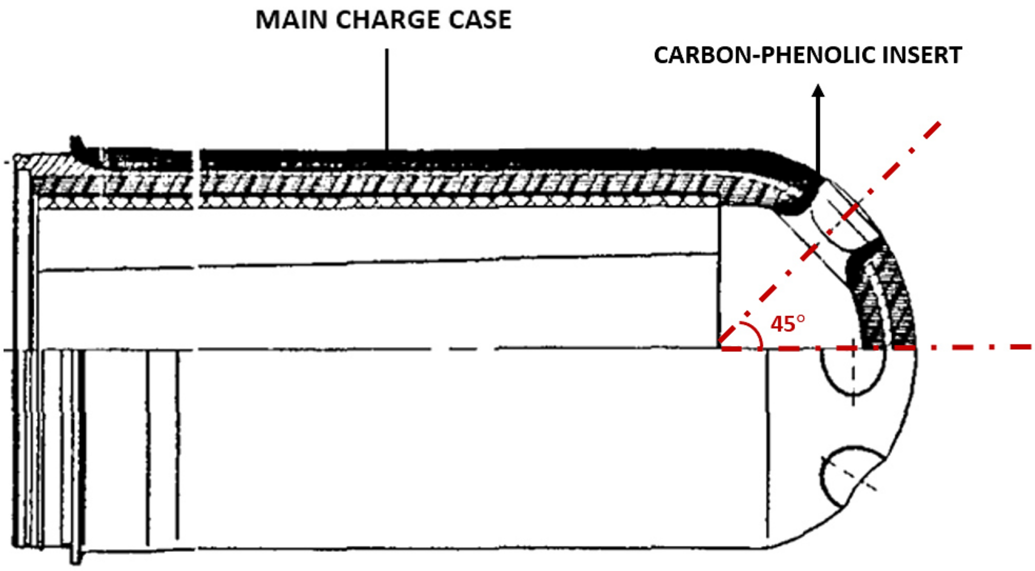


*Figure 1.24.* P230 main pyrogen igniter nozzle details [9]

### 1.4.4. VEGA – P80, Z23, Z9 and Z16 Pyrogen Nozzle Configurations

The family of VEGA subsystem solid rocket motors (P80, Z23, Z9 and Z16) and their pyrogen igniters have some distinguishing features compared to other solid rocket motors investigated in the literature. First of all, cases of these pyrogen igniters are made composite material, instead of metal. Nozzles located in the dome section are integrated with the carbon epoxy wounded motor case (see Figure 1.19). Motor cases and their integrated nozzles do not have inner or outer insulation due to the fact that carbon epoxy can withstand harsh conditions inside grand SRM; furthermore, because of the same reason nozzles do not have nozzle inserts either. After static firings (Figure 1.25), it is concluded that erosion of carbon epoxy material in the nozzle sections are acceptable (Figure 1.26) [12].

*Figure 1.25.* P80 pyrogen igniter static firing [12]


(a) (b)

*Figure 1.26.* Z9 Igniter cases and nozzles after static Firing of Z9 (a) and Z23 (b) [12]

Although their manufacturing methods, technologies and topological features are quite similar, pyrogen igniters of VEGA subsystem solid motors differ from each other by means of their nozzle configurations. Z16 pyrogen has three radial nozzles with 100% radial igniter mass flow rate (See to Figure 1.27). These three nozzles are located 35° above the longitudinal axis of the pyrogen igniter itself. On the other hand, Z9, Z23 and P80 all have six radial and one axial nozzles having 80% radial – 20% axial, 60% radial – 40% axial and 50% radial – 50% axial mass flow rates, respectively [3].

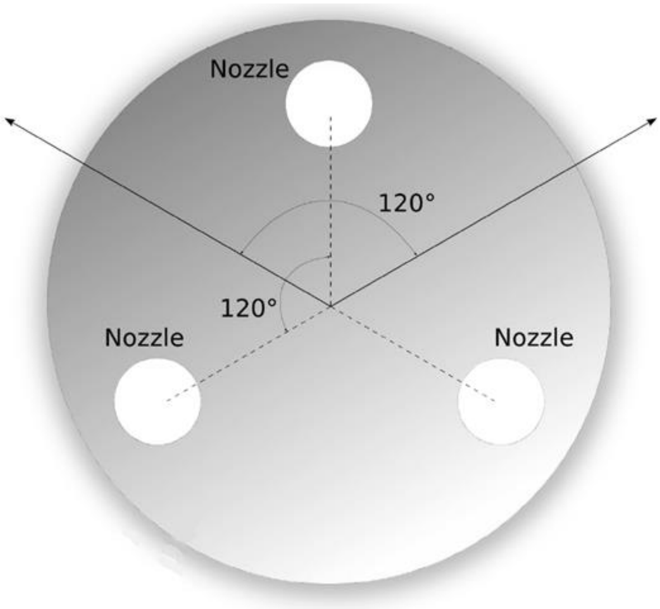


*Figure 1.27.* Zefiro 16 nozzle configuration (top view) [3]

Because of composite winding manufacturing process, pyrogen igniters of all Vega sub-system solid rocket motors have only convergent nozzle geometries, not convergent-divergent as in standard rocket motor nozzles. Thus, the flow that is departing the pyrogen cannot reach supersonic regime, it is always sonic or close to sonic. Which means chocked flow conditions are achieved in a very short time interval throughout the nozzles. Therefore, the jet flow leaving the pyrogen igniter and travelling across grand system SRM propellant shows an underexpanded behavior [3].

As can be figured from all reference pyrogen igniters, unlike standard solid rocket motor nozzle configurations, pyrogen igniters have more than one nozzle in their assembly. Most of the pyrogens have 5 or 6 radial nozzles. Although it is not mentioned above, pyrogen igniter of S200 SRM, developed and manufactured in India, also possesses five radial nozzles (see Figure 1.28) [19].

In these type of configurations, the hot jet flow leaving the igniter hits the main SRM propellant in 60° or 72° intervals, with the aim of covering and igniting the surface of that propellant circumferentially. Also, if one of the pyrogen nozzles clogs, ignition can still be achieved with the help of flow passing through other nozzles. However, this situation must be avoided because of the fact that if more than nozzles gets in clog state, the igniter might become over pressurized and burst in the SRM.


(a) (b)

*Figure 1.28.* S200 Pyrogen igniter (a) and its Static Firing (b) [19]

### 1.5. Motivation and Objectives of The Thesis

At first glance, solid rocket motors seem like simple propulsion systems which have certain known components showing predictable behavior. However, during an SRM design, production and test phases very intricate and complex phenomena occur: some of which happen in milliseconds in extreme conditions, some of which happen in years in room conditions; some of which cannot be simulated in a simple manner or some of which can be triggered by multiple other causes. From the first sketch till the flight mission, these phases take lots of thinking and effort, which is also not inexpensive.

Ignition transient is only one of these complex phenomena, starts and ends in milliseconds and happens in severe transient temperature and pressure conditions. In large solid rocket motor systems, things get a bit more complicated because one extra element is added to the ignition chain sequence, namely a pyrogen igniter. Pyrogen igniter is both an igniter and a solid rocket motor. Its igniter behavior is somehow similar to its minor pyrotechnics system; whereas, its motor behavior shows similar characteristics as its major SRM system.

The pressurization effect that is created by the pyrogen igniter in the main SRM, which is directly linked to ignition transient, is affected from various reasons. Type of propellant used in the pyrogen, performance of its own pyrotechnics, grain geometry of the propellant, pressurizing fluid used in SRM system etc. are some of these factors. Nozzle geometry also plays an important role in this type of pressurization. The mass flow ejected into the main SRM propellant, its speed as well as its direction is determined by the nozzle design of the pyrogen.

In the open literature, there exists only few studies about nozzle design of pyrogen igniters and these studies are not directly about nozzle design, they generally cover some information or mathematical model in their various chapters. Scientific papers, articles and documents related to pyrogen igniters contain some trivial information related system's pyrogen nozzles; however, the design logic of the nozzle geometry, orientation and configuration can only be interpreted by the reader himself/herself. At best, comparisons between different systems can be made to have an idea and develop some feasible visions about the nozzle design of a pyrogen igniter. There is no reference/bedside guide for this kind of design procedure, in the open literature.

By this motivation, in this thesis work the first objective is to determine and mathematically model the dominant factors for a pyrogen nozzle design which shortens the ignition transient phase of the main SRM via a design of experiment (DOE) approach. These factors will be number, angle and diameter of nozzle openings for a given pyrogen design. The pressurization effect problem will be solved by a "Fully Coupled Compressible Solver for Turbulent Perfect Gas Flows" code constructed with the academic research carried out by Kalpaklı, with wide range of combination of the factors aforementioned [20]. After the recessive factors eliminated, the optimum nozzle geometry will be selected by this kind of method. Before this procedure, the results of an atmospheric pyrogen firing will be compared to design outputs of the code which run with the same tested pyrogen (and its nozzle) geometry in an atmospheric environment, in order to verify the numerical solver. Thus, if numerical and test results match, optimum nozzle geometry found in DOE approach will make the shortest and the most effective pressurization in the SRM, even though optimum nozzle itself is not tested.

### 1.6. Structure of The Thesis

The organization of the thesis work is explained below:

Chapter 1 is the introduction of solid rocket motors, pyrogen igniters, and nozzle configuration of pyrogen igniters. Literature research and information background is constructed and objective of the thesis work explained in this chapter.

Chapter 2 represents governing equations, mathematical model and the features of the solver. Then, an experimental verification study for the solver found in the literature is explained and the comparison of the outcomes of the solver with the experiment results are discussed.

Chapter 3 introduces design of experiment procedure first. After that, the fixed parts of the test geometry, initial and boundary conditions are introduced. The test matrix that is constructed according to the nozzle parameters, topologies of the test cases in the matrix, and also extreme cases are discussed at the end of the chapter.

In Chapter 4, the mesh independency study is carried out in the beginning. Then, a sample test case and its simulations results are discussed. Comparison of the pressure, Mach number and temperature outcomes of each test case are made and the effects of nozzle design parameters on these outcomes are discussed relatively in a detailed manner. Later in this chapter ballistic performance and ignition transient behavior of the pyrogen nozzle designs are compared and the optimum nozzle geometry is selected for the given problem. Furthermore, the effects of dominant factors in the nozzle design of a pyrogen igniter are presented. In the end, the feasibility and the availability of these designs, optimization logic and test results are discussed and interpreted by citing their inter-correlations. and possible future work studies regarding to this thesis work are mentioned in the last sections of this chapter.

In the last chapter, Chapter 5, first of all a summary of the thesis work is written. Then, conclusions deducted from this work, benefit to the open literature and possible other usage areas of this study are discussed. Suggested future works are also pointed out at the end of the chapter.

# CHAPTER 2

# MATHEMATICAL ANALYSIS

## 2.1. Introduction

As mentioned in Section 1.2, ignition transient in solid rocket motors is a complex phenomenon which includes a variety of unstable and successive events in an extremely short time interval. The main purpose of this thesis work is to determine the effect of the nozzle configuration (including number of nozzles, angles and dimensions) of a pyrogen igniter on ignition transient of its grand SRM system. In order to achieve this goal, a DOE procedure is carried out. Different nozzle geometries are simulated and tested numerically in order to specify the dominant parameters in the design and to obtain an effective (shorter) ignition transient. During this task, the findings of the doctoral thesis work of Kalpaklı and CFD Solver constructed from his work which is called "Fully Coupled Compressible Solver for Turbulent Perfect Gas Flows" is utilized [20]. The solver is able to approach different kinds of gas dynamic problems (cases) in both implicit and explicit manners. It can be used from incompressible flow conditions to hyper-sonic flow regimes and is suitable for investigating ignition transient behavior due to the following reasons:

- Since ignition transient phenomena occurs in a very short time duration – which is in milliseconds range – blast waves and acoustic phenomena dominate the port volume of main SRM, rather than pressure waves which are following behind. Here, explicit problem-solving approach is more suitable than implicit one because in implicit solver, time accuracy degenerates while dealing with problems mainly containing acoustic phenomena. Therefore, in the cases of this thesis work, a fast converging explicit discretization approach is more suitable to investigate the mentioned phenomena in a detailed manner [20].

- When the igniter jets blow out of pyrogen igniter and reach main solid rocket motor propellant surface, the flow speed decreases significantly. Mach number value of this flow is approximately 1 near pyrogen igniter nozzle exit and drops to 0.2 - 0.3 near main SRM propellant regions; thus, the flow becomes incompressible. The solver is not a pressure-based or density-based solver only; it behaves as it is hybrid of these two approaches and therefore more suitable for covering these varying flow regimes.
- During SRM operation and ignition transient intertangled events occur simultaneously and affect each other. In addition to fundamental governing equations which are continuity, momentum and energy equations, additional equations and terms are introduced in order to cover the phenomena in a complete manner. Therefore, solving equations and obtaining variables namely, pressure, velocity, temperature, turbulent parameters, and species mass fractions, in a coupled manner is more suitable approach for this problem rather than solving equations in a segregated way.
- Rather than using commercial CFD solvers like FLUENT, a solver which can cover acoustic phenomena in a widespread manner is selected in order to simulate and solve real compressible acoustic cases.

## 2.2. Governing Equations of Gas Dynamic Model

The fundamental governing equations used can be formulated as follows [21]:

- In a control volume the conservation of mass in integral form can be written as,

  $$\frac{\partial}{\partial t}\int_{CV}\rho d\mathrm{V} + \int_{CS}\rho\, \boldsymbol{v} d\mathrm{A} = 0 \qquad (2.1)$$

  where $\rho$ is the fluid density and $\boldsymbol{v}$ is the fluid velocity for control volume $\underline{d}$V and control surface $d$A.

- In a control volume the conservation of momentum in integral form can be written as,

  $$\frac{\partial}{\partial t}\int_{CV}\rho \boldsymbol{v} d\mathrm{V} + \int_{CS}\rho\,(\boldsymbol{v}\boldsymbol{v}) d\mathrm{A} = \sum F \qquad (2.2)$$

  where $\sum F$ is net body forces acting on control volume.

- In a control volume the conservation of energy in integral form can be written as,

  $$\frac{\partial}{\partial t}\int_{CV}\rho(e+\frac{v^2}{2}) d\mathrm{V} + \int_{CS}\rho\,(e\ +\ \frac{v^2}{2})\,(\boldsymbol{v}) d\mathrm{A} = \sum \dot{Q} + \sum \dot{W} \qquad (2.3)$$

  where $e$ is thermal energy of the fluid particles, $\sum \dot{Q}$ is net volumetric heat generation and $\sum \dot{W}$ is net work done on the control volume.

## 2.3. Boundary Conditions

The boundary conditions used in "Fully Coupled Compressible Solver for Turbulent Perfect Gas Flows" can be classified as follows [20]:

- For mass flux => Mass Flow Inlet BC in order to provide mass flow rate at a boundary (Mass flux, total temperature and static pressure is provided)

First, the density ($\rho$) of ideal gas is calculated as,

$$\rho = \frac{p}{RT} \tag{2.4}$$

where p is static pressure, T is static temperature and R is the gas constant. With the provided $T_0$ in the mass flow inlet condition,

$$\frac{T_0}{T} = 1 + \frac{(k-1)\boldsymbol{u}^2}{2a^2} \tag{2.5}$$

where a is the speed of sound, $\boldsymbol{u}$ is the normal velocity and $k$ is ratio of specific heats.

$$a = \sqrt{\frac{kp}{\rho}} \text{ and } u = \frac{\dot{m}}{\rho} \tag{2.6}$$

Then, the density can be found as,

$$\rho = \frac{kp + \sqrt{k}\sqrt{2R\dot{m}^2(k-1)T_0 + kp^2}}{2a^2} \tag{2.7}$$

- For wall velocities => Viscous Wall BC since the flow type is viscous. A ghost cell is used with a state,

$$U_{g=} \begin{bmatrix} p_d \\ p_d u_d \\ p_d v_d \\ E_d \end{bmatrix} \tag{2.8}$$

where gradients of velocity vectors ($\boldsymbol{u}$ and $\boldsymbol{v}$) can be calculated as,

$$\frac{\partial \boldsymbol{u}}{\partial \boldsymbol{x}} = \frac{\boldsymbol{u}}{\Delta \boldsymbol{x}}, \frac{\partial \boldsymbol{v}}{\partial \boldsymbol{x}} = \frac{\boldsymbol{v}}{\Delta \boldsymbol{x}}, \frac{\partial \boldsymbol{u}}{\partial \boldsymbol{y}} = 0 \text{ and } \frac{\partial \boldsymbol{v}}{\partial \boldsymbol{y}} = 0 \tag{2.9}$$

Here $\Delta \boldsymbol{x}$ is the difference between cell center and face center. In this thesis work, the investigated phenomenon is the filling of main SRM port volume by the gaseous products ejecting from pyrogen nozzles, mainly. Thus, mass flow inlet (e.g. pyrogen nozzle openings) and wall (e.g. main SRM propellant surfaces) boundary conditions are used while running the simulations.

Furthermore, as an important note, boundary layer phenomenon did not take into account while dealing with boundary conditions or investigating the parameters (pressure, density, etc.) at the wall since the utilized solver has no capability of solving heat transfer and/or pyrolysis equations or any wall interactions.

### 2.4. Calculation of Thermochemistry Properties

In order to obtain thermochemistry properties, the solver is utilizing the same thermodynamic database (library) used by NASA Chemical Equilibrium with Applications (CEA) software [22]. In this thesis work the gas mixture, which is ejecting from pyrogen nozzle and filling the port volume of the main SRM is assumed to be composed of perfect gases. That means their thermodynamic properties are functions of temperature. The mass specific enthalpy ($h_k$), the mass specific energy ($e_k$) and the mass specific entropy ($s_k$) of the $k^{th}$ species in the gas mixture can be defined as follows:

$$h_k = \int_{T_0}^{T} c_{p,k} dT + \Delta h_{f,k}^0 = h_{s,k} + \Delta h_{f,k}^0 \tag{2.10}$$

$$e_k = \int_{T_0}^{T} c_{v,k} dT + \Delta h_{f,k}^0 - R_k T_0 = e_{s,k} + \Delta h_{f,k}^0 \tag{2.11}$$

$$s_k = \int_{T_0}^{T} \frac{c_{p,k}}{T} dT + s_{k,0} \tag{2.12}$$

where, $c_{p,k}$ is constant pressure specific heat, $c_{v,k}$ is constant volume specific heat and $R_k$ is gas constant. $R_k = \frac{R}{W_k}$ where universal gas constant $R$ = 8.314 $\frac{J}{K.mole}$ and $W_k$ is the molecular weight of the $k^{th}$ species. Furthermore, $\Delta h_{f,k}^0$ term in equation (2.4) is the enthalpy of formation at reference state temperature $T_0$ and $s_{k,0}$ term in equation (2.6) is the reference state entropy at $T_0$. In calculations reference temperature $T_0$ is taken as 298.15 K.

Specific mixture properties are calculated using specific properties of each species having mass fractions $Y_k$ as follows:

$$h_s = \sum_k^N Y_k h_{s,k}(T)\ , \quad e_s = \sum_k^N Y_k e_{s,k}(T, p_k),\ \ s_s = \sum_k^N Y_k s_{s,k}(T, p_k) \qquad (2.13)$$

where $p_k$ is the partial pressure of the $k^{th}$ species. Gas constant and molecular weight of the mixture is calculated as follows:

$$R = \sum_k^N R_k Y_k\ , \qquad \frac{1}{W} = \sum_k^N \frac{Y_k}{W_k} \qquad (2.14)$$

## 2.5. Solution Scheme

The solution scheme (flowchart) of the serial solver used in this thesis work is illustrated and can be investigated in Figure 2.1.

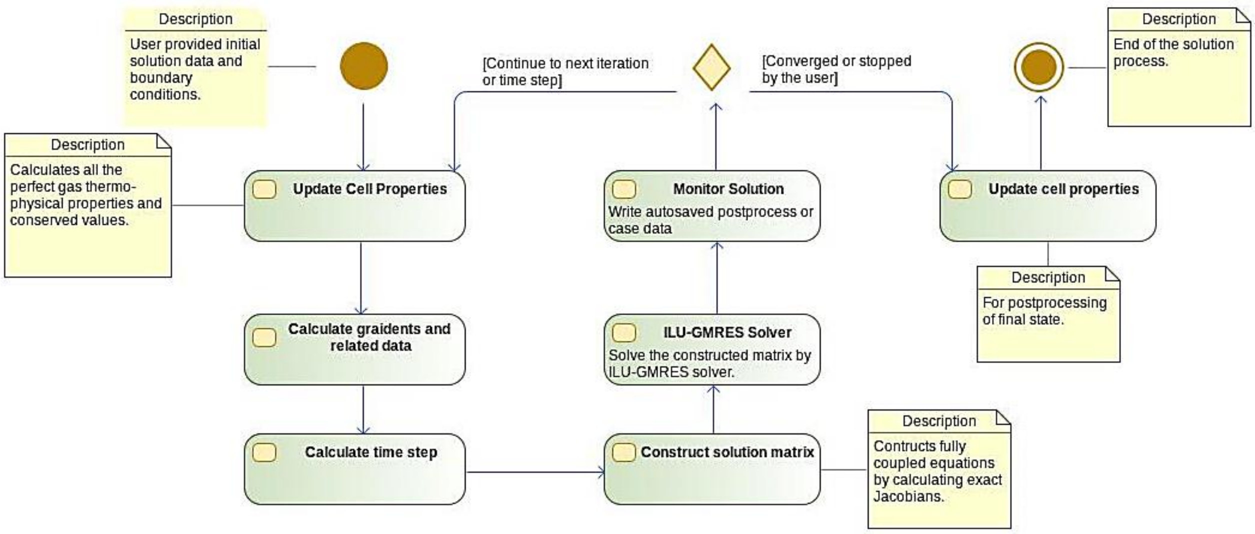


*Figure 2.1.* Flowchart of the fully coupled compressible solver for turbulent perfect gas flows

In a detailed approach, first of all, the user introduces the meshed geometry of the test case with providing boundary (inlet, wall etc.) and initial conditions (temperature, pressure, velocity, CEA outputs etc.) as well. Then, the solver options (1st order, 2nd order etc.) and flow characteristics (viscous, inviscid, with or without particle species etc.) are defined. Iteration starts via updating the cell properties. A solution matrix is then created by constructing fully coupled equations after gradients of the parameters and time step are calculated, precedingly. This constructed matrix is solved by iterative matrix solver and the results are saved and monitored in the visual interface of the solver. This procedure is repeated by the next iteration (starting from updating cell properties with the most recent data that have been stored) until the solution converges to a pre-defined value for a particular parameter or the solver is stopped by the user. After convergence or termination of the iterations, the cell properties are updated for the last time for postprocessing purposes and the flow simulation reaches to an end.

### 2.6. Reference Verification Experiment

In order to test the solver, a study in the literature is examined in a detailed manner and its outcomes of original test case are compared to the outcomes of the solver used in this study [23]. The examined study is "Experimentally Validated 3-D Simulation of Shock Waves Generated by Dense Explosives in Confined Complex Geometries" written by Rigas and Sklavounos in January 2005. The aim of this work is to compare the data gathered from an explosion experiment with the data obtained from the simulation of the same event, in pressure and Mach number points of view in order to foresee the effects of blast waves of an explosion and take safety measurements prior to production of these kind of systems involving explosives. To carry out the process, a test geometry shown in Figure 2.2 is constructed. As shown in Figure 2.2 (a), an explosive is planted between the confined extensive volume and the pipes. The aim of the experiment is to detect the pressure data via the sensors placed in the pipe system before (point 1) and after (points 2 and 3) the branching point.

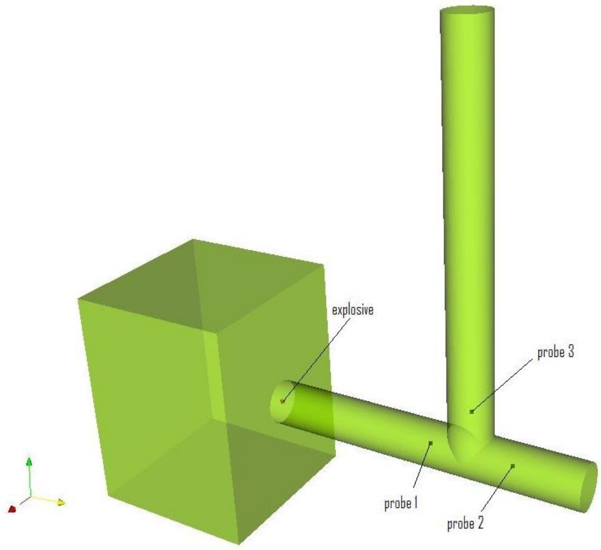


*Figure 2.2.* Constructed test geometry in the reference study [23]

In this thesis work, the data obtained from the experimental results of the reference study are compared with the outcomes of the simulations made by the fully coupled solver used in this work, whose solution scheme is introduced in Section 2.5. The pressure outcomes of this comparison can be analyzed in Figure 2.3. The results obtained from the solver are in good agreement with the experiment results and the simulation successfully predicts the pressurization behavior with an acceptable error margin.

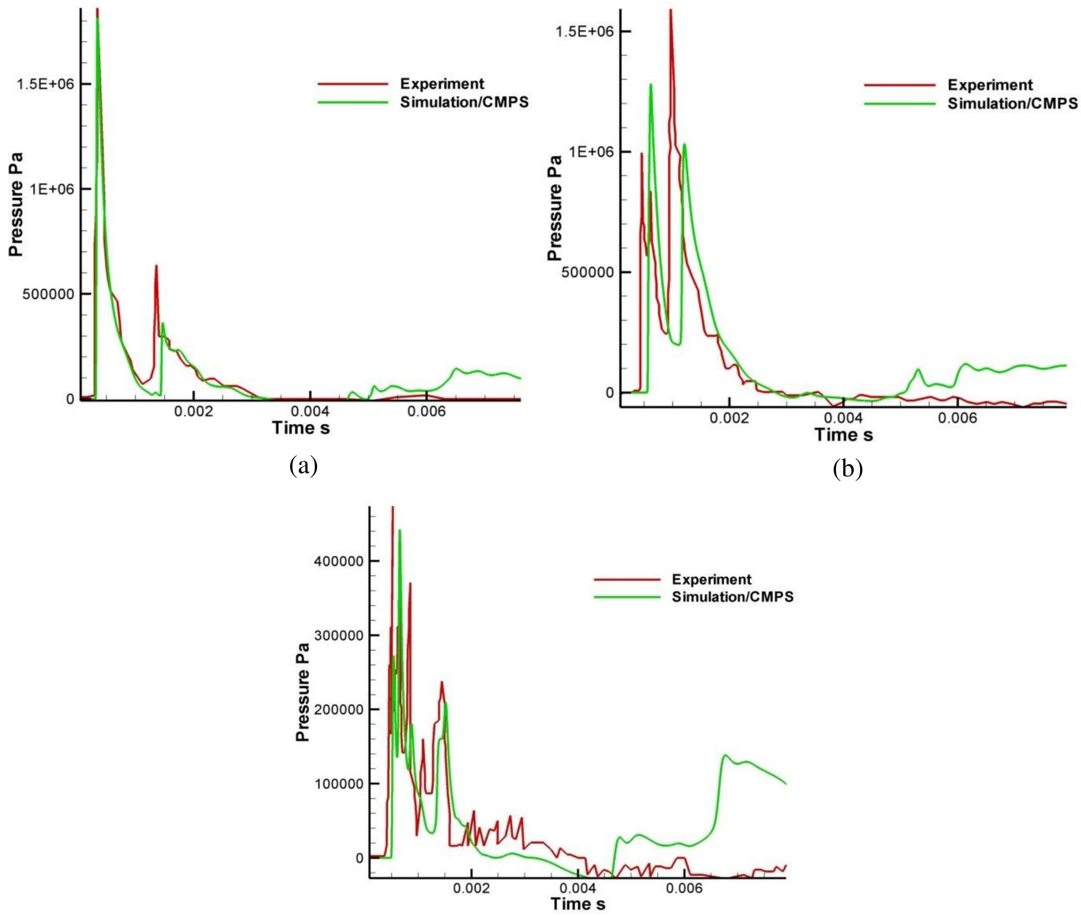


(c)

*Figure 2.3.* The comparison of pressure outcomes of the solver used in thesis work and the experimental results in the reference study in probe locations 1 (a), 2 (b) and 3 (c)

Moreover, the pressure and Mach number visualizations can be analyzed in Figure 2.4 and the propagation of the shockwave and pressure peaks can be seen in the 60th millisecond of the simulation (similar illustrations are also made in the reference study with its own numeric solver). In the reference study it is concluded that the free expansion of the gases (products of the explosion) in the tubular sections is restricted, unlike it is in the extensive large volume; therefore, higher pressure values obtained in those parts of the experimental setup. Likewise, in the extensive volume Mach number of the gases drop below sonic limit (Ma=1); whereas, it increases in the pipe section with the propagating shockwaves. Thus, narrowing down the exit ways/areas/volumes of any sort of explosive flow is not recommended [23].

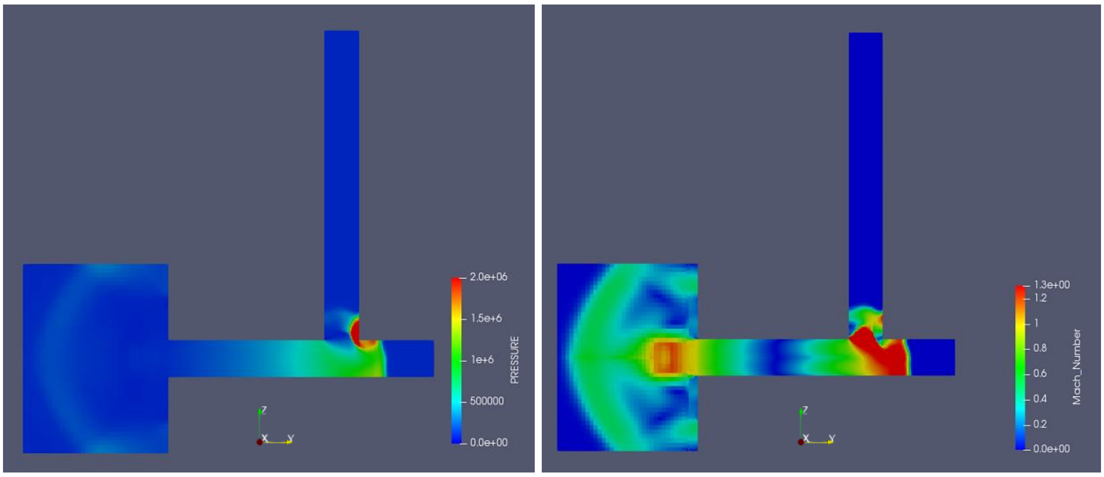


(a) (b)

*Figure 2.4.* The pressure (a) and Mach number (b) behaviors in the 60th millisecond of the simulation made by the solver used in this thesis work

After analyzing Figure 2.3 and Figure 2.4 it can be concluded that results obtained from the solver used in this thesis work are coherent with the results of the experiment carried out in the reference study. Therefore, by this assessment, 'fully coupled compressible solver for turbulent perfect gas flows' is opted as suitable tool to investigate the pressurization behavior of a pyrogen igniter inside a grand SRM system in the first milliseconds of its ignition.

# CHAPTER 3

# NUMERICAL MODEL

## 3.1. Full Factorial Design Experiment

Design of Experiment (DOE) is a statistical tool that constructs a mathematical expression between the outputs and the inputs (which are thought to be affected from those outputs) of a phenomenon, problem, process etc. DOE offers a systematical solution to the problems and helps to manage the outputs in a numerical way. It also places the problem on an analytical approaching basis rather than just experience or common knowledge [24].

There are several experimenting methods such as, Trial and Error method, One-Factor-at-a-Time method and Designed Experiments. The input parameters in a given problem might have no relationship with the outputs of that problem. Therefore, if Trial and Error method is used for experimenting problems with lots of input parameters, access time and effort can be consumed by the experimenter [24].

The problems with One-Factor-at-a-Time method is that it supplies no information about the interactions of the inputs (if any); as well as, the outcomes of the problem when multiple influencing input effects are combined. That is the reason why finding an optimum solution for a given test case is problematic when using One-Factor-at-a-Time method [24].

Designed Experiments such as Full Factorial, Fractional Factorial or Surface Response Methodologies, aim to obtain maximum amount of information with minimum amount of data via using the resources at hand in an iterative and efficient manner. They also point out how individual and/or combined existence of inputs affect the output(s) that is/are desired to be observed.

In Full Factorial Design approach every combination of the given factors (inputs) is examined in a test plan/matrix; whereas, in Fractional Factorial Design approach some of these combinations are eliminated. Therefore, Fractional Factorial Design approach has less number of experiments than Full Factorial one; and thus, the experiment approaches to the conclusion faster than the one examined by Full Factorial approach. However, due to the fact that some combined factors have been omitted, some amount of information is lost in Fractional Factorial Design approach. Whether this lost information is crucial for interpreting the outcomes of the experiment or not, is a choice in the experimenter's own thinking and hands.

In this study, in order to investigate the dominant parameters in the nozzle design of a pyrogen igniter, a Full Factorial DOE approach is utilized. With predetermined geometric and ballistic performance features (which are compatible with the literature and will be explained in a detailed manner in Sections 3.2 and 3.3) every combination and scenario of three design parameters of the nozzle of a pyrogen igniter will be investigated. These three design parameters are radial nozzle number, radial nozzle angle and the radial mass flow rate ejected from nozzle openings of a pyrogen igniter nozzle also having an axial nozzle opening, for pivoting. The outcome that will be investigated is the pressurization efficiency of the (same) grand SRM system having that particular pyrogen igniter for igniting its own propellant grain. Since the number of the consequent test cases is not extreme ($3^3 = 27$) and the software utilized to solve these cases is fast enough, a Full Factorial Design approach is selected rather than Fractional one in order to map the entire problem domain, in a fully covered manner. Besides, two more extreme pyrogen igniter cases having only full axial or radial mass flows for pressurization of the grand SRM system will be investigated for a complete comparison and understanding of the problem.

## 3.2. Test Geometry and its Features

The isometric views of the grand SRM propellant and its pyrogen igniter used in the test cases are shown in Figure 3.1 and Figure 3.2. Because of test purposes, the SRM geometry is simplified and only its propellant in a closed volume has been left. The fixed geometric features of the closed SRM propellant and the pyrogen igniter can be seen in Figure 3.3 and Figure 3.4 respectively.

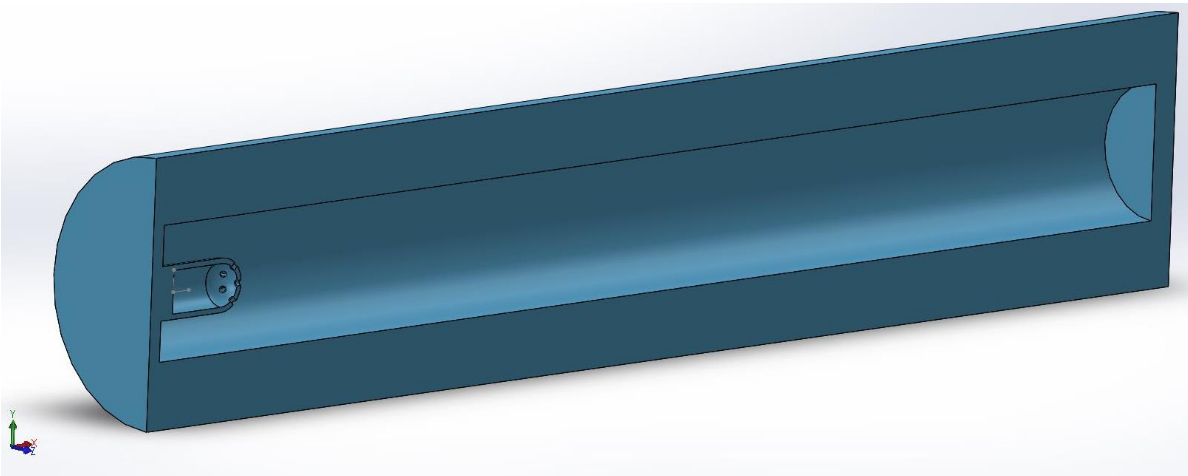

*Figure 3.1.* Isometric view of the grand SRM propellant

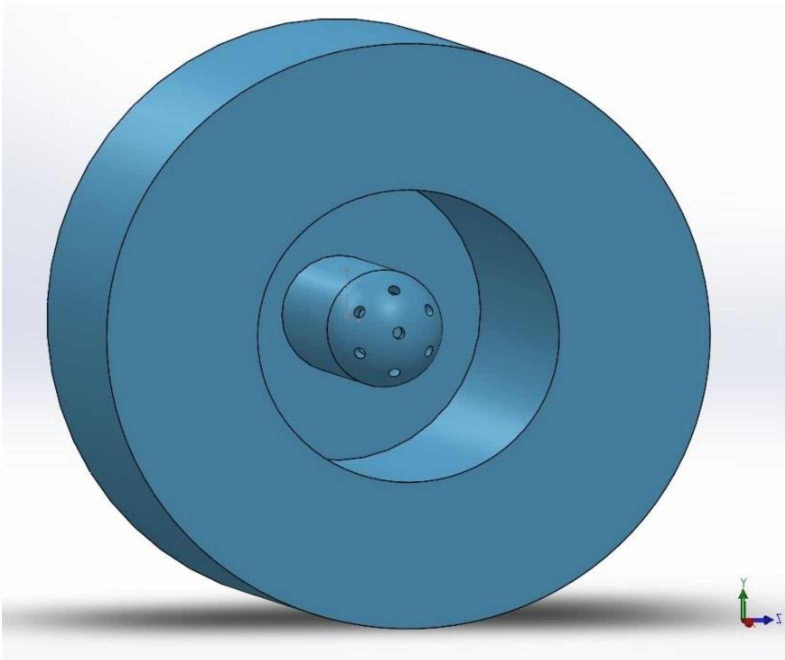

*Figure 3.2.* Isometric view of the grand SRM pyrogen igniter

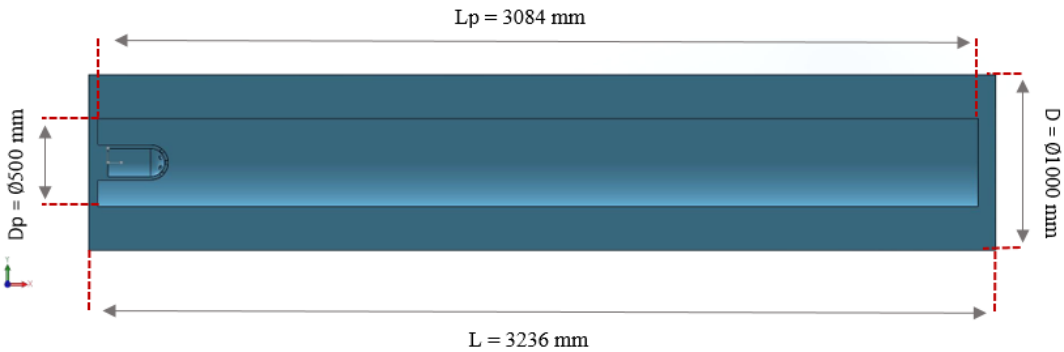


*Figure 3.3.* Geometric features of the SRM

The length of the empty volume inside grand SRM propellant (Lp, port length) is 3084 mm; whereas, its port diameter (Dp) is 500 mm. These two parameters constitute the port volume, also known as combustion chamber free volume, of the SRM propellant.

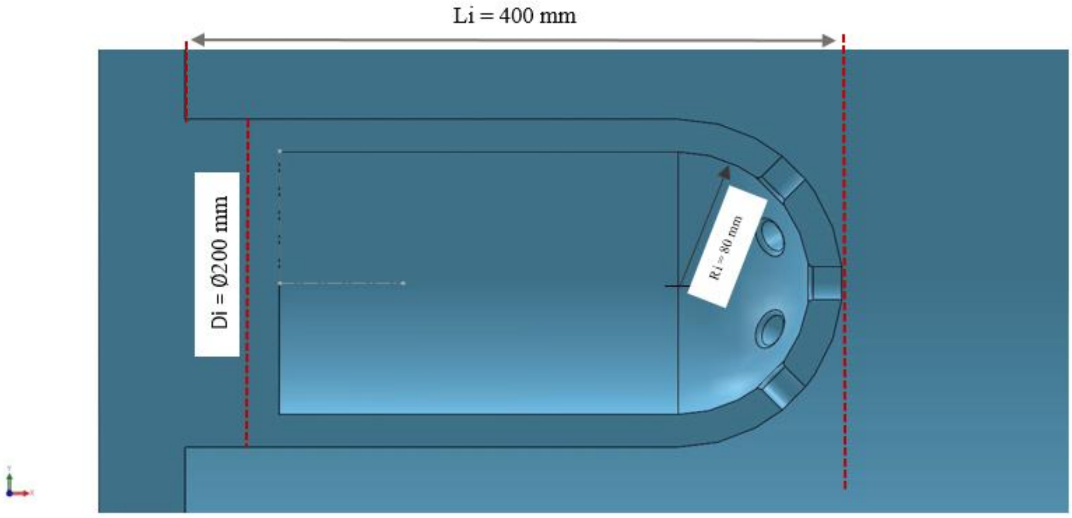


*Figure 3.4.* Geometric features of the pyrogen igniter

The designed pyrogen igniter for this thesis work (see Figure 3.4. Geometric features of the pyrogen igniter) has 400 mm of length (Li) and 200 mm of diameter (Di). Its inner port radius (Ri) is 80 mm. Thus, 20 mm of bulk thickness (200 – 80x2 = 20 mm) is left in order to simulate pyrogen motor case and insulation thicknesses. The geometric features that are not fixed are the parameters related to the nozzle openings: angle, diameter and the total number. These dimensional features are related to the test case matrix of this work and will be mentioned in detail in Section 3.4. However, the total nozzle exit area shared by all test configurations is fixed and its value is 1500 mm$^2$, in order to establish a controlled experiment.

With the port volume of the pyrogen igniter itself, the flow volume of the grand SRM propellant (see Figure 3.5, subtracted geometry from solid body) for exhaust products of pyrogen igniter, and filling that particular volume of SRM, becomes exactly 600 liters.

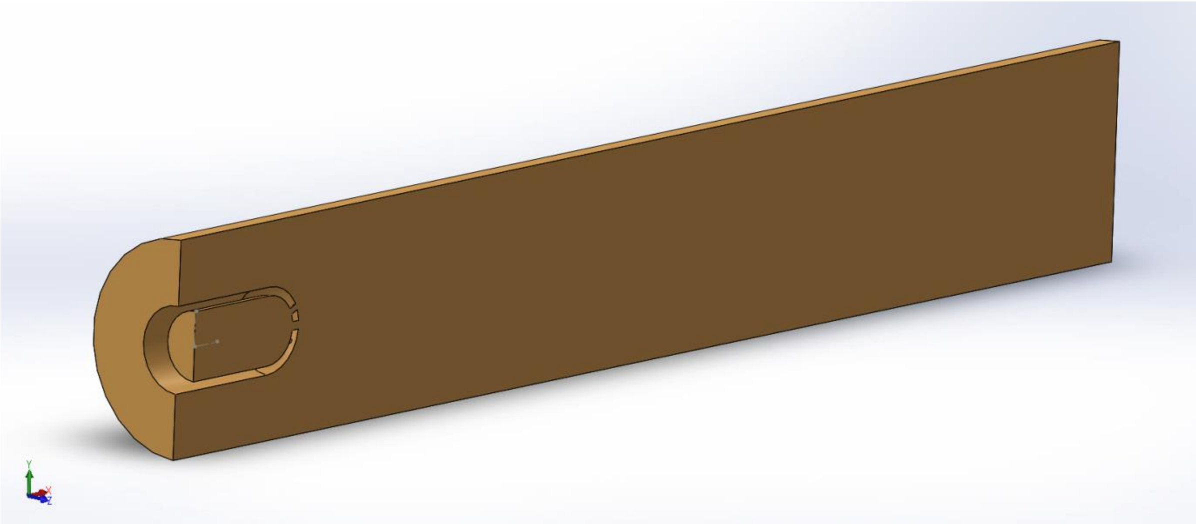

*Figure 3.5.* The flow volume

Here, port volume value and pyrogen igniter sizes explained above are selected in a generic manner in accordance with the literature. The technological demonstration SRM of VEGA Launcher, Zefiro 16 has approximately 900 liters of port volume; whereas, the older third stage of VEGA Launcher, Zefiro 9 (not 9A, the newer version) has 660 liters of port volume. As seen from Table 1.2, the length of the pyrogen igniters of both Z16 and Z9 is between 500-550 mm, and their diameter changes between 200-260 mm. Both of these igniters have 3-4 kg of propellant having 13-16-star geometry grain and they operate between 1500-2000 psi of working pressure in 0.2-0.5 seconds [3]. Therefore, rather than selecting arbitrary values, a pyrogen igniter having diameter of 200 mm and length of 400 mm, and filling 600 liters of port volume (close to the value of Z9) is selected for the model in this work.

Furthermore, the mass flow rate ejected from pyrogen igniter nozzles to grand SRM propellant port volume, is designed in a generic manner. The pyrogen igniter of Zefiro 9 SRM produces approximately 12 kg/s mass flow rate in less than 100 milliseconds and this flow rate decreases rapidly until it reaches almost zero in 500 milliseconds. This type of ballistic behavior of a SRM is called regressive burning: producing its maximum pressure, force, mass flow rate etc. in the launching stage and then reaching to burnout stages rapidly (see Figure 1.10 for this type of SRM behavior). Therefore, as can be seen in Figure 3.6, a pyrogen igniter showing a regressive ballistic behavior with 10 kg/s maximum value of mass flow rate is constructed for this work.

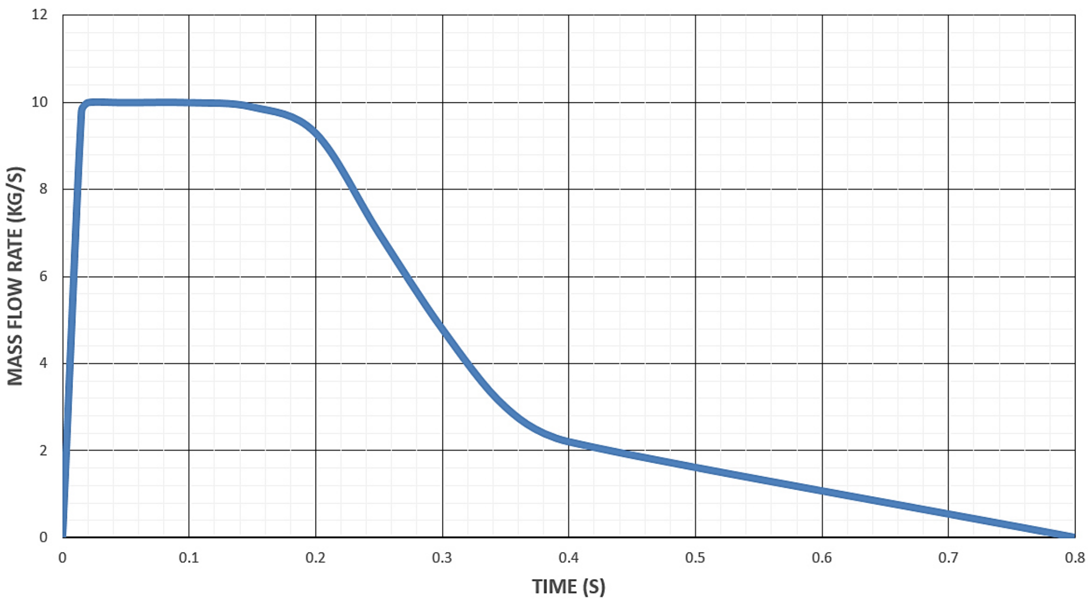


*Figure 3.6.* The ballistic behavior of the pyrogen igniter

### 3.3. Boundary and Initial Conditions

From the geometric point of view, there are two boundary conditions (BC) for the flow volume shown in Figure 3.5: inlet and wall. The visualization of inlet BC is shown in Figure 3.7. There are three red surfaces shown in the figure (modelled via ANSYS-Workbench 2019 Academic Edition): the head-end of the pyrogen igniter and two half-cylindrical sidewalls. On the other hand, the snapshot of the wall BC can be seen in Figure 3.8.

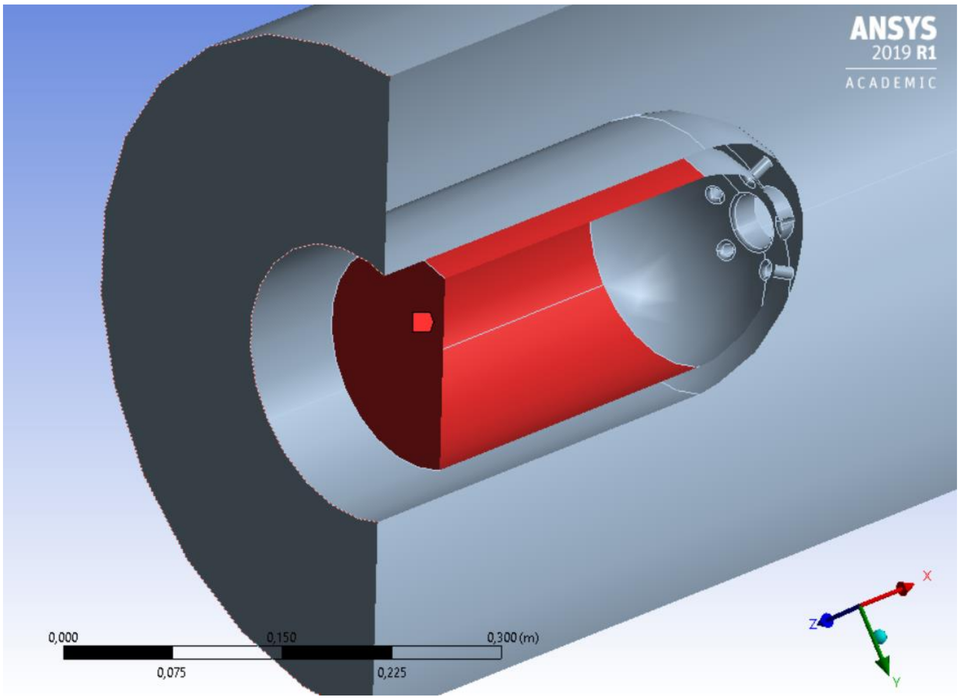


*Figure 3.7.* Inlet boundary conditions

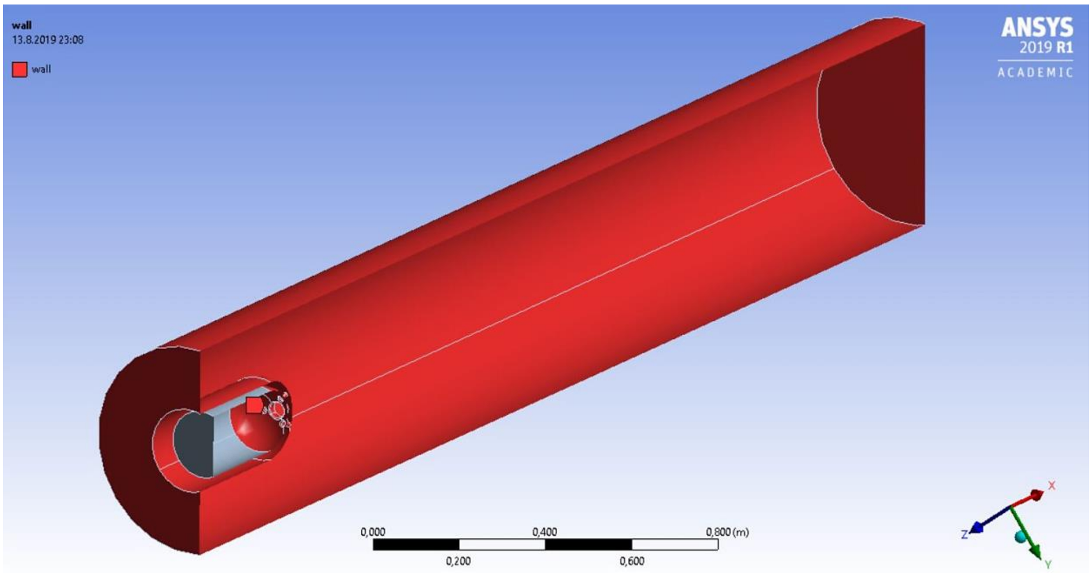


*Figure 3.8.* Wall boundary conditions

From ballistic performance point of view, mass flow rate data shown in Figure 3.6 enters into the flow volume from the inlet faces shown in Figure 3.7. Initially, the flow volume is filled only with nitrogen ($N_2$) gas at room conditions: 300 K and 100 kPa. As a side note, before static firings or flight missions, solid rocket motors are pressurized between 100-150 kPa with nitrogen, helium or their mixture gases in order to carry out gas leakage test as a common practice. Their temperature conditioning however, differs according to the aim of the mission. Therefore, selecting 300 K temperature and 100 kPa pressure as initial conditions is suitable for this system. What is more, the $N_2$ gas filling the flow volume is assumed to be in thermal, kinetic and chemical equilibrium with the system, so all the velocity vectors (in x,y and z directions) are zero at the beginning.

Starting from t = 0 seconds, the mass flow rate of the pyrogen igniter reaches its peak value of 10 kg/s in 15 milliseconds (see Figure 3.6). The combustion products of the pyrogen igniter first start to fill the port volume of pyrogen igniter itself and then, they are ejaculated into the port volume of the grand SRM in at least sonic speed levels (Mach number = 1) via the various configuration of nozzle openings. Combustion products are assumed to be at 3500 K and 6 MPa, as initial conditions in order to simulate the hot gas flow. Calculated mass fractions of combustion products that enter the flow due to pyrogen burning are as follows [22]: 0.33% $CH_2O_{(g)}$, 0.30% $HCl_{(g)}$, 0.08% $H_2O_{(g)}$, 0.12% $CO_{2(g)}$, and the rest is $N_{2(g)}$. Here, at t=0 initial time step, the mass fractions of all these combustion products are zero. They start to increase and fill the port volume with the start of the solver; in other words, the ignition of pyrogen igniter.

As the last notable concept to be mentioned, these products do not include Aluminum (Al) or Alumina ($Al_2O_3$). In common practice, most of the SRMs and their pyrogen igniters that are used in ballistic missile systems or space missions use aluminized propellants as fuel. The reason of this phenomena is that Al is a highly energetic material that increases the net force gained from the combustion of unit weight of propellant compared to non-aluminized propellants. However, the existence of Al or

$Al_2O_3$ in the flow, which are solid and/or liquid particles, converts single phase gaseous flow into two or three phase mixture flows. Therefore, in this thesis work, for numerical simplicity reasons, the propellant of the pyrogen igniter is assumed not to include aluminum; and also, the gas mixture that fills the port volume of both pyrogen and the grand SRM is assumed to be only in gaseous state.

## 3.4. Test Matrix

In order to compare the pressurization of the same grand SRM system, three nozzle parameters namely, number of the radial nozzles, angle of the radial nozzles, radial mass flow rate (ejaculated in to the grand SRM port volume) and their combined effects are tested. As mentioned in Section 3.2. the nozzle exit area for all pyrogen igniter simulation cases is fixed and its value is 1500 $mm^2$. All configurations have one axial nozzle which creates the axial flow rate coming out of the pyrogen. Radial flow rate on the other hand, is controlled by the diameter of radial nozzles since mass flow rate ejected out of pyrogen igniter is directly proportional to the exit area of the nozzles. The related parameters are shown in Table 3.1.

Table 3.1. *Nozzle Parameters*

| | |
|---|---|
| **Radial Nozzle Angle (˚)** | 25, 50, 75 |
| **Radial Nozzle Number (#)** | 3, 5, 7 |
| ***Radial Mass Flow Rate (%)** | 20, 50, 80 |

**% = (Radial Mass Flow Rate / Total Mass Flow Rate) x 100**

These parameters shown in Table 3.1, are selected in such manner that it should not conflict the geometric boundaries of the pyrogen igniter explained in Section 3.2; that is, the test subject. For example, radial nozzle angle of 75° simulates the condition where radial nozzles are too far apart from the axial nozzle and the longitudinal axis of the pyrogen igniter. The value indeed, could be 80° or 85° or even 90°. However, the more the angle is increased, the more the nozzle openings get away from the aft dome of the pyrogen igniter and start to approach to the pyrogen motor case. Therefore, maximum angle of 75° is suitable for test purposes. In addition, the minimum nozzle angle degree is selected as 25° in the parameter chart. If the value is decreased further, radial nozzles and axial nozzle start to coalesce and this creates abrupt shapes of nozzles. The change of the nozzle configurations with respect to the angle of the radial nozzles can be seen in sample configurations in Figure 3.9. The full radii data is available in Table 3.2.

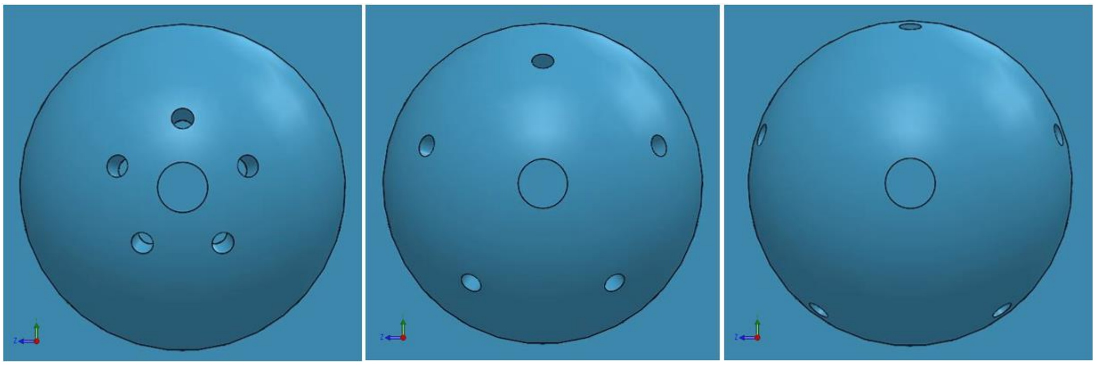

(a) (b) (c)

*Figure 3.9.* The change of the nozzle configurations with respect to the angle of the radial nozzles: 25° (a), 50° (b) and 75° (c)

The other parameter to be mentioned is the number of the radial nozzles. As seen in Table 2, the comparison of the pyrogen igniters in the literature, the number of radial nozzles differ from three to six from system to system. In this work, the minimum value is selected as three. The second value is five, and the last value is seven rather than six in order to attain the symmetry between the minimum and the maximum, with the number five in the middle. The change of the nozzle configurations with respect to the number of the radial nozzles can be seen in sample configurations in Figure 3.10.

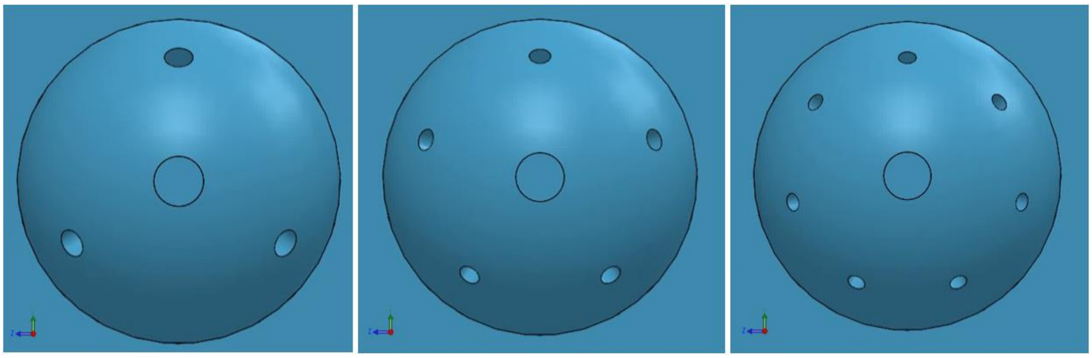

(a) (b) (c)

*Figure 3.10.* The change of the nozzle configurations with respect to the number of the radial nozzles: 3 (a), 5 (b) and 7 (c)

As the last parameter, 20% radial mass flow rates represent the situations where axial flow coming out of the pyrogen igniter is dominant; whereas, 80% represents the radially dominant flow conditions. That is why the existence of the axial nozzle helps to create the test matrix in order to compare the radial nozzle effects. If the pyrogen had only an axial nozzle or only radial nozzles, these situations would create singularities in the test matrix. 100% axial flow means no radial nozzles exist in the system; thus, parameters like radial nozzle angle or radial nozzle number become meaningless. With the same approach, if there was no axial nozzle (100% radial flow), only radial nozzle number and angle parameters would become meaningful. However, in order to observe the behavior of these extreme cases and compare with the ones in the test matrix (and not to miss any information), two more cases are constituted, namely full axial and full radial configurations, and solved separately. The change of the nozzle configurations with respect to the nozzle radius (i.e., mass flow rate) can be seen in sample configurations in Figure 3.11. The nozzle configurations of the two extreme cases can be seen in Figure 3.12.

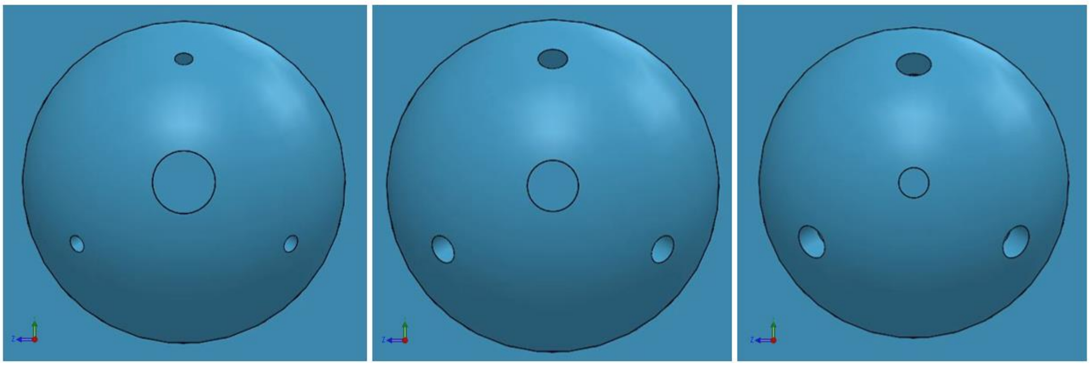

(a) (b) (c)

*Figure 3.11.* The change of the nozzle configurations with respect to the nozzle radius for 20% radial mass flow rate (a), for 50% (b) and for 80% (c)

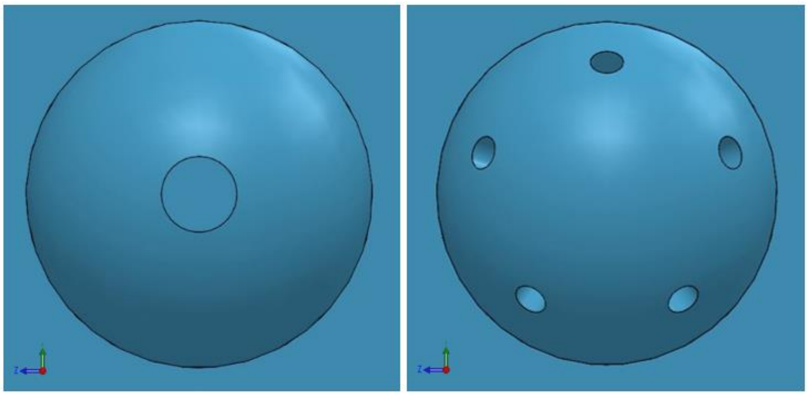

(a) (b)

*Figure 3.12.* The nozzle configurations of the two extreme cases: full axial (a) and full radial (b)

Since there are three different parameters each having three sub-levels in Table 3.1, a total of 27 test case is formed for this work. With the addition of two extreme cases the number of geometries that are tested is increased to 29. As a side note regarding the extreme cases, there is only one case for full axial pyrogen igniter condition for sure; since there is only one axial nozzle. However, for full radial flow conditions, as mentioned previously, radial nozzle angle and radial nozzle number are also meaningful parameters. Thus, each having three sub-levels, a number of $3^2 = 9$ test cases form. However, every comparison that could be made with full radial configurations can also be made with configurations having axial nozzles; therefore, eight of full radial flow configurations are omitted and only one of them is analyzed for demonstration purposes.

As mentioned earlier in this section, the exit area of all pyrogen igniters is 1500 mm$^2$. First, this area is divided between radial and axial flow regimes. For example, if the radial flow is 20%; then, a total 300 mm$^2$ radial nozzle area is required for radial nozzles. That is because as mentioned in Chapter 1, in rocket motor physics the mass flow rate is directly proportional to the exit area of the nozzle. The remaining 1200 mm$^2$ is for axial flow and determines the axial nozzle radius ($r_{axial} = \sqrt{1200/\pi}$ = 19.54 mm). Then, according to the number of the radial nozzles, the radial nozzle area is again divided evenly. Let's say the number of radial nozzles is five, then exit area of one radial nozzle is 300/5 = 60 mm$^2$. After that, the only job is to find out the radius of individual nozzle ($r_{radial} = \sqrt{50/\pi}$ = 4.37 mm).

This procedure is made for all nine combinations for one angle of radial nozzles (for example 25°) and geometric parameters shown in Table 3.2 are obtained. The obtained radius values are the same for 50° and 75°; therefore, three exactly same matrices shown in Table 3.2 and a total of 27 cases have been formed.

These calculations are all made with the assumption that each nozzle type used in the system, whether axial or radial, is cylindrical. They are not converging-diverging type of nozzles because as a common practice in both pyrotechnic and pyrogen systems, the exhaust products are opted to leave the pyrogen in sonic conditions. They reach supersonic conditions with the sudden expansion in the large flow volume but with this way the effect is kept at a minimum. If the pyrogen jets leave the nozzles in supersonic conditions, in high speeds with high Mach numbers, they might damage the propellant surface of the grand SRM, which might increase the burn area of the SRM in an undesired manner.

Table 3.2. *The Test Matrix for numerical simulations, for 25° radial nozzle angle (The parameters are exactly the same for 50° and 75° angles, as well).*

| ***Radial Nozzle Number (#) vs. Radial Mass Flow Rate (%)*** | | **3** | **5** | **7** |
|---|---|---|---|---|
| ***20 %*** | **Case #** | **1** | **2** | **3** |
| | $r_{radial}$ **(mm)** | 5.64 | 4.37 | 3.69 |
| | $r_{axial}$ **(mm)** | 19.54 | 19.54 | 19.54 |
| ***50 %*** | **Case #** | **4** | **5** | **6** |
| | $r_{radial}$ **(mm)** | 8.92 | 6.91 | 5.84 |
| | $r_{axial}$ **(mm)** | 15.45 | 15.45 | 15.45 |
| ***80 %*** | **Case #** | **7** | **8** | **9** |
| | $r_{radial}$ **(mm)** | 11.28 | 8.74 | 7.39 |
| | $r_{axial}$ **(mm)** | 9.77 | 9.77 | 9.77 |

In the upcoming Section 4, the pressurization behavior of these cases with respect to time is analyzed and the result are compared.

# CHAPTER 4

# RESULTS AND DISCUSSION

## 4.1. The Methodology and Mesh Independency

In this Section, all of the test cases are analyzed in an exhaustive manner. In the beginning, an example case is selected, the Case #5 shown in Table 3.2 for more detailed analysis. This selected case owns a pyrogen igniter with 1 axial and 5 radial nozzles. The angle of the nozzles of this sample pyrogen igniter with respect to the longitudinal axis of igniter itself is 50°. Furthermore, the mass flow rate is divided evenly (50% - 50%) between axial and radial flows. This case is suitable to be investigated as a sample case because it is in the middle point of all of the test matrix. The parameters that are analyzed are pressure and Mach number behaviors in the longitudinal axis of the grand SRM and pressure behavior on the SRM propellant surface, with respect to time. Also, visual images of the pressure and Mach numbers and additionally the static temperature of the combustion products in the flow volume is demonstrated. Finally, the distributions of these parameters that have been mentioned are interpreted in two cross-sectional areas of the flow volume: the exit of pyrogen and the place where pyrogen exhaust jets hit the SRM propellant surface.

Then, all of the test cases (except extreme ones mentioned in Section 3.4) are analyzed. The investigated parameters in this particular work are pressure and Mach number behaviors in the longitudinal axis of the grand SRM and pressure behavior on the SRM propellant surface at 20 milliseconds of the simulation. Furthermore, the results obtained (especially on pressure and Mach number basis) in this work are interpreted by referencing the outcomes of the doctoral thesis of Stefano Zaghi, 'SRM Igniter Jet Simulation, Multidimensional Unsteady Gasdynamics' which is one of the most important reference guides of this work [3].

These solved cases are compared and discussed; as well as, the dominant factors in the pressurization of the grand SRM with respect to the different pyrogen configurations are pointed out from a design of experiment point of view.

After that, two extreme cases having fully axial and fully radial pyrogen flows are analyzed and compared with previous test cases. Also, additional discussion and interpretation is made for these cases.

But first, one of the most important parts to be urged upon in this chapter is the mesh independency issue. As it will become clear in Section 4.3, the critical domain that is investigated while comparing the test cases is the propellant surface of the grand SRM in the flow domain. The compared parameter is the pressure on those surfaces. For the mesh independency study, the case having a pyrogen igniter with 75° radial nozzle angle, 3 radial nozzles and 80% radial mass flow rate is selected.

In all 29 test cases (27 from test matrix and 2 extreme cases), unstructured tetrahedral meshing is used with element size of 0.1 m since the flow volume is too large (600 liters). Overall, the statistics of meshing are formed of 130.000-140.000 nodes and around 700.000 elements. Same number of elements tried to be kept for all test cases via changing the growth rate sizing between 1.07 and 1.09 and keeping maximum size at 0.15 m.

The mesh structure of the mentioned test case can be seen in Figure 4.1 both in general and detailed views. Obviously, the meshing is denser in the nozzle parts of the pyrogen igniter, for the characteristics of the flow changes in these parts as seen in Mach number illustrations in this chapter. In order to catch the shock formations and rarefactions parts before, middle and after of nozzle openings, meshing frequency is increased.

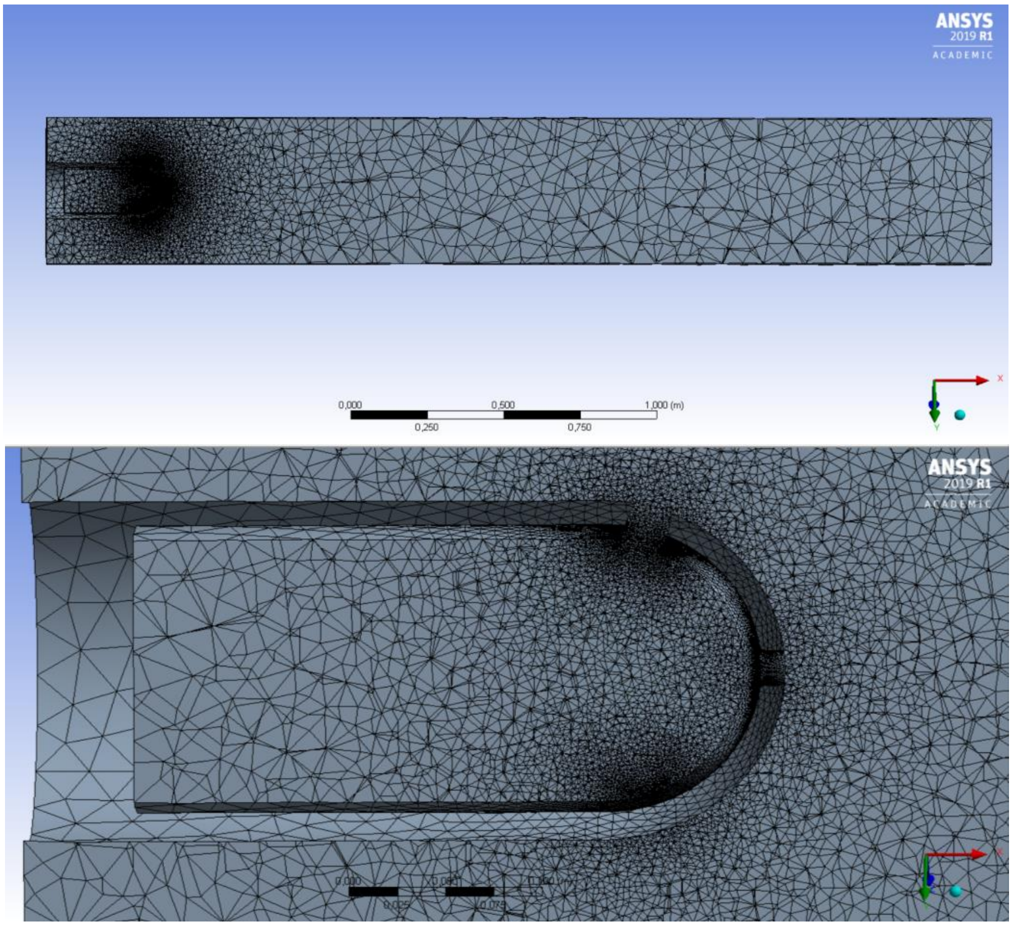


(a)

(b)

Figure 4.1. General (a) and detailed (b) front views of mesh structure of test Case #7 in Table 3.2 having 75° of nozzle angle

For the mesh independency study, same case geometry is solved with 350.000, and 1.400.000 mesh elements in addition to standard 700.000 element number. The solver lasted for 15 milliseconds, which is an adequate time duration in order to gather information about the mesh independency. Pressure variations on the propellant surface of the SRM for each different mesh scenario can be observed in Figure 4.2.

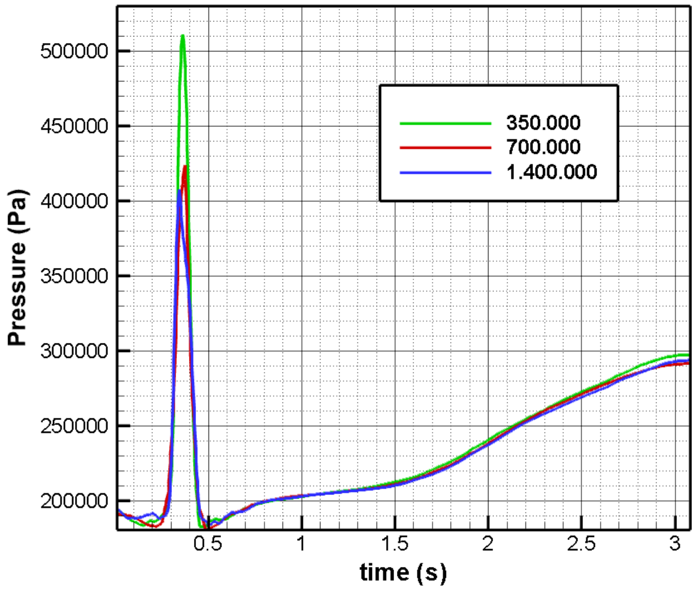


Figure 4.2. Pressure variations on the propellant surface of the grand SRM for each mesh-case scenario

When Figure 4.2 is analyzed, it can be seen that the mesh-case having least number elements has an overshoot in the peak pressure zone compared to the ones having finer meshes. The error, in terms of pressure, is 3.66% for the case having 700.000 elements compared to the finest mesh-case scenario; whereas, it is 24.40% for the case utilizing 350.000 elements.

However, the computational time required for solving the meshing scenario having 1.400.000 elements is approximately 170 hours by utilizing a 32-core processor using the fully coupled solver. By using the same settings, the time required for the scenario having 700.000 elements is 70 hours; whereas, it is 60 hours for the scenario having 350.00 elements.

Therefore, since the deviation from the finest mesh-case scenario is negligible and the computational time advantage is significant, all test cases are opted to have 700.000 elements in this work.

## 4.2. The Sample Test Case

As mentioned in Section 4.1., the simulation case #5 in the test matrix shown in Table 3.2 is explained in this Section. The geometrical features and the boundary and inlet conditions of the SRM flow volume is as explained in Sections 3.2. and 3.3. The nozzle configuration of the pyrogen igniter to be tested has five radial nozzles with 50° nozzle angles. The radial and axial mass flow rates coming out of the pyrogen jets are equal and 50%. Therefore, according to the nozzle radius calculations mentioned in the Section 3.4., the radius of the axial nozzle is 15.45 mm and the radius of one of the similar radial nozzles is 6.91 mm (also see Table 3.2).

### 4.2.1. Investigation of the Pressure Behavior of the Sample Test Case

First of all, the pressure behavior in the longitudinal axis and the propellant surface of the grand SRM is investigated. The longitudinal x-axis and the visual outcomes of the pressurization of the flow volume with the effect of the pyrogen igniter ejecting maximum mass flow rate of 10 kg/s hot combustion products (see Figure 3.6) can be seen in Figure  and the graphical results can be seen in Figure 4.4, in a 10 kPa (room conditions) to 1 MPa pressure range in 22.5 milliseconds with 2.5 milliseconds of time increments.

As can be seen in Figure 4.3 the product gasses start to pressurize the flow volume of the pyrogen igniter in the first milliseconds of ignition. When the jet flow starts to come out of the cylindrical nozzles of the pyrogen igniter, they over expand in the 100 kPa pressurized environment of the SRM flow volume. However, as the time duration increases, the pressure inside the SRM starts to pile up. At about 15 milliseconds pressure waves hit to the rear surface of the SRM and reflect back. This phenomenon increases the pressure more in the posterior time increments (from 15 milliseconds to 22.5 milliseconds). When Figure 4.4 is analyzed, it can be deducted that the pressure increase in the first milliseconds of the firing is lesser when compared with the last milliseconds, because the pressure gap between the time increments increases as the time increases.

The mass flow rate of the pyrogen igniter reaches to its maximum value of 10 kg/s at 15 milliseconds and stabilizes (see Figure 3.6), and the reflection of this stabilization in the flow volume of the grand SRM can also be observed in Figure 4.4. The pressure in the aft part of the SRM (after 2 meters) does not increase aggressively as it increases till to 17.5 milliseconds.

At 22.5 milliseconds, due to the pile up phenomenon, the pressure reaches to its maximum value of 600 kPa at pyrogen igniter exit and 380 kPa in the rest of the flow volume. Since this is the sample case, the time duration is extended to 22.5 milliseconds for more information. However, in the upcoming Section, when all pressurization behavior of the matrix will be investigated, the simulations will last long 20 seconds. Therefore, in Figure 4.5, a detailed view of pressure waves coming out of the pyrogen igniter can be observed at the 20$^{th}$ millisecond time step. The flow coming from all of the nozzle experience shocks and their pressure decreases rapidly, as also can be seen in the graphic in 0.6 m distance (Figure 4.4) with the overexpansion.

This phenomenon is observed in all test cases and also in the literature [3]. In the doctoral thesis of Stefano Zaghi, the behavior is explained as, ‘The jets leaving the pyrogen igniter are obliged to reduce its pressure because these jets exit the simple convergent nozzles in sonic (or more than sonic) speeds with higher pressure value than the pressurizing gas in the SRM chamber. It endures an expansion with strong rarefaction (opposite of compression, a wave or continuous disturbance which decreases the density and pressure of the isentropic flow of a compressible fluid). Then the jet experiences a shockwave and its pressure decreases. This rarefaction and shockwave duo is repeated until pyrogen jets reach the same pressure value with the pressure of the gas in the SRM chamber.’ [3].

The last notable subject to be mentioned about pressurization of the flow volume is the pressure distribution at the SRM propellant surface, which is 245 mm away from the pyrogen igniter according to the geometry. The pressure piling up at the SRM propellant carries a vital importance. The igniter jets should not damage the propellant surface of the SRM because this creates unwanted increase in the burning area of the SRM propellant which is ignited by the pyrogen itself. In Figure 4.6, it can be observed that pressurization shown similar pattern to the pressurization of the longitudinal axis of the SRM but lesser in value. After 22.5 milliseconds of time, the maximum pressure observed on the propellant surface of the SRM is 400 kPa in the average. This value, and also the logarithmic rank of this value (between 100kPa to 1 MPa) is an acceptable and a desirable value. The reason will be much clear when Mach distribution will be investigated in the upcoming Section 4.2.2; however, as a preliminary knowledge, pyrogen jets should not hit the propellant surface of the SRM with very high speeds and should not damage or deform it. The difference of the pressure between the outlet of the nozzles of the pyrogen igniter and the SRM propellant surface can be also analyzed visually in Figure 4.5.

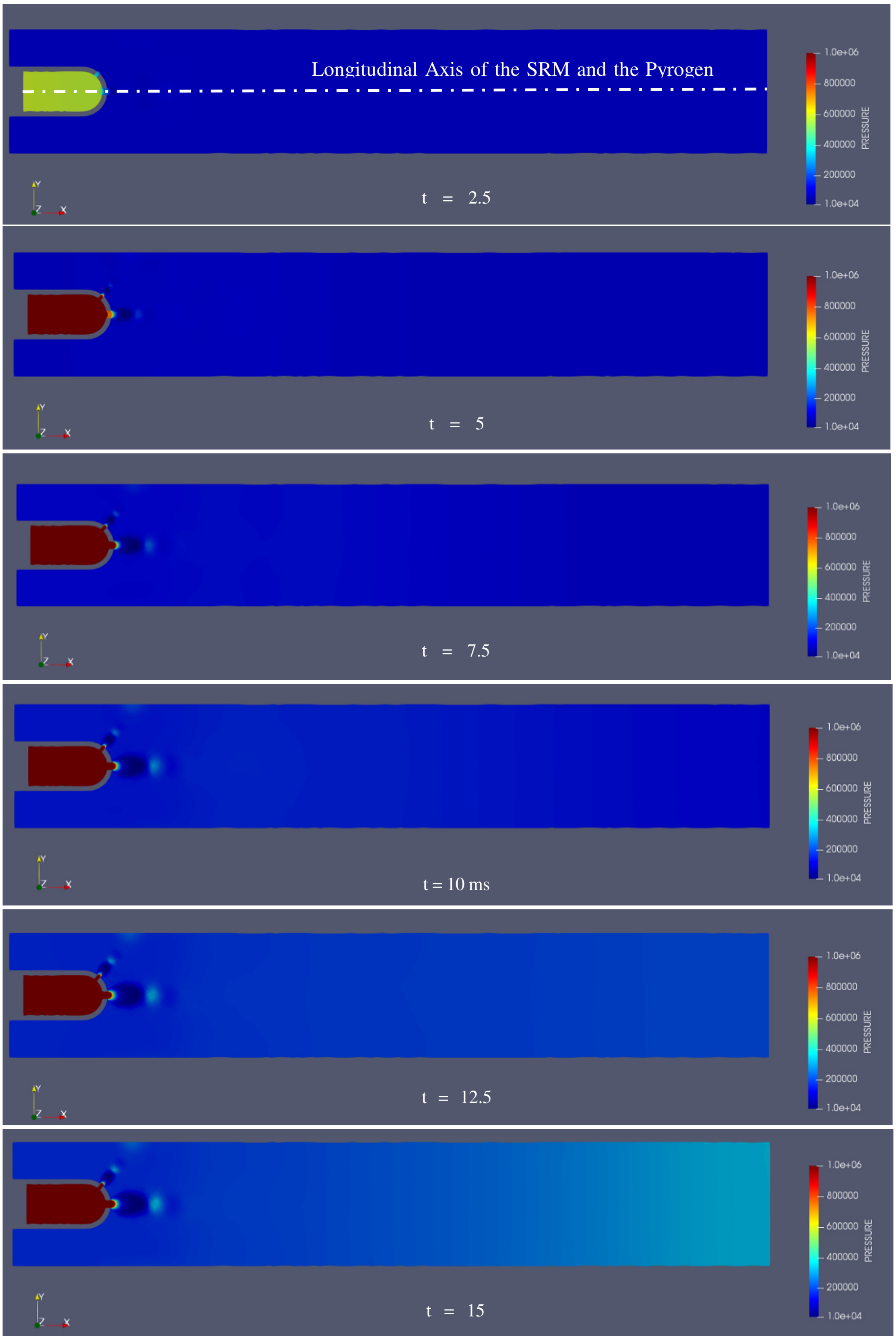


*Figure 4.3.* Pressure distribution of the sample Case # 5 in the SRM flow volume, changing with time

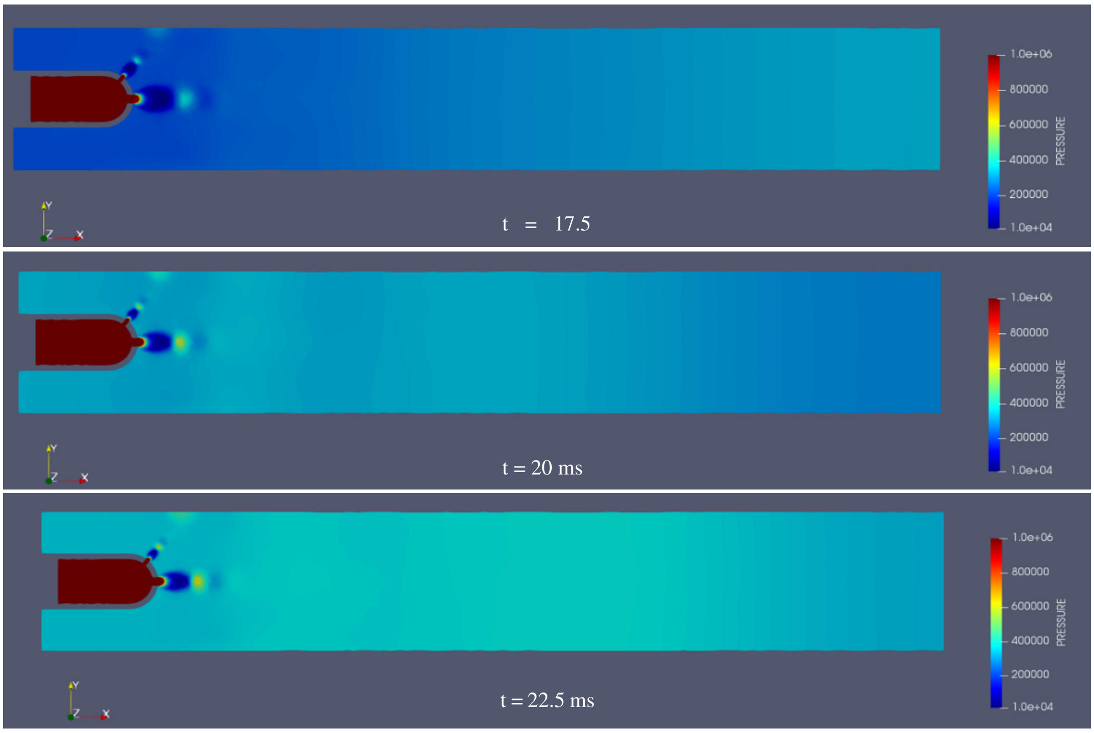


*Figure 4.4.* (Continued)

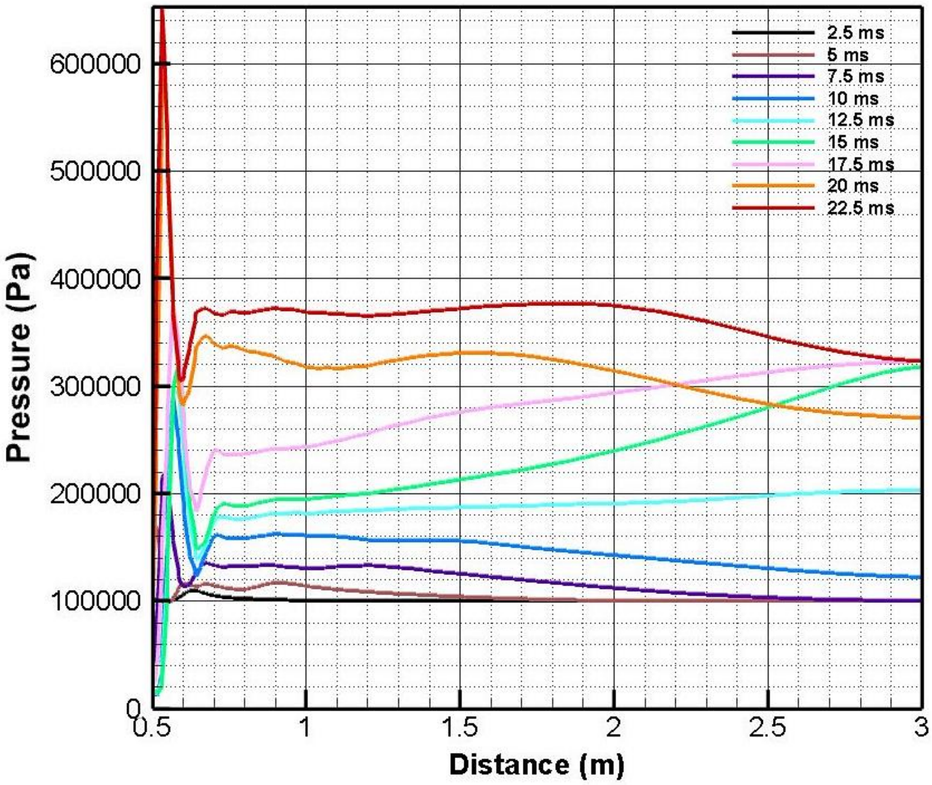


*Figure 4.4.* Graphical representation of the pressure distribution in the longitudinal axis of the SRM of the sample Case # 5

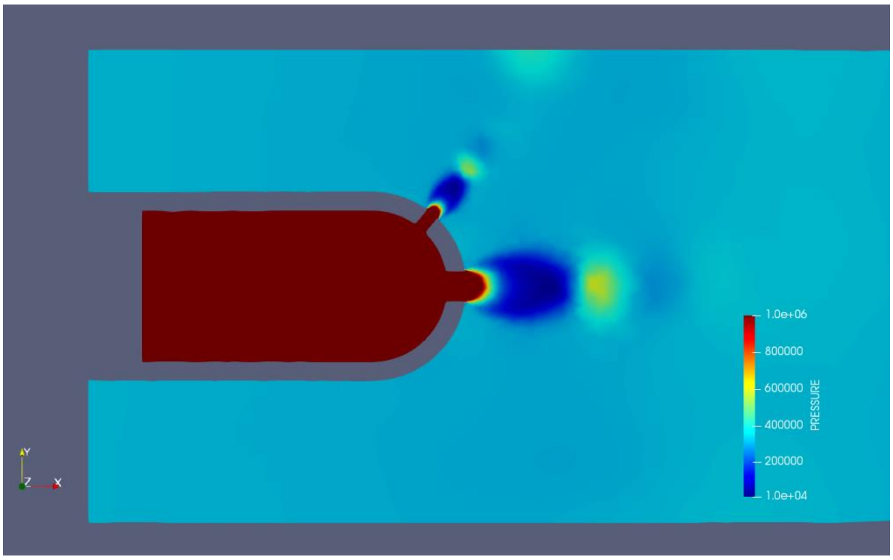


*Figure 4.5.* Detailed view of pressure waves of the sample Case # 5 at 20 milliseconds

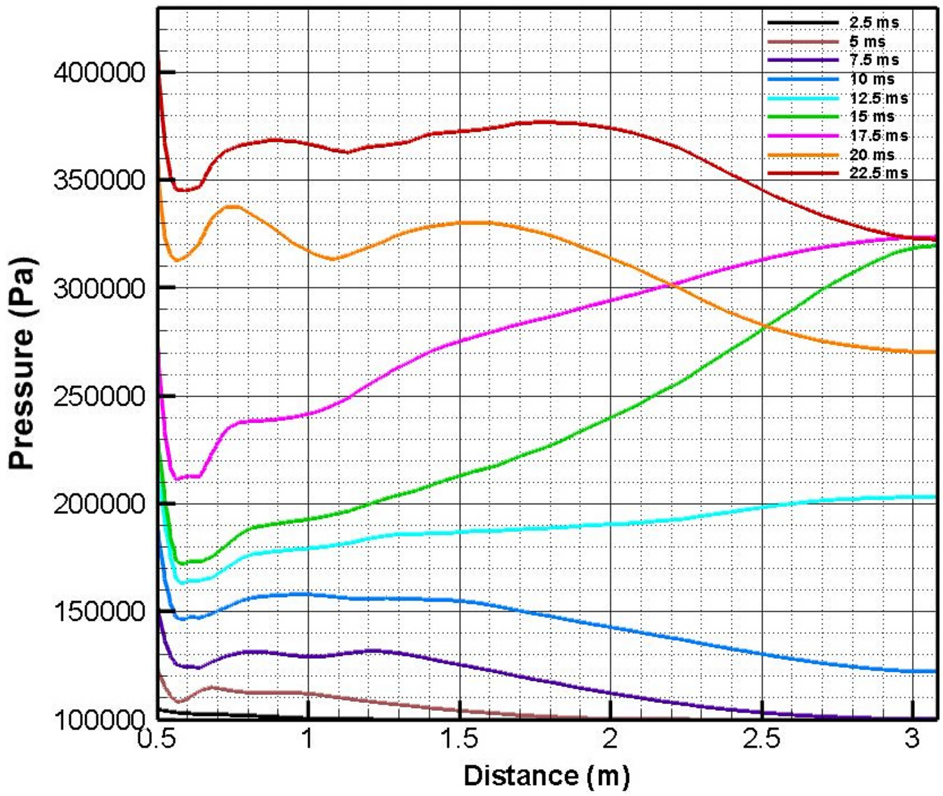


*Figure 4.6.* Graphical representation of the pressure distribution on the propellant surface of the SRM of the sample Case # 5

### 4.2.2. Investigation of the Mach Number Behavior of the Sample Test Case

Secondly, the Mach number behavior in the longitudinal axis of the grand SRM is investigated. The visual results of the Mach number distribution of the flow volume due to the effect of the pyrogen igniter ejecting maximum mass flow rate of 10 kg/s hot combustion products can be seen in Figure 4.7 and the graphical results can be seen in Figure 4.8, in a 0-3.5 Mach range in 22.5 milliseconds with 2.5 milliseconds of time increments.

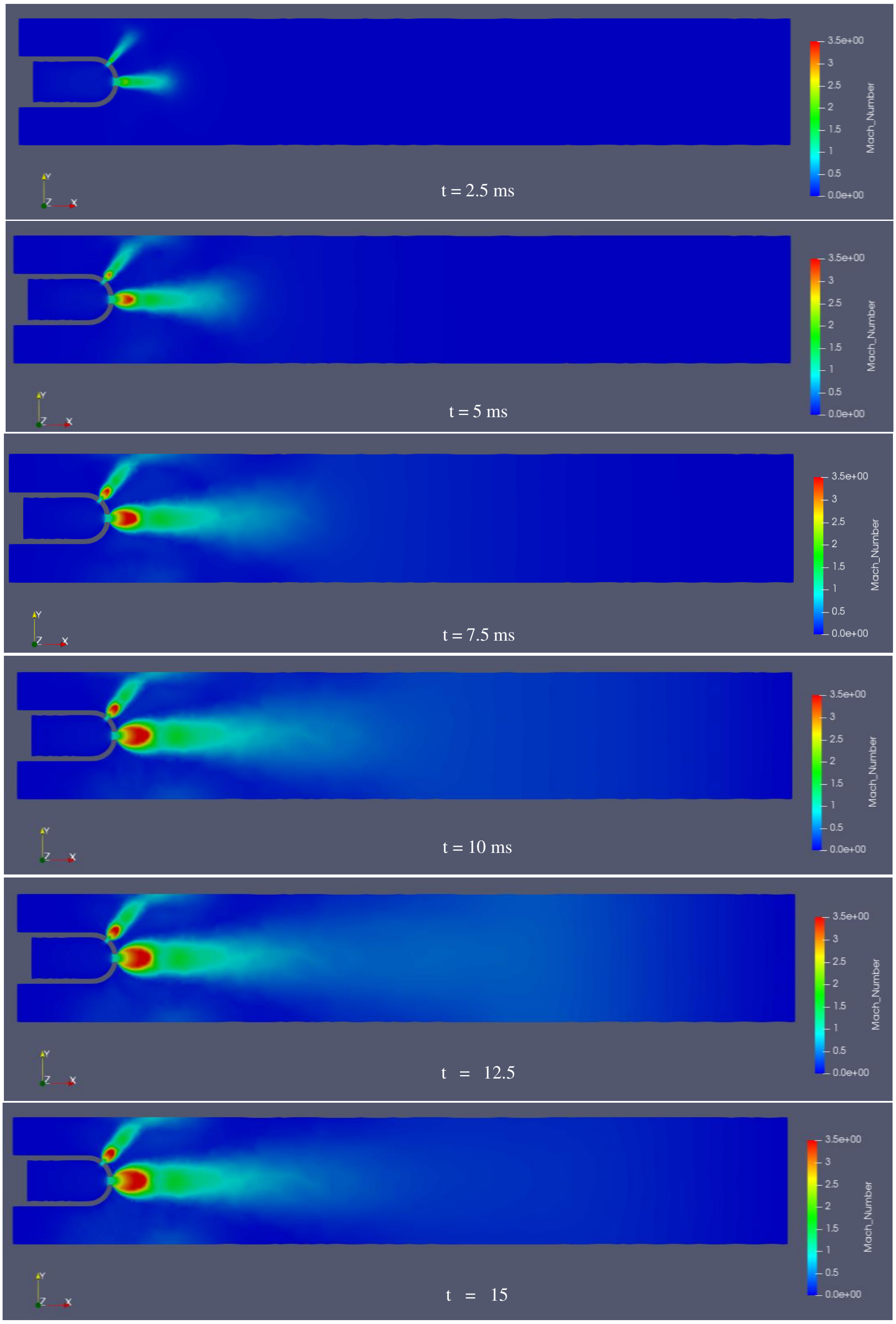


*Figure 4.7.* Mach number distribution of the sample Case # 5 in the SRM flow volume, changing with time

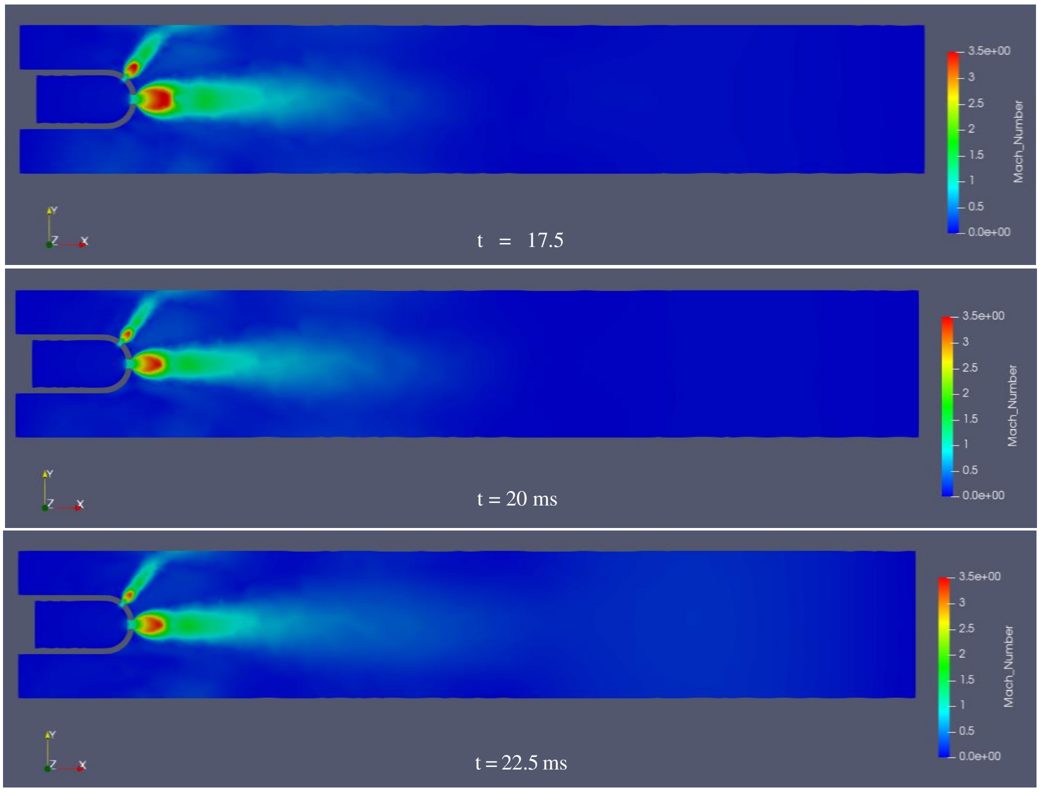


*Figure 4.8.* (Continued)

As can be seen in Figure 4.7 the hot gas combustion products leave the pyrogen igniter in supersonic speed levels in the very first-time steps. The value of Mach number of the jet flow leaving the pyrogen igniter is approximately 2 at 2.5 milliseconds. This value increases with time and jets coming from both axial and radial nozzles tend to grow larger and larger until 15 milliseconds. At 15 milliseconds, the Mach number reaches to 3.5 at its maximum in the location before the flows experience shocks. That time step is the point where pyrogen mass flow rates reaches to its maximum value and stabilizes as mentioned before (see Figure 3.6). After occurring shocks, Mach number decreases drastically, from 3.5 to 2 and from 2 to transonic level with the continuation of the flow (see color patterns turning from red to yellow to blue in Figure 4.7).

After 15 milliseconds of time duration, with stable burning and ejecting mass flow with no rate of increase, the Mach number at the exit of the pyrogen nozzles tends to decrease. This occurrence can also be observed in graphical outcome, in Figure 4.8. On the contrary to pressure behavior, the maximum Mach number lines are pointed at $15^{th}$ and $17.5^{th}$ milliseconds (light and dark blue lines) not at $22.5^{th}$ milliseconds. The other subject that is different form pressure plots is that, as the distance gets further away from the pyrogen igniter, Mach number in the flow volume decreases rapidly. In pressure plots (Figure 4.4 and Figure 4.6), the values of pressure lines were linear and arithmetically averageable in all time steps. However, scenario changes in Mach plots, they represent regressive behavior. This means, although the pressure waves go back and forth in the SRM flow volume very quickly and pressurize in SRM chamber almost evenly in the majority of the chamber, since the "matter" – exhaust products in this case – travels slower than waves, Mach distribution in any time step in unbalanced in the first milliseconds of the operation of the pyrogen igniter.

Furthermore, a detailed view of Mach number behavior of this simple case can be seen in Figure 4.9. As mentioned in Section 4.2.1. the surface of the SRM propellant experiences a jet flow with transonic speed levels at 22.5 milliseconds. The behavior is also the same at 15 milliseconds, when Mach number shows its largest values. The fact that the pyrogen jets are not hitting to the surface of the SRM propellant in supersonic speed with pressure values in megapascal rank is convenient in design point of view, as also mentioned in the last part of Section 4.2.1.

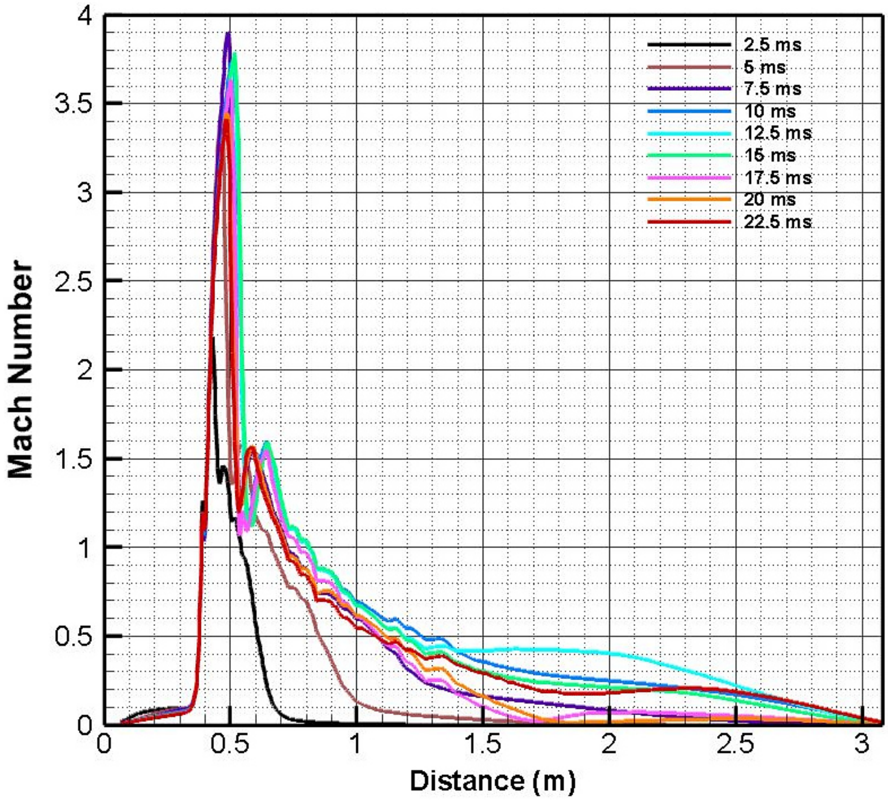


*Figure 4.8.* Graphical representation of Mach number distribution in the longitudinal axis of the SRM of the sample Case # 5

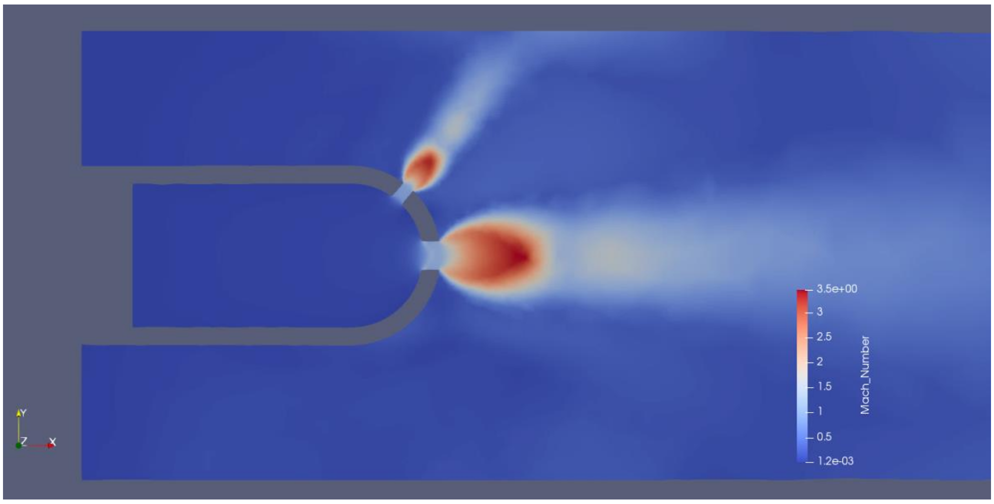


*Figure 4.9.* Detailed view of Mach behavior of the sample Case # 5 at 20 milliseconds

### 4.2.3. Investigation of the Temperature Behavior of the Sample Test Case

Third, the static temperature (the temperature of the fluid moving with a velocity in compressible flows) distribution in the longitudinal axis of the grand SRM is investigated. The visual results of distribution of static temperature outcomes inside the flow volume due to the effect of the same pyrogen igniter can be seen in Figure 4.10. The temperature range starts from 300 K (room conditions) and ends in 3500 K, in 22.5 milliseconds with 2.5 milliseconds of time increments.

The temperature behavior has been found out to be in concordance with the pressure behavior. As time passes, the inside temperature starts to rise and also start to become evenly distributed across the head end of the SRM flow volume, after heating the pyrogen igniter itself in a full manner, up to 3500K. One of the reasons of this phenomena is the existence of evenly distrusted radial nozzles (as it will be come much clear in Section 4.3). It can be clearly concluded that, the temperature distribution will be even in all of the flow volume, not just the head-end part because of two reasons. First, the pyrogen will still operate after 22.5 milliseconds until 200 milliseconds in maximum flow rate conditions, where its regressive behavior will become dominant thereafter. The second reason is that heat transfer, due to both conduction, convection and radiation takes time to establish. The rate of rise in the temperature is not as fast as the rate of rise in the pressure because the fact that pressure waves travels at very high speeds in the SRM chamber; however, eventually, temperature effect will also kick in for the ignition of the propellant of the grand SRM.

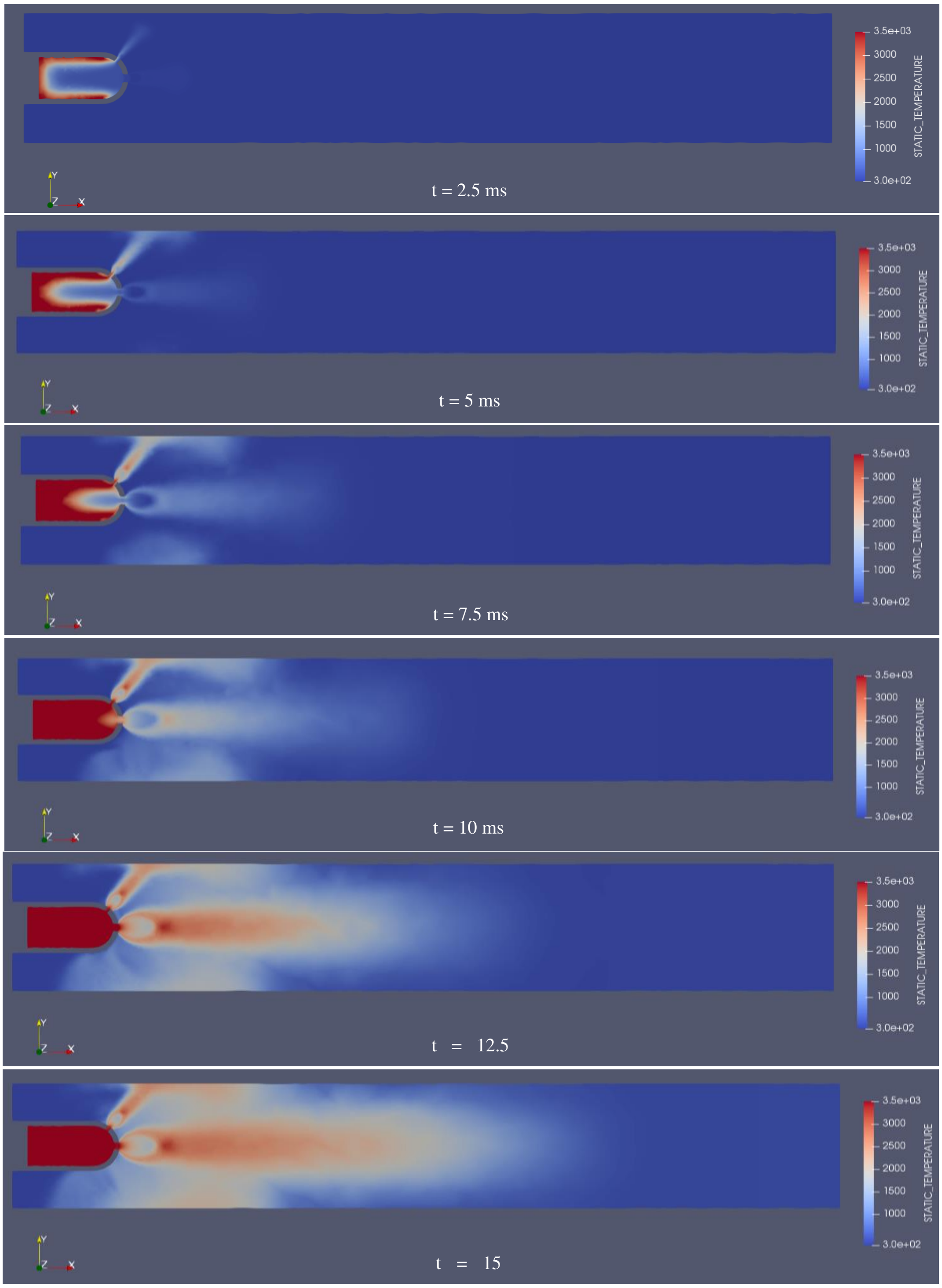


*Figure 4.10.* Temperature distribution of the sample Case # 5 in the SRM flow volume

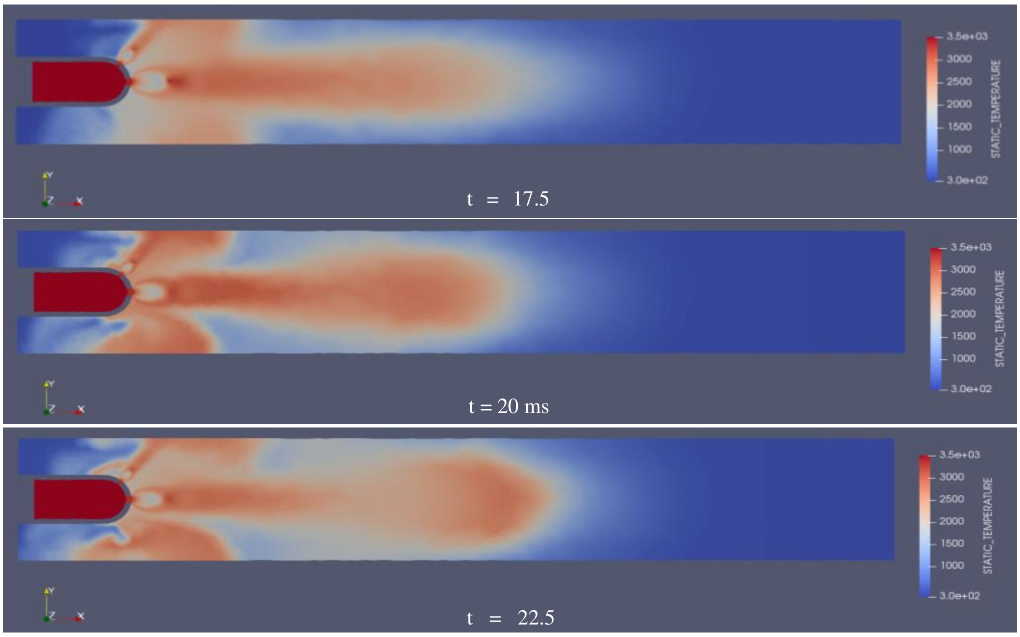


*Figure 4.11.* (Continued)

### 4.2.4. Investigation of the Parameter Behaviors of the Sample Test Case in Cross-Sectional Views

Lastly, the changes of the aforementioned parameters (pressure, Mach number, and static temperature) is investigated in the cross-sectional area of the flow volume. The first cross-section is taken 400 mm away from the head-end of the pyrogen igniter, the section where marks the end of pyrogen igniter's axial nozzle. For better envisage, the picture of the first cross-section place can be analyzed in Figure 4.11. Furthermore, the place where the pyrogen jets of this sample case hit to the propellant surface of the grand SRM is investigated in cross-sectional view. For this particular case, it is located 480 mm from the head-end of the pyrogen igniter; however, when the nozzle angle and the configuration changes, the point where jets hit also change geometrically. The snapshot of this second cross-sectional area can be seen in Figure 4.12. The change of pressure, Mach number, and static temperature in both of these cross-sectional areas can be examined between Figure 4.13 and Figure 4.18.

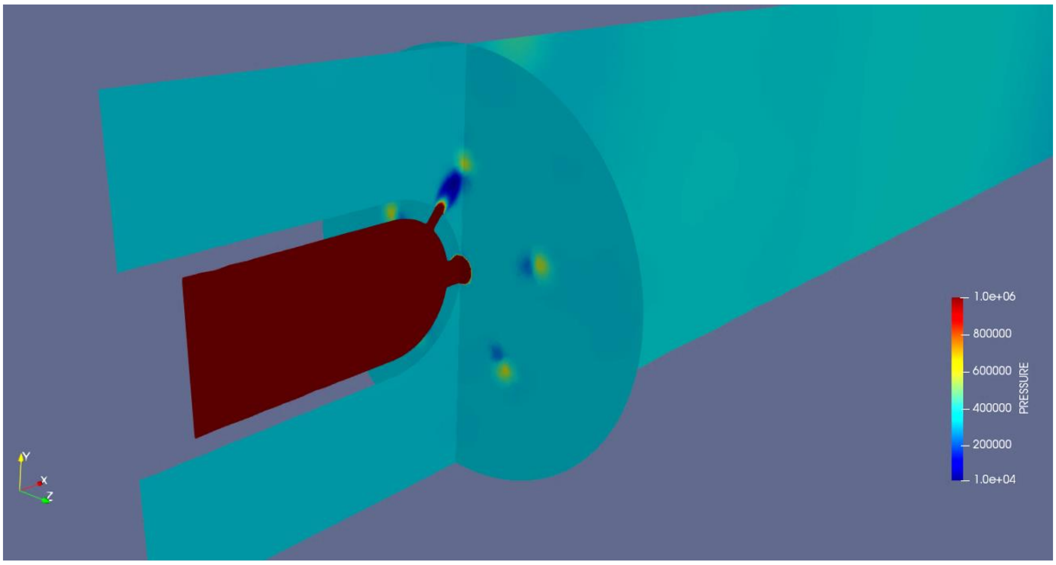


*Figure 4.11.* First cross-sectional view – the exit of the axial nozzle of the pyrogen igniter (at x = 400 mm)

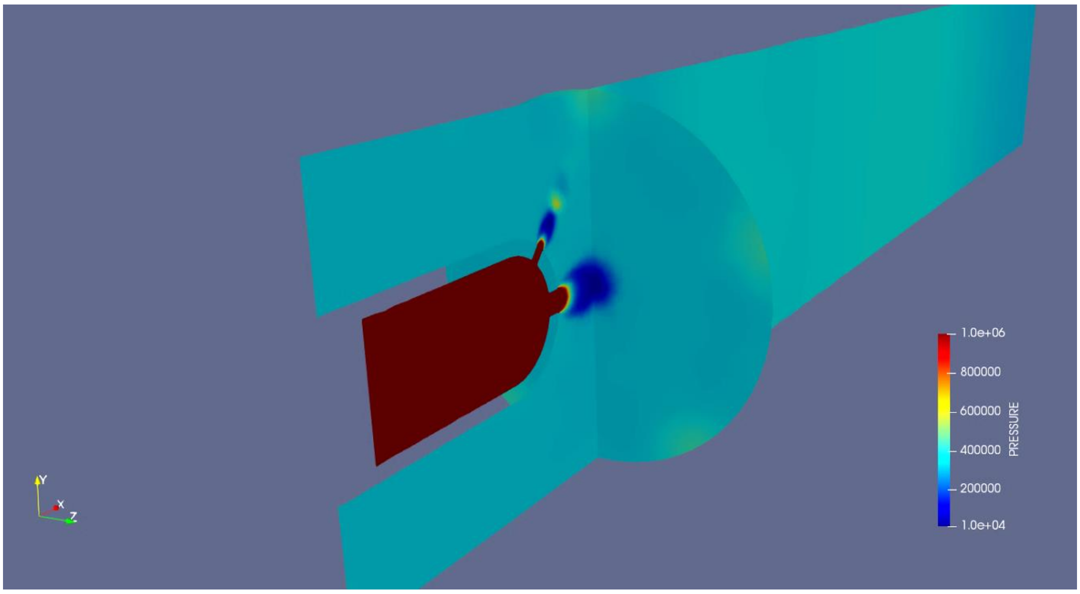


*Figure 4.12.* Second cross-sectional view – the location where pyrogen jets hit to the SRM propellant surface (at x = 480 mm)

Figure 4.13 displays the pressure distribution in the first cross-section with 2.5 milliseconds of time increments. Figure 4.14 displays the Mach number distribution; whereas, Figure 4.15 displays the static temperature distribution, in the first cross-section with the same manner. Figure 4.16, Figure 4.17 and Figure 4.18 are corresponding plots in the second cross-section for the mentioned parameters, respectively. For the first cross-section visuals, the arguments that are mentioned in Sections 4.2.1, 4.2.2 and 4.2.3 are still valid and all discussion made in pressure, Mach number and temperature could be interpreted in the same manner but from a different view.

For the second cross-section visuals, the situation is little bit different. In Figure 4.16 and Figure 4.18 it can be observed that pressure and temperature is distributed almost evenly all over the cross-sectional areas in all time instances, except little portions where the pyrogen jets hit, which is totally different from their corresponding first cross-section visuals. At 22.5$^{th}$ millisecond of the time duration, the pressure value reaches its maximum value of 550 kPa; as well as, the temperature value reaches to its maximum value of 3500 K. In Section 4.3, it will become clear that, the difference between these little portions of highly pressurized and heated local regions are the decisive factors while comparing all of the test cases in terms of ignition transient. Therefore, analyzing the pressure, Mach number and temperature behaviors of the test cases in second cross-sectional area, where the pyrogen jets hit to the propellant surface of the SRM is important.

Moreover, it can be observed in Figure 4.17 that Mach number trend in the second cross-sectional areas is not too much different from the trend observed in first cross-sectional areas. As the time moves on, Mach number in the localized regions where jet flows pass by increases up to certain duration. However, after 17.5$^{th}$ millisecond, it starts to regress as the pyrogen igniter reaches to its maximum stable mass flow rate with zero rate of change. This phenomenon also observed in Section 4.2.2, where the Mach number behavior inside the whole domain was investigated.

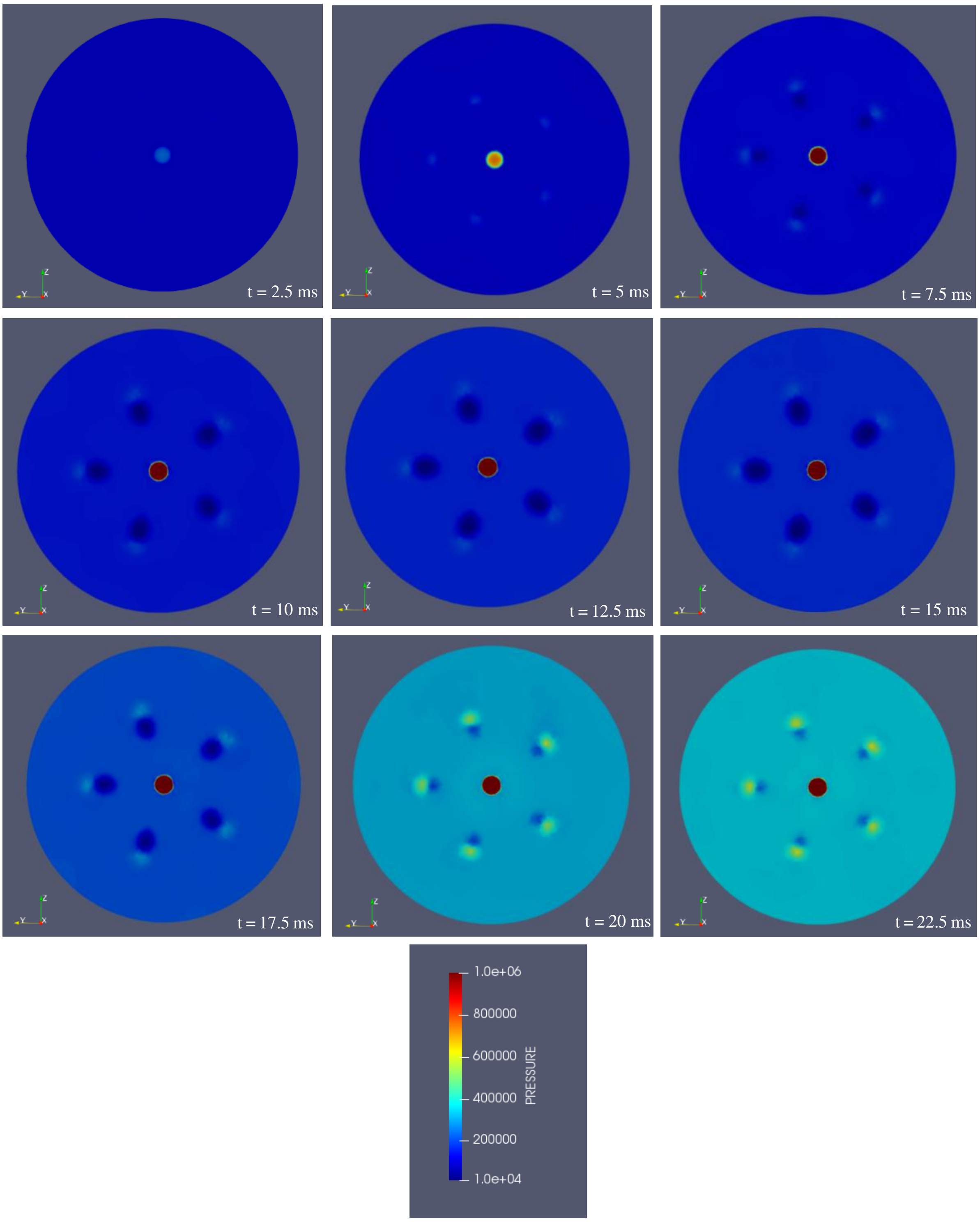


*Figure 4.13.* Pressure [Pa] distribution in the first cross-sectional (at x = 400 mm) view

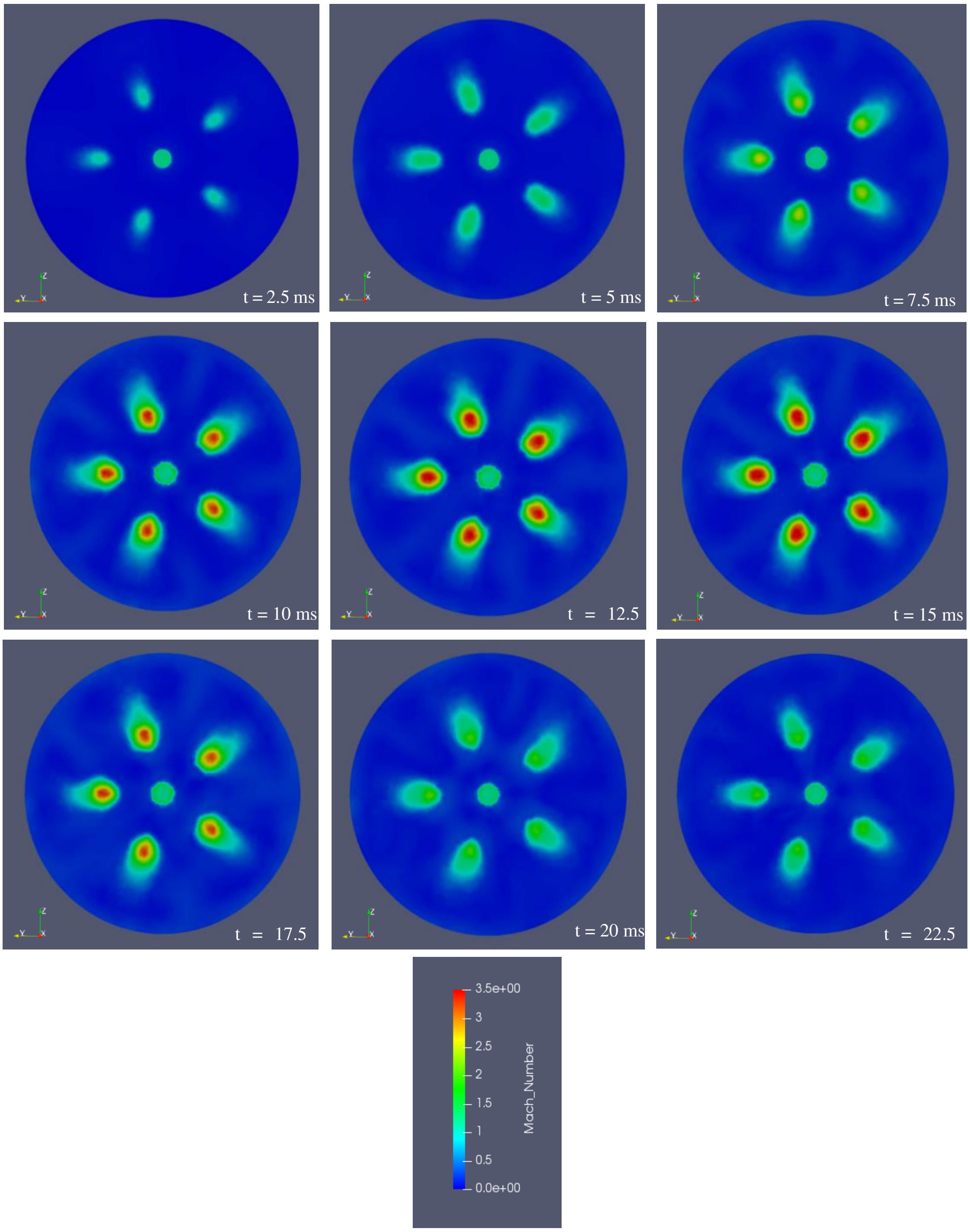


*Figure 4.14.* Mach number distribution in the first cross-sectional (at x = 400 mm) view

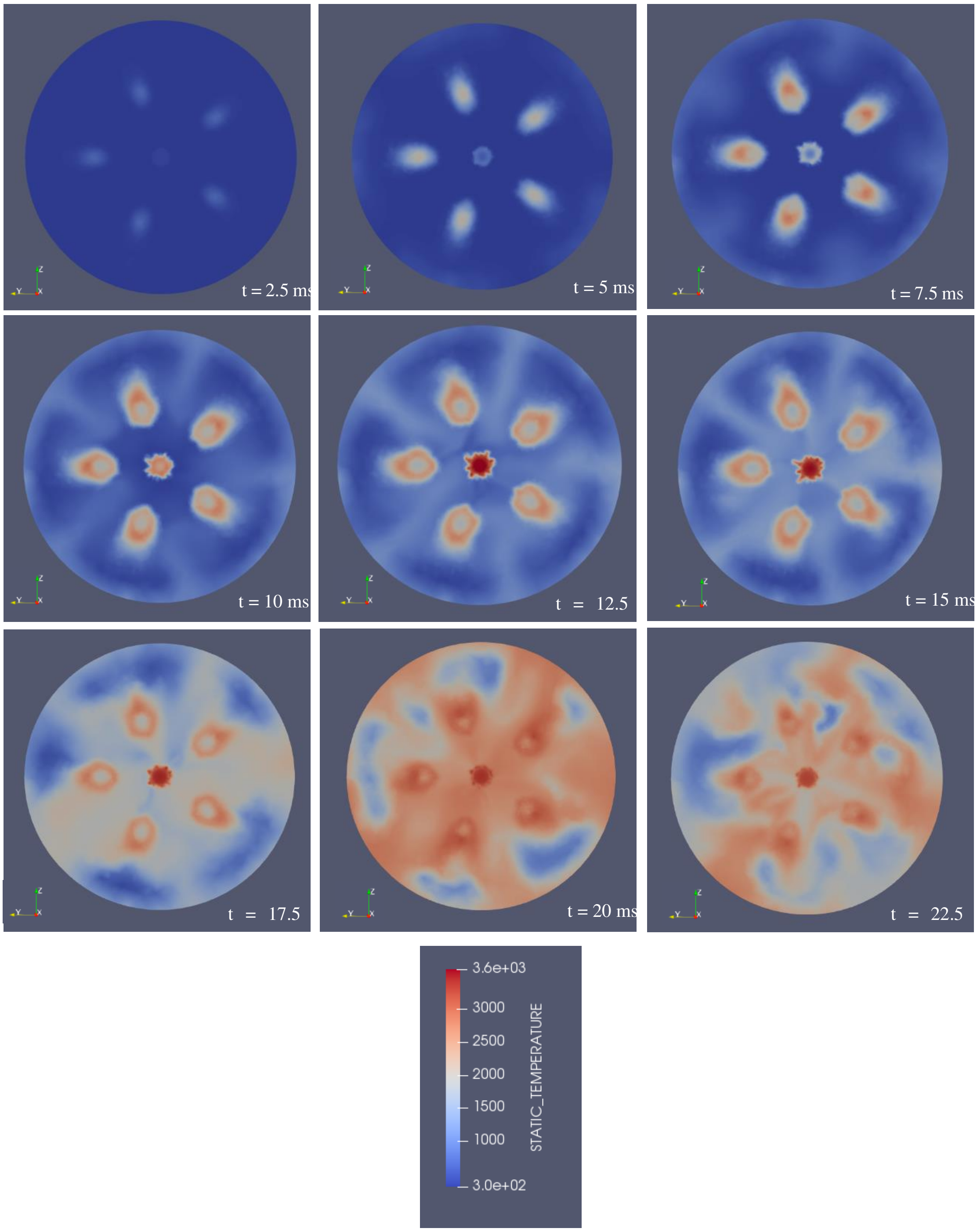


*Figure 4.15.* Static temperature [K] distribution in the first cross-sectional (at x = 400 mm) view

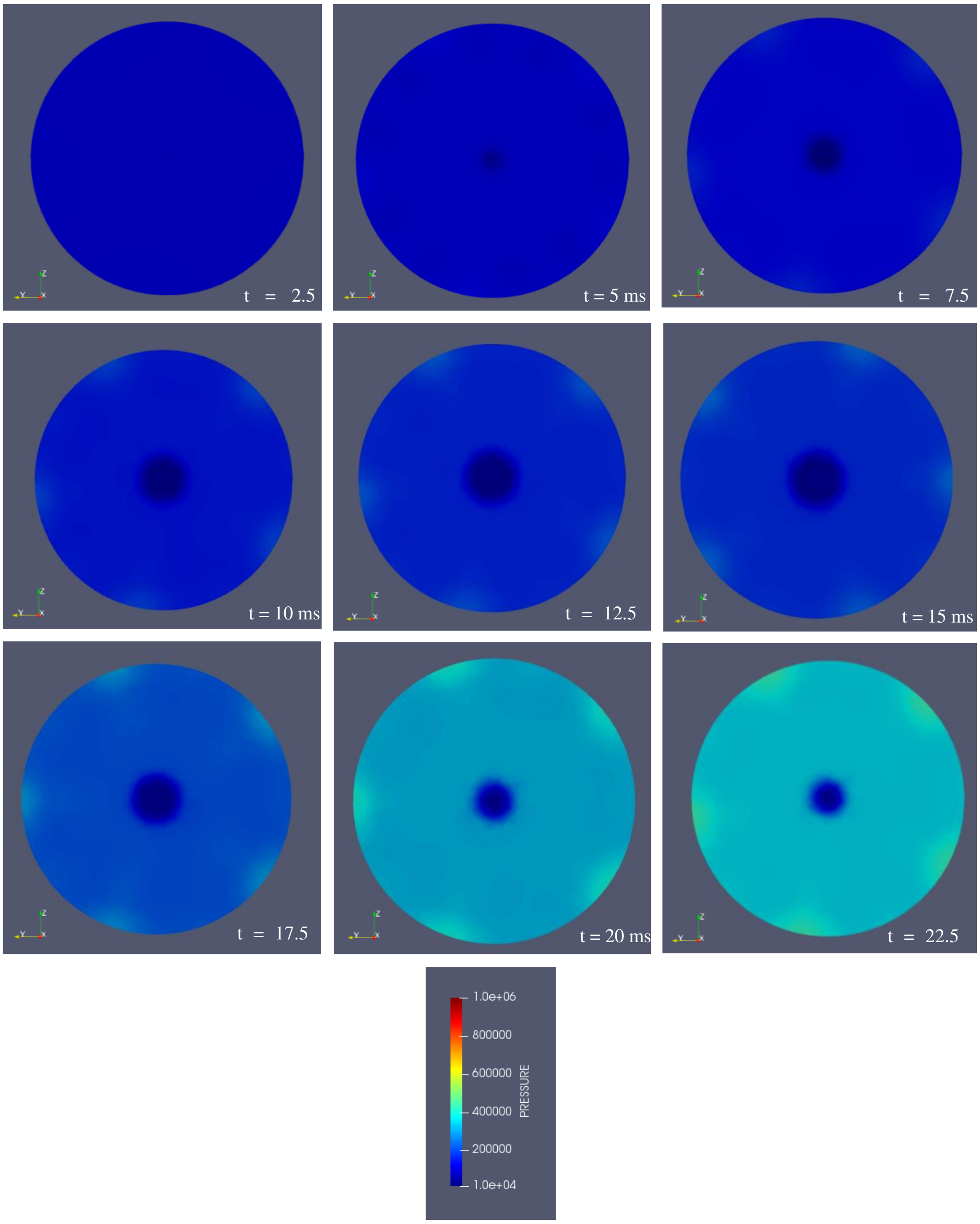


*Figure 4.16.* Pressure [Pa] distribution in the second cross-sectional (at x = 480 mm) view

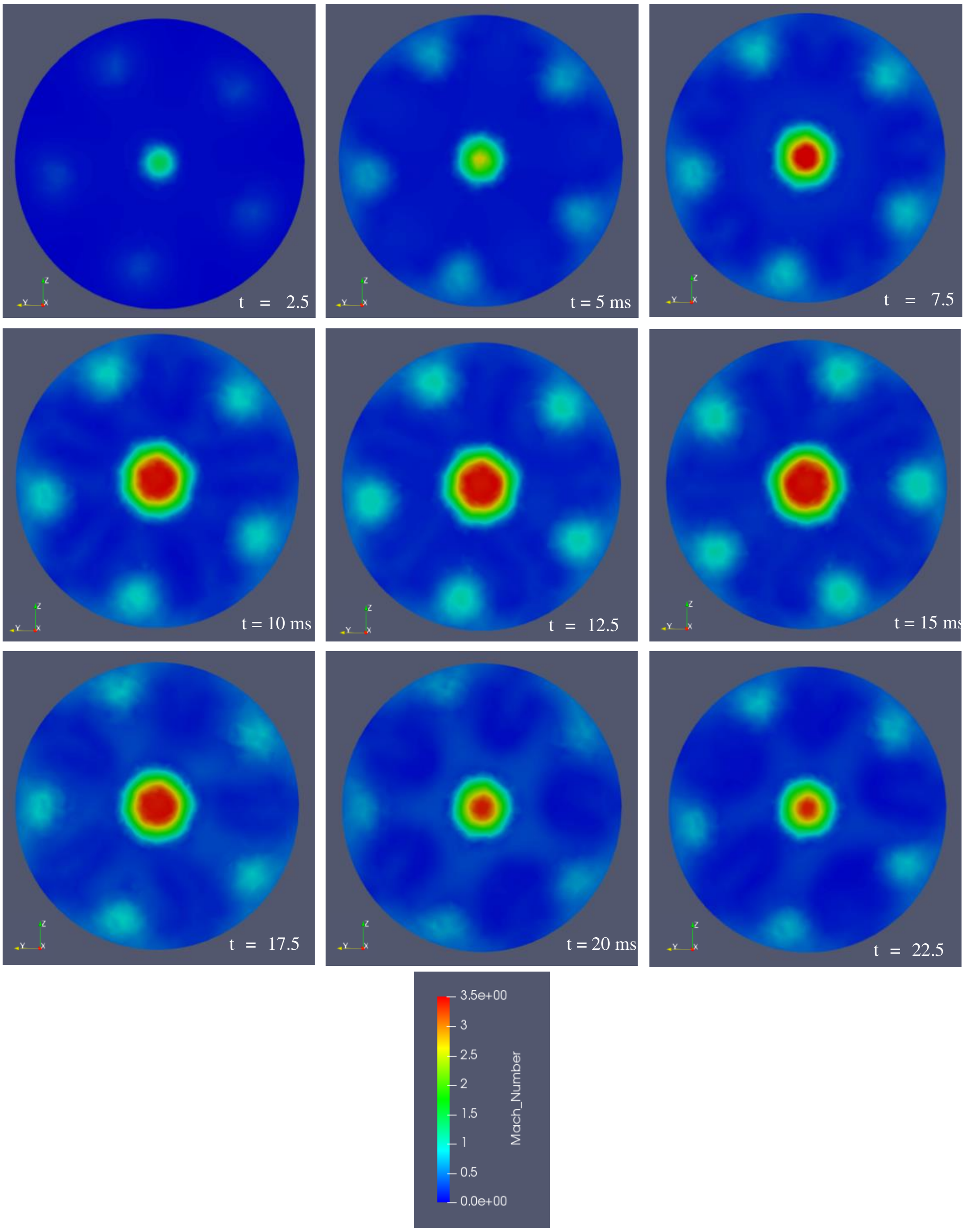


*Figure 4.17.* Mach number distribution in the second cross-sectional (at x = 480 mm) view

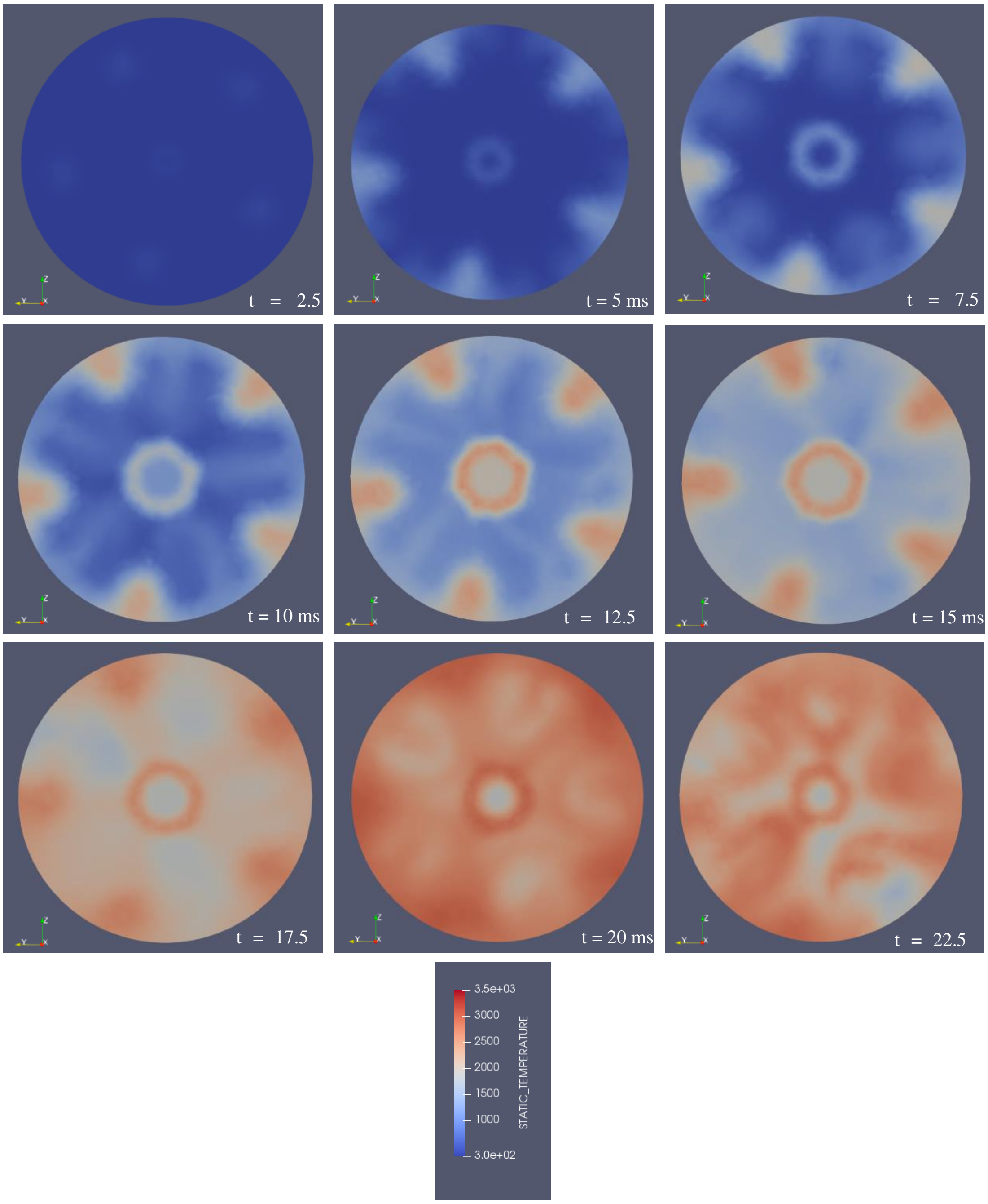


*Figure 4.18.* Static temperature [K] distribution in the second cross-sectional (at x = 480 mm) view

## 4.3. Comparison of the Test Cases

This section is divided into three parts. First, the comparison of the change of radial nozzle number and how it effects the pressurization of the grand SRM flow volume with the effect of pyrogen igniter is investigated. Then, the comparison of the change of radial mass flow rate ejected out of pyrogen and how it effects the pressurization of the grand SRM flow volume is analyzed. Last, the comparison of the change of radial nozzle angle and how it effects the pressurization of the grand SRM flow volume is investigated. In the upcoming Section 4.4, these individual effects as well as their combined interactions are discussed.

To begin with, while making the comparisons, the first thing to be analyzed is the mean pressures in the longitudinal axis of the grand SRM because the aim was to express how the pyrogen igniter pressurized it. As seen in Figure 4.4 the pressure plot inside the SRM volume (chamber) skyrockets in the area close to the end of the pyrogen igniter (where pyrogen jets first introduced to the SRM chamber), then it falls down drastically. This change occurs between 0.5 meters and 0.7 meters of the SRM volume in the longitudinal axis before even the jet flow reaches to 1 meters of length. After these peak and depth points, pressure tends to stabilize compared to these extremes; and even it is increasing or decreasing, this change occurs in a smooth transition manner. Therefore, since the general characteristics of the pressure in the longitudinal axis the SRM chamber is vital in this point, while making the comparison of the cases, the first parts of the SRM chamber where the extremes occur are omitted.

For better visualization, the parts that are omitted and urged upon in the graphical plots are illustrated in Figure 4.19. Again, the data of the example case #5 is used for this demonstrative figure at the 20$^{th}$ millisecond of the simulation.

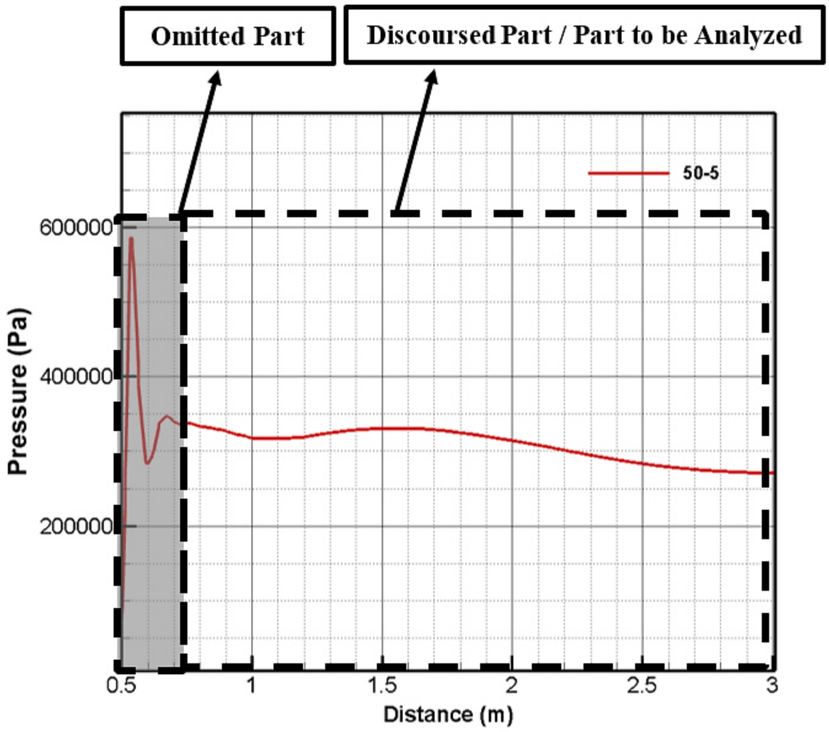


*Figure 4.19.* Demonstration of the parts omitted and used in the comparison of the test cases

The results of this comparison however, seemed not useful. Although there are small rise and fall trends, the mean pressure in the longitudinal axis of the SRM chamber for all cases is very close to each other. As it is clearly shown in Figure 4.20, the gap between the highest and the lowest pressures is merely 90 kPa at maximum, less than the atmospheric pressure, for any arbitrary comparison. Also, all pressure values vary inside this gap from 260 kPa to 350 kPa. In this workspace, comparison is not meaningful since all cases are showing the same behavior with slight changes occurring. For more convenience, the omitted (extreme) parts in Figure 4.19 are also checked: the changes in the pressure value is not more than 5-10 kPa.

However, the story changes when the pressure plots in the SRM propellant surface are investigated. The pressure variation of the test cases is more apparent on the propellant surface, especially in the areas where pyrogen igniter jets hit. On the remaining surfaces close to the head or aft end of the SRM, the pressure behavior is similar to the behavior in the longitudinal axis. Also showed in Figure 4.21, the change of mean pressures in those areas are again merely 5-10 kPa in a 90-100 kPa pressure distribution.

Thus, in this study, a test case showing better ignition transient means that it has higher pressure value where the radial pyrogen jets hit to the propellant surface. Therefore, from this point on, the comparison of the test cases will be made based on the variation of the pressure behavior on the propellant surface in the critical area (shown in Figure 4.21). Furthermore, these comparisons will be supported by Mach number and temperature figures of the test cases.

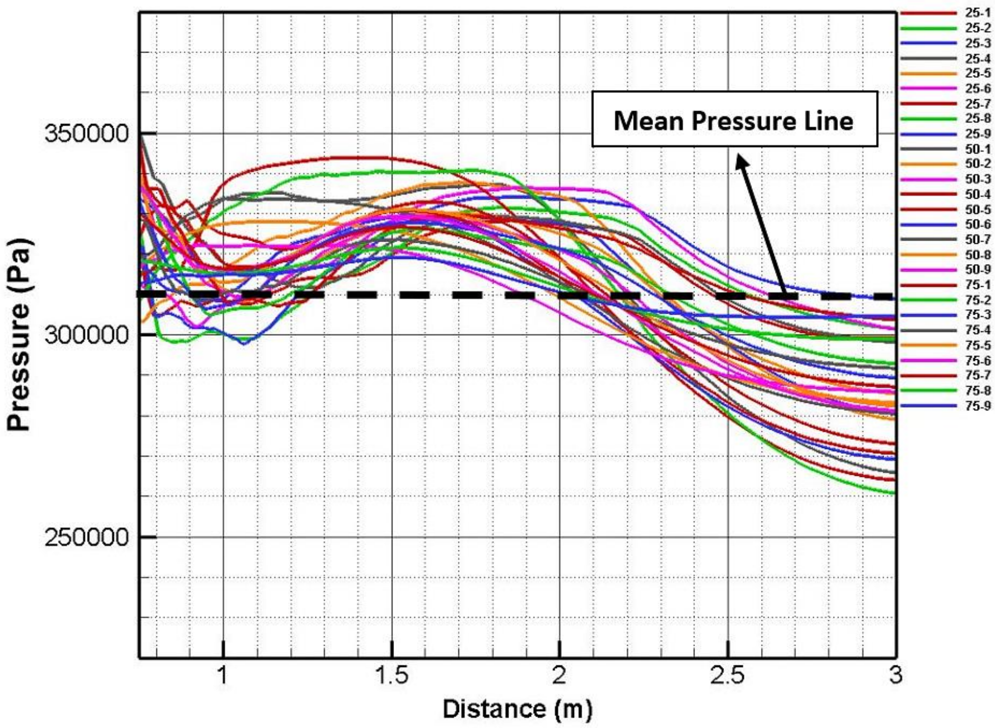


Figure 4.20. Comparison of the pressure plots in the longitudinal axis of the SRM for all test cases

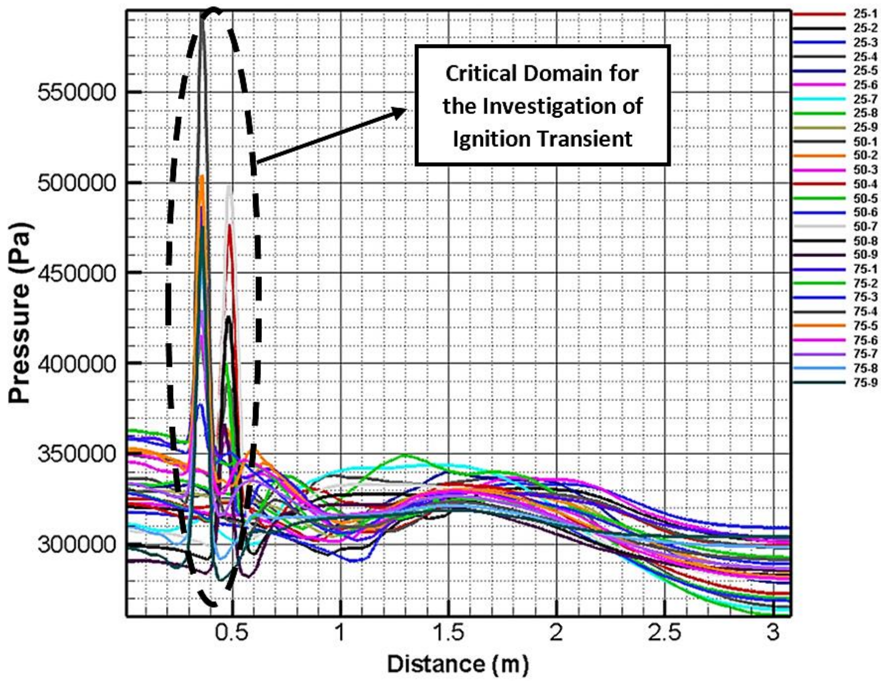


Figure 4.21. Comparison of pressure plots on the propellant surface of the SRM for all test cases

As mentioned in Section 4.1., the time instance when comparisons between the test cases are made is the 20th millisecond. This time duration is suitable for analyzing the pressurization behavior of a pyrogen igniter since the ignition transient phenomena (mentioned in Section 1) in solid rocket motor systems occur in very short time periods (milliseconds range) and the firing of the motor initiates thereafter. Also, in the reference thesis [3], these types of 3-D simulations lasted for similar time durations for the investigation of the same phenomena. Since all of the test cases were solved until they have reached to the exactly same time instance, the higher pressure a case has in the SRM chamber or propellant surface, the better option it becomes in terms of ignition transient. The comparison of the performance of different configurations of pyrogen igniter nozzle designs and the following discussion is made with this idea and assessment.

### 4.3.1. Comparison of the Effect of the Radial Nozzle Angle

The first comparison subject is the investigation of how the change of angle of the radial nozzles affects the pressurization the flow volume of the grand SRM system. All of the test cases in the Table 3.2 are analyzed individually with having 25°,50° and 75° radial nozzle angle configurations. All other parameters, axial and radial nozzle dimensions and radial mass flow rate, are kept exactly similar for these comparisons.

The results of each comparison are shown in Figure 4.. First group is originated from case #1. It has three radial nozzles in addition to one axial nozzle and has radial mass flow rate of 20% as fixed parameters. The variable parameter is radial nozzle angles: 25°,50° and 75°. Likewise, other groups are based on remaining cases in Table 3.2. As it can be clearly seen it Figure 4., as the nozzle angle grows up, the pressure where pyrogen igniter jets hit become increases. This type of behavior can be observed in all randomly selected cases (and in the cases which are not show here, for simplicity).

Let's choose an arbitrary case for the analysis: Case #4, the upper-right plot in Figure 4.22. It seems when all other parameters are fixed, the 25° nozzle angle configuration has lowest pressurization at the SRM propellant surface. Indeed, the pyrogen jets have not reached to propellant surface yet; thus, in the area where they supposed to reach the surface, the pressure is approximately 330-340 kPa. This hypothesis will be proved in Figure 4.23, the comparison of temperature behavior at the SRM propellant surface. The 50° nozzle angle configuration has a pressure peak of 470 kPa at the propellant surface, almost 1.5 times than 25° configuration. What's more, 75° nozzle angle configuration has a pressure peak of 500 kPa, the highest value of all. As mentioned before, the situation is similar in other cases as well.

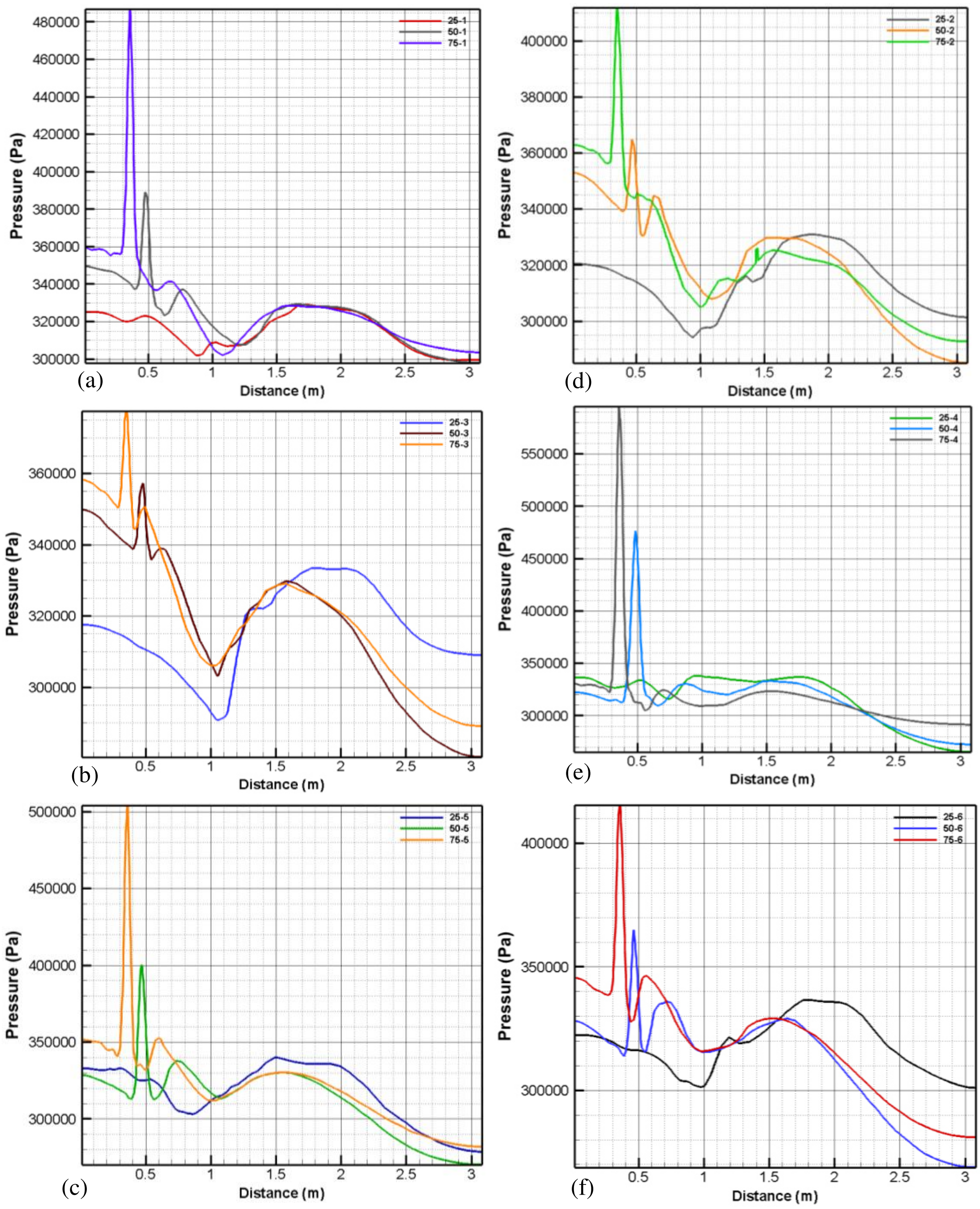


Figure 4.22. Comparison of pressure plots on the propellant surface of the SRM for all test groups, (a): case #1, (b): case #2, (c): case #3, (d): case #4, (e): case #5, (f): case #6, (g): case #7, (h): case #8 and (i): case #9

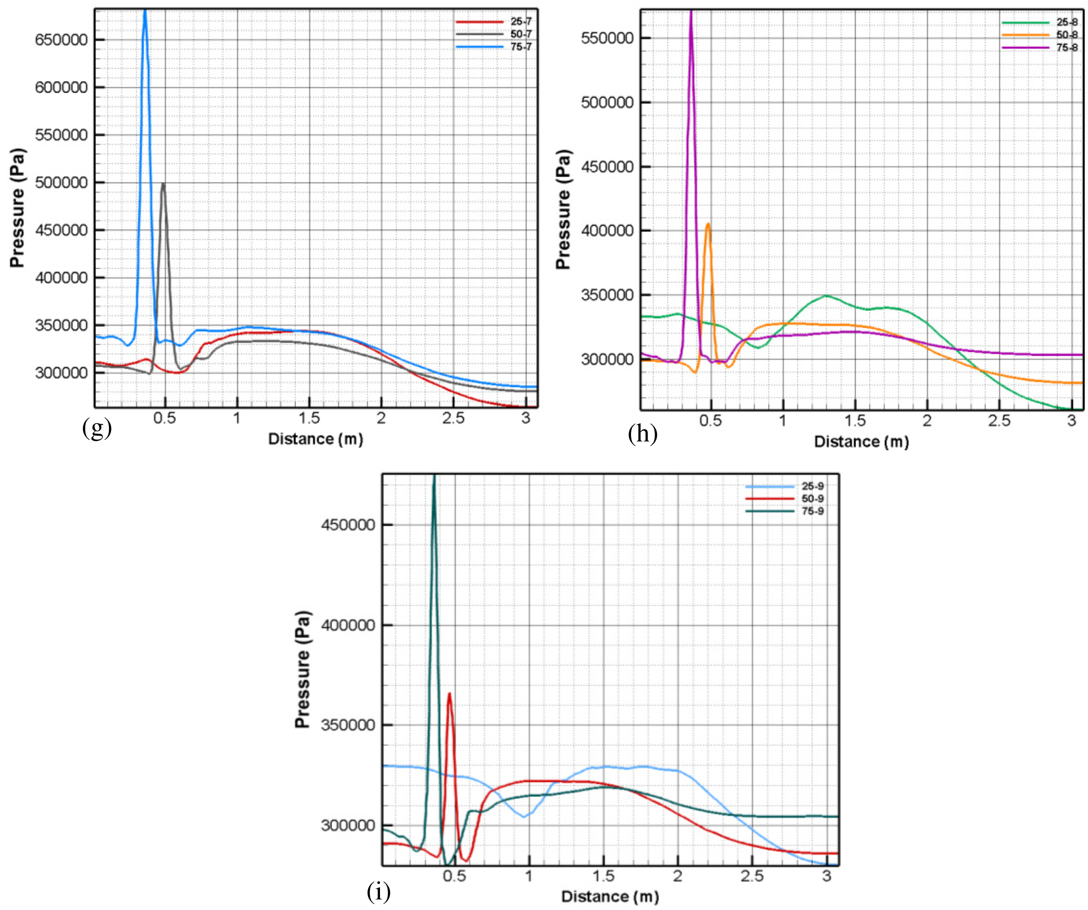


*Figure 4.23.* (Continued)

In Figure 4.23, the argument that has been presented is shown, in temperature-wise. The picture of 25° radial nozzle angle configuration is at the top, 50° is in the middle and 75° is at the bottom. The proposed idea was the fact that jets of 25° radial nozzle angle configuration have not reached to the SRM propellant surface at 20$^{th}$ millisecond of the simulation. Due to the angular orientation, this proposition seems corrected. Since the angle is lower compared to other two cases, the flow is close to full axial flow instead of having radial features. However, as mentioned in Section 4.3. when the pressures in the longitudinal axis are compared, there was not much of a difference for cases; whereas, the variation is originated from the pressurization of the SRM surface. Temperature distribution is also seeming much or less similar in Figure 4.23.

75° radial nozzle configuration has largest pressure (500 kPa) and temperature (3500 K) zones in the SRM propellant surface which makes it best option from the ignition transient point of view. This means that jet flow in 75° configuration reaches to propellant surface much faster than 25° configuration, staring to heat and pressure it much earlier, which is better for ignition transient. Indeed, it is. Since the geometrical distance these jets travel is shorter than 25° configuration, they seem to hit the surface in 10$^{th}$ millisecond as proven in Figure 4.24.

50° radial nozzle configuration has also some amount of hot jet flow hitting to the same surface, more than 25° configuration but not as great as 75° configuration; thus, it is the second-best choice in this comparison from ignition transient point of view.

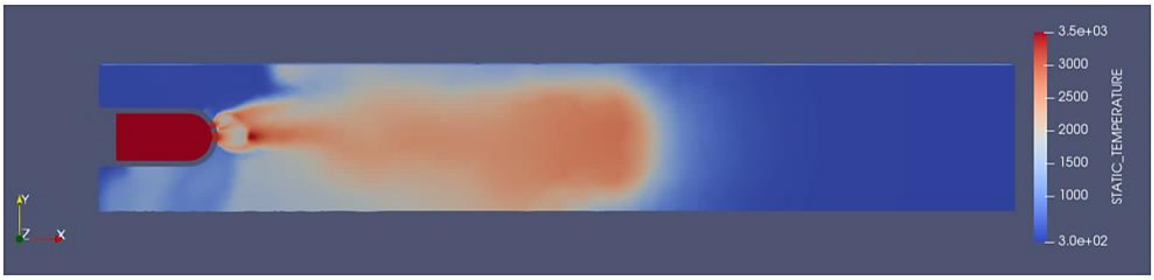


(a)

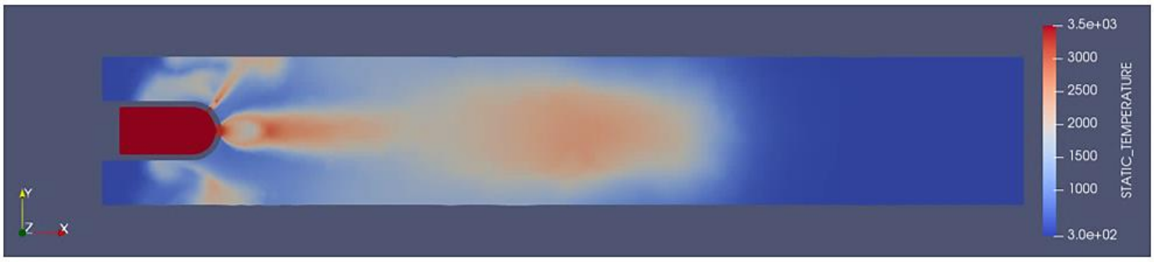


(b)

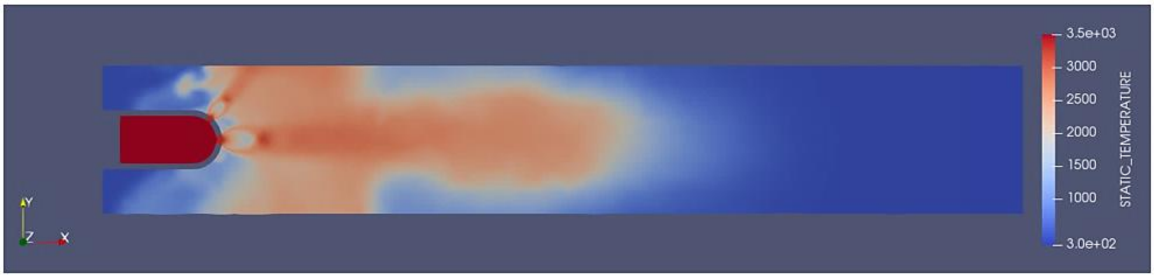


(c)

Figure 4.23. Comparison of temperature behavior on the propellant surface of the SRM for test Case # 4 with varying radial angles: 25° (a), 50° (b) and 75° (c)


Figure 4.24. Temperature behavior of the test Case # 4 having 75° of radial nozzle angel, at the $10^{th}$ ms

Therefore, it can be concluded from the analysis of the data is that the rise in the radial nozzle angle of pyrogen igniter, increases the pressure on the propellant surface of the SRM and favors of ignition transient phenomena. The further disscussion about this subject is made in Section 4.4 and the concluding remarks of this comparison regarding the ignition transient phenomena is presented there.

### 4.3.2. Comparison of the Effect of the Radial Nozzle Number

When the Table 3.2 is examined, it can be concluded that using case # 1-2-3 group, 4-5-6 group and 7-8-9 group is suitable for the comparison of how the change of radial number of the pyrogen igniter nozzle design affects the pressurization the flow volume and the propellant surface of the grand SRM system. Having one fixed axial nozzle, cases 1,4 and 7 have three, cases 2,5 and 8 have five and cases 3,6 and 9 have seven radial nozzles.

For the first group (cases 1,2 and 3) the fixed nozzle design parameters are the dimension of the axial nozzle, the radial nozzle angle (25°) and the radial mass flow rate (25%). The changing parameter is the radial nozzle number and as proceeding from case # 1 to case # 3, radial nozzle radius decreases since the radial nozzle number increases (see Figure 4.25). For the second group (cases 4,5 and 6) the fixed nozzle design parameters are the dimension of the axial nozzle, the radial nozzle angle (25°)

and the radial mass flow rate (50%); whereas, for the third group (cases 7,8 and 9) the fixed nozzle design parameters are the dimension of the axial nozzle, the radial nozzle angle (25°) and the radial mass flow rate (80%). Since these groups showing the same pattern as the first group, the radial nozzle number increases as proceeding from cases 4 and 7 to cases 6 and 9, while the radius of the individual radial nozzle decreases.

| **Radial Nozzle Number (#) vs. Radial Mass Flow Rate (%)** | | **3** | **5** | **7** |
|---|---|---|---|---|
| **20 %** | **Case #** | **1** | **2** | **3** |
| | $r_{radial}$ **(mm)** | 5.64 | 4.37 | 3.69 |
| | $r_{axial}$ **(mm)** | 19.54 | 19.54 | 19.54 |

*Figure 4.25.* Partial view of the Test Matrix (Table 3.2.) for the first radial nozzle number comparison group

The results of the comparison of the pressure inside the majority volume of the SRM chamber can be seen in Figure 4.26. As seen from the figure, all comparison cases show similar behavior and the main pressure difference between all locations of the cases is solely 5-10 kPa. Although in all plots, the configurations with least nozzle number (three) has the most pressurization effect on SRM propellant wall, the difference is minor and needs to be checked. All these cases have fixed 25° of radial nozzle angle in their design configurations. Therefore; the examination must be expanded by checking the same cases with 50° and 75° of radial nozzle angles. However, it must not be forgotten that variable parameter here is the radial nozzle number, not the radial nozzle angle. Nozzle angle will be fixed again in the same grouping system but its value will be increased in order to gather more information. Therefore, cases having 50° and 75° of fixed radial nozzle angle with changing nozzle number configurations are also analyzed. The results obtained this time is more satisfying and improves the intuition made with 25° radial nozzle angle configuration results.

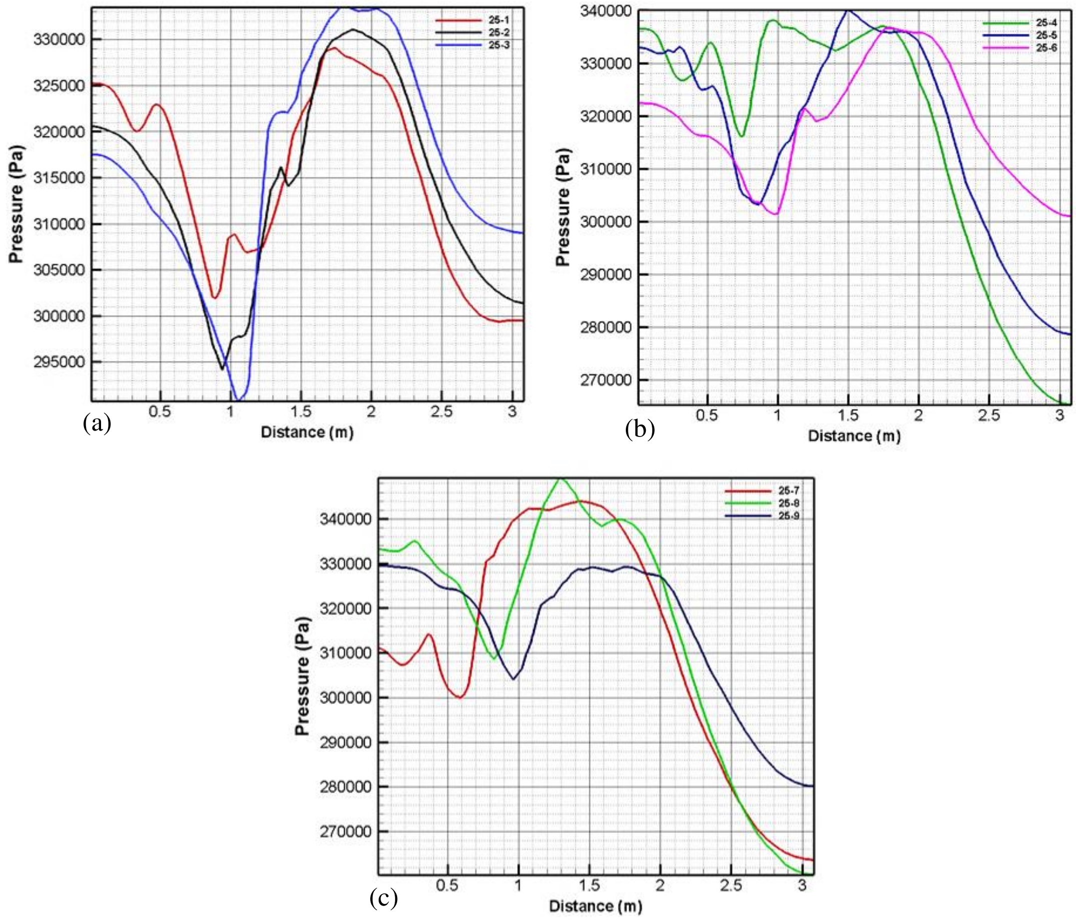


*Figure 4.26.* Pressure plots on the propellant surface of the grand SRM of the comparison group 1 ((a) cases 1,2 and 3), group 2 ((b) cases 4,5 and 6) and group 3 ((c) cases 7,8 and 9) with 25° radial nozzle angle

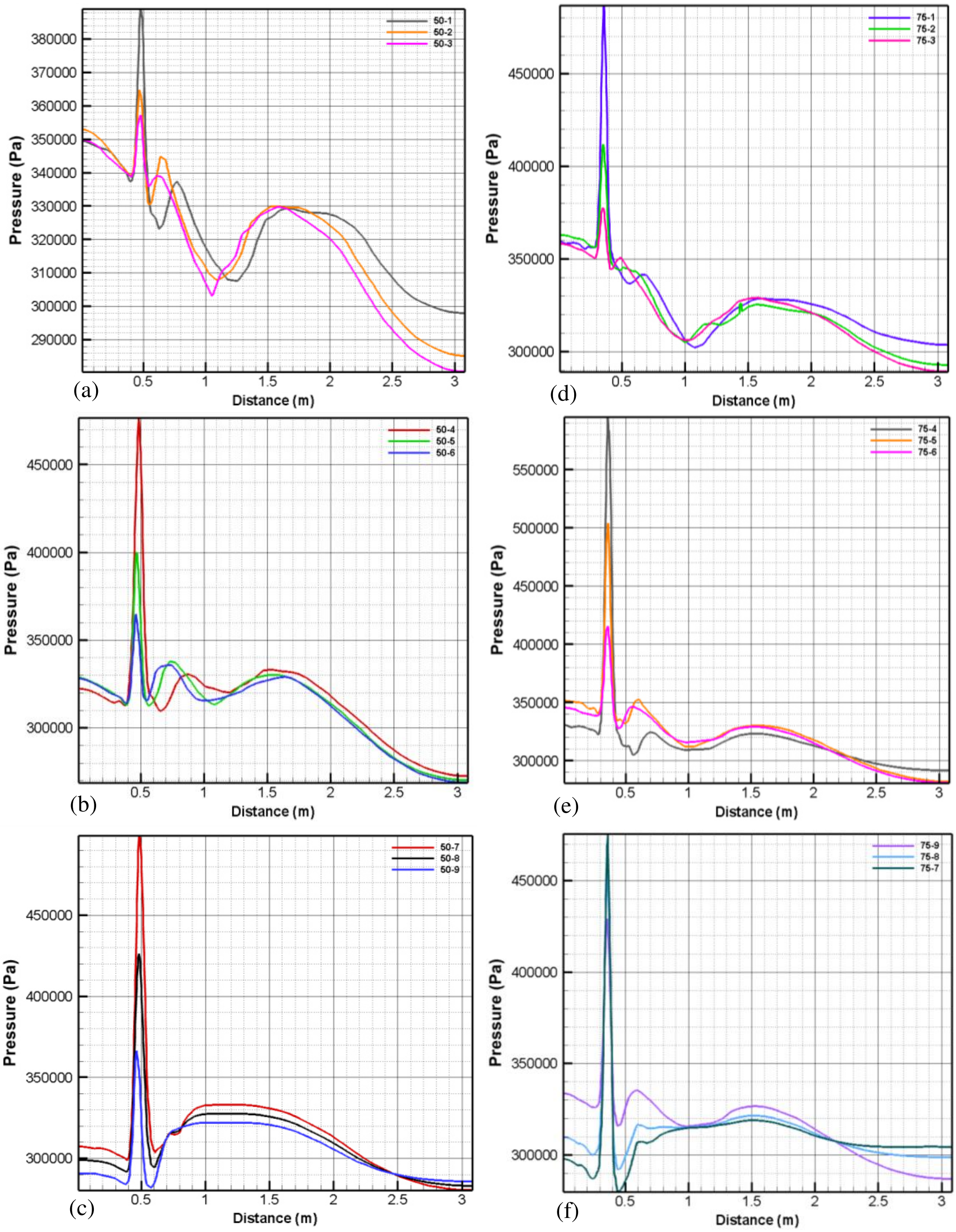


*Figure 4.27.* Pressure plots on the propellant surface of the grand SRM of comparison groups, 4(a), 5(b), 6(c), 7(d), 8(e) and 9(f)

As seen in Figure 4.27, in all comparison groups, the pressure where the pyrogen jets hit decrases with the increasing radial nozzle number. Let's investigate a sample group: Comprasion of group 2 -cases 4,5 and 6- having 50° of radial nozzle angle (Left column, middle pressure plot in Figure 4.27). When all other parameters are fixed, using three radial nozzle jumps the pressure on the propellant surface to 475 kPa. When five radial nozzle are utilized in the configuration, this value decreases to 400 kPa and when the radial mass flow rate is divided into seven, the pressure value increases to 365 kPa. This means that instead of dividing the radial mass flow rate via increasing the radial nozzle number, concentrating it into less number of radial nozzles improves the ignition transient. This proposition is illustrated better across the SRM chamber, using Mach number distrubition visuals this time. In Figure 4.28, visuals of the same comparison group that has been mentioned are shown: configuration having three radial nozzles is at the top, five is in the middle and seven is at the bottom. While the speed and magnitude of the axial jet flow remains constant in all cases, the same virtues of radial flow diminish as the number of the radial nozzles increases.

Therefore, it can be comfortably concluded that the number of radial nozzles have inversely proportional relationship with the pressurization of the propellant surface of the SRM; and thus, the ignition transient phenomena. As the number of the radial nozzles increase, the radial flow becomes disaggregated and ineffective, which in turn retards the ignition of the SRM. Concentrating the radial flow with less radial nozzles seems more practical for the system. The further disscussion about this subject is made in Section 4.4 and the final remarks of this comparison regarding the ignition transient phenomena is presented there.

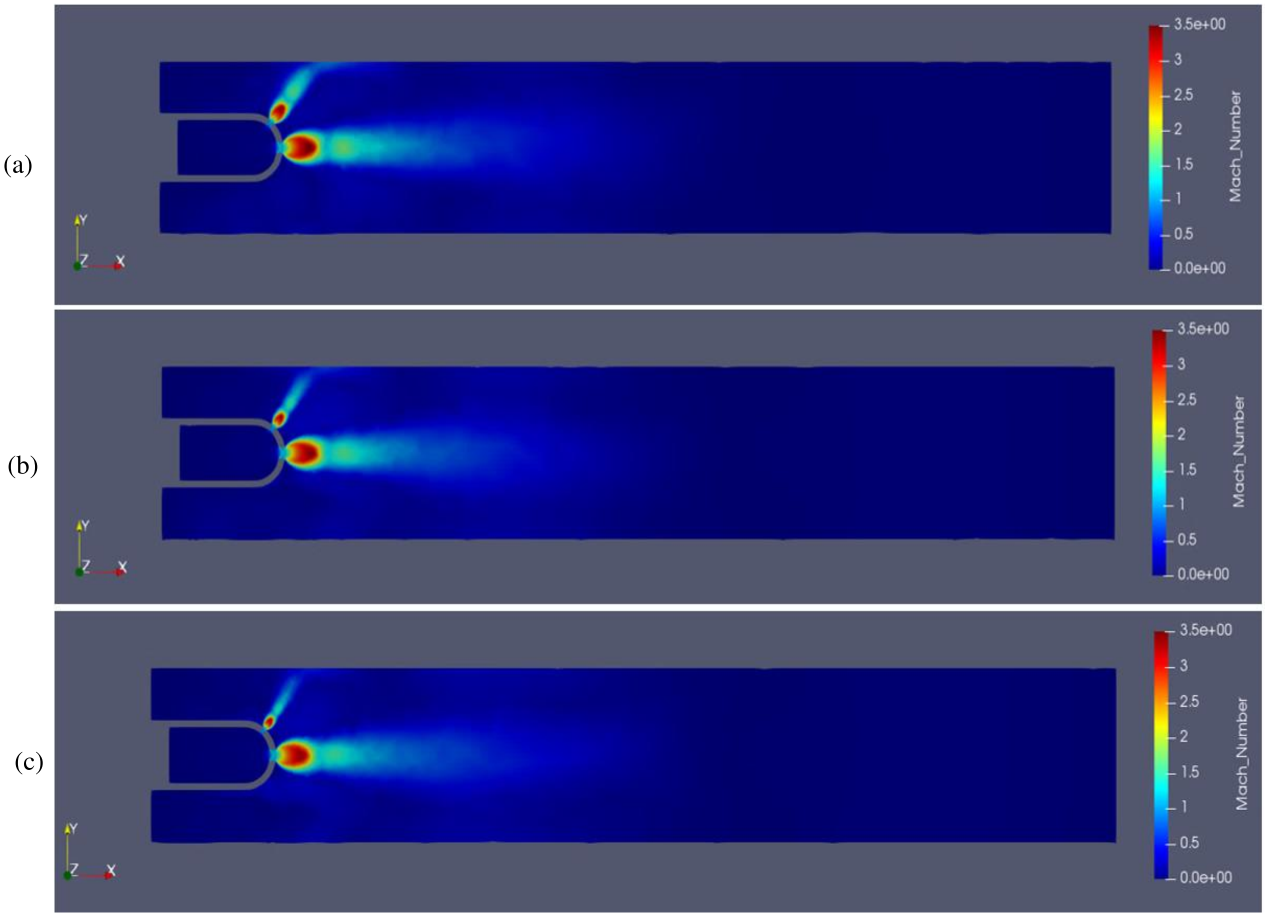


Figure 4.28. Comparison of Mach number behavior on the propellant surface of the SRM for Test Group 2 (3 radial nozzles (a), 5 (b) and 7 (c)) having 50° of radial nozzle angle

### 4.3.3. Comparison of the Effect of the Radial Mass Flow Rate

The last comparison subject is how the change of degree of the radial mass flow rate ejected out of the pyrogen igniter nozzles affects the pressurization the flow volume of the grand SRM system. Again, referenced from Table 3.2, comparison groups are formed for the same radial nozzle number and radial nozzle angle.

For the first group (cases 1,4 and 7) the fixed nozzle design parameters are the radial nozzle angle (25°) and the radial nozzle number (3). The variable parameter is the radial mass flow rate and as proceeding from case # 1 to case # 4, the radial mass flow rate increases from 20% to 80% with the enlargement of the radius of radial nozzles and shrinking of the radius of the axial nozzle (see Figure 4.29). For the second group (cases 2,5 and 8) the fixed nozzle design parameters are the radial nozzle angle (25°) and the radial nozzle number (5); whereas, for the third group (cases 3,6 and 9) the fixed nozzle design parameters the radial nozzle angle (25°) and the nozzle number (7). Since these groups showing the same pattern as the first group, the radial mass flow rate increases as proceeding from cases 2 and 3 to cases 8 and 9, while the radius of the individual radial nozzle increases.

| ***Radial Nozzle Number (#) vs. Radial Mass Flow Rate (%)*** | | **3** |
|---|---|---|
| ***20 %*** | **Case #** | **1** |
| | $r_{radial}$ **(mm)** | 5.64 |
| | $r_{axial}$ **(mm)** | 19.54 |
| ***50 %*** | **Case #** | **4** |
| | $r_{radial}$ **(mm)** | 8.92 |
| | $r_{axial}$ **(mm)** | 15.45 |
| ***80 %*** | **Case #** | **7** |
| | $r_{radial}$ **(mm)** | 11.28 |
| | $r_{axial}$ **(mm)** | 9.77 |

*Figure 4.29.* Partial view of Test Matrix (Table 3.2.) for the first radial mass flow rate comparison group

The results of the comparison of the pressure inside the majority volume of the SRM chamber can be seen in Figure 4.30. When the results are analyzed same pattern mentioned in Section 4.3.2 is observed. Comparing the result of configurations having 25° fixed nozzle angle does not yield healthy results because pressure plots are very close to each other having similar trends and mean values. Configurations having more radial mass flow rate seems higher pressurization in the SRM propellant surface but this proposition must be checked for convenience.

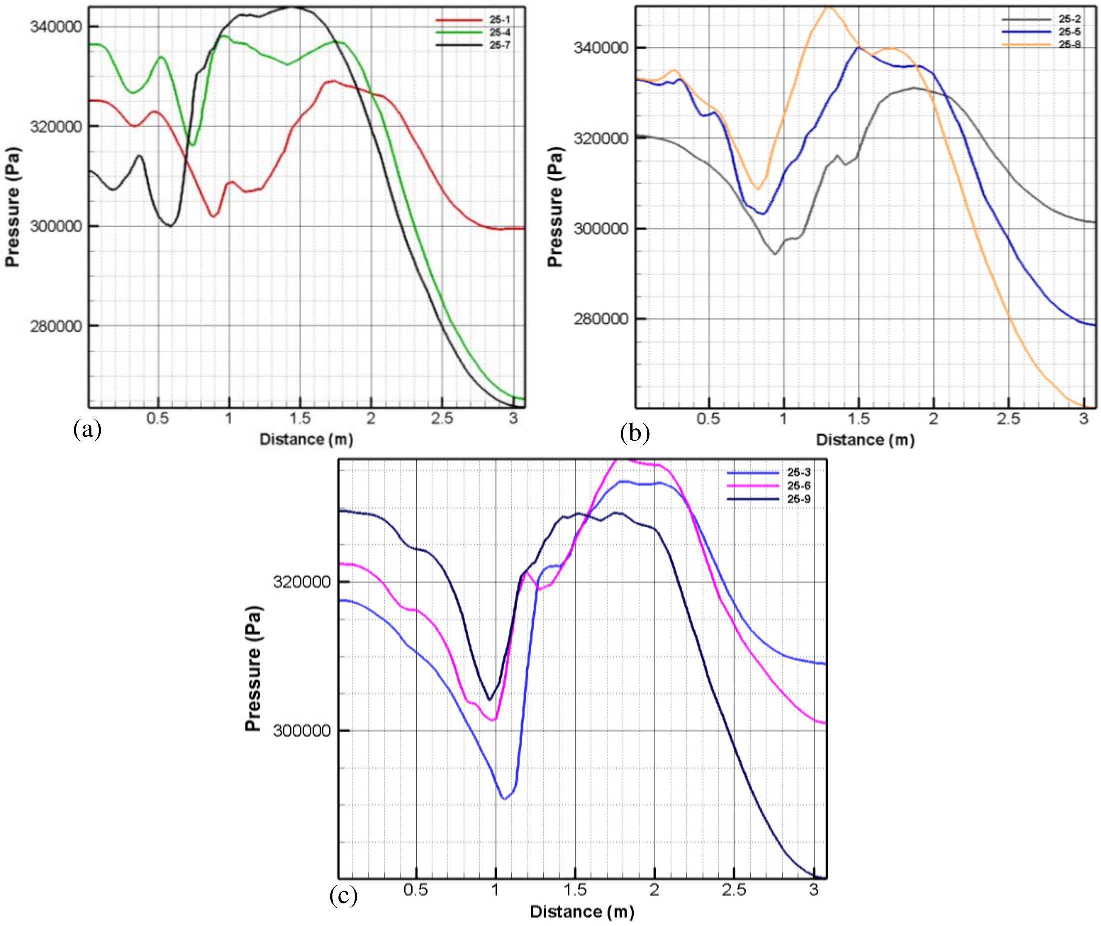


*Figure 4.30.* Pressure plots on the propellant surface of the grand SRM of comparison group 1 ((a) cases 1,2 and 3), group 2 ((b) cases 4,5 and 6) and group 3 ((c) cases 7,8 and 9) with 25° radial nozzle angle

Therefore, same grouping system is applied to cases having fixed 50° and 75° radial nozzle angles. Nozzle angle will not change again in the exactly similar grouping system but its value will be increased in order to gather more information, like before. The varying parameter is radial mass flow rate. The results obtained wit this procedure is again more satisfying and enhances the proposition made with 25° fixed radial nozzle angle configuration results.

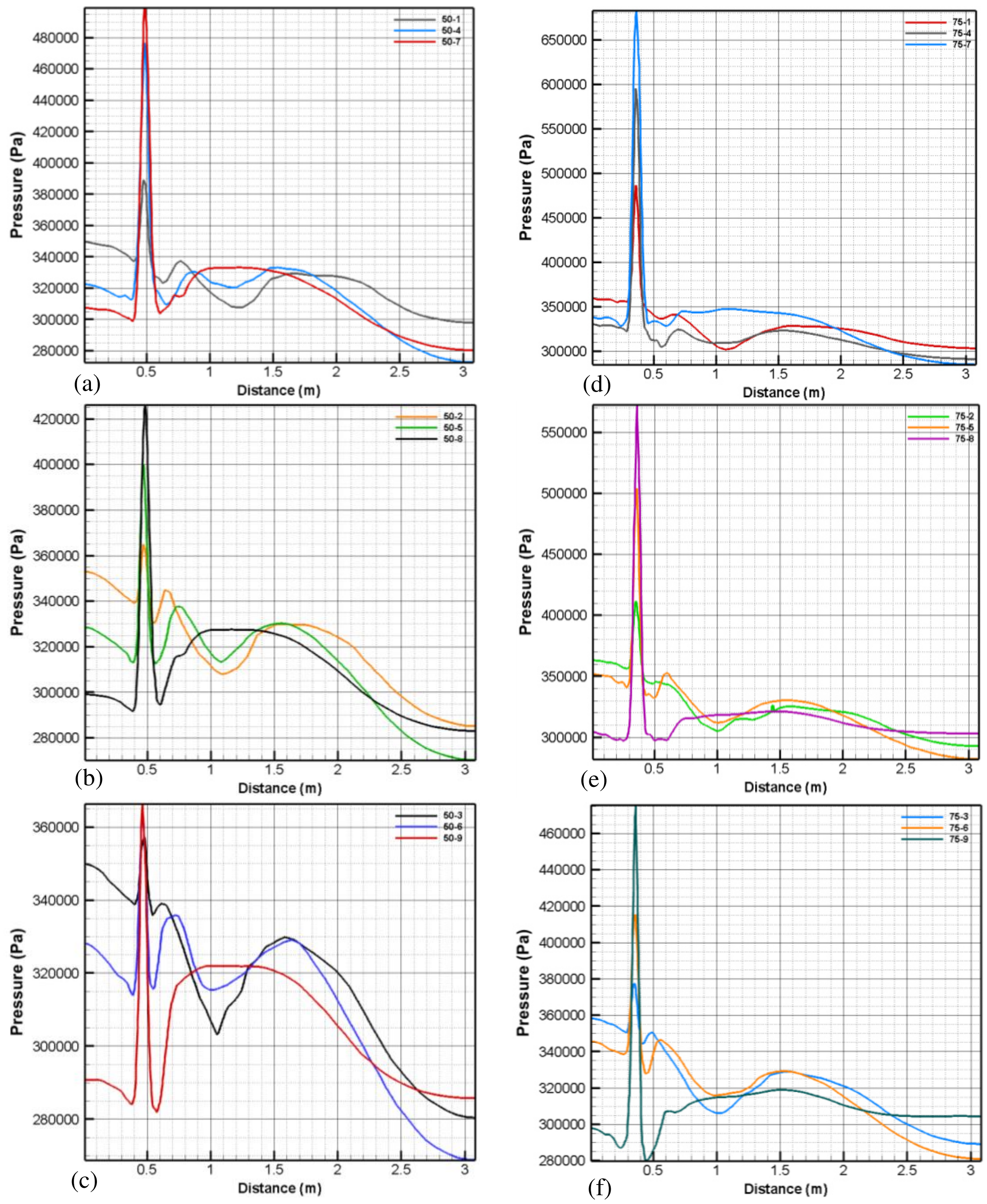


*Figure 4.31.* Pressure plots on the propellant surface of the grand SRM of comparison groups 4(a), 5(b), 6(c), 7(d), 8(e) and 9(f)

As seen in Figure 4.31, in all comparison groups, the pressure on the propellant of the SRM increases with the increasing radial mass flow rate. In order to investigate this logic a sample group is again chosen: Comprasion of group 3 -cases 3,6 and 9- having 75° of radial nozzle angle (Right column, bottom pressure plot in Figure 4.31). When all other parameters are fixed, pyrogen igniter ejecting 20% of its combustion products in radial direction pressurizes the SRM propellant surface up to 410 kPa at its maximum value. If this ratio is increased to 50% then, the maximum pressure value increases to 460 kPa. When the ratio is its peak level, 75%, the maximum pressure value passes 500 kPa slighlty. This means the more the flow ejected out of the pyrogen igniter is radial, the more SRM propellant surface is pressurized, the faster ignition transient occurs.

This phenomena is illustrated across the SRM chamber, using both Mach number and temperature distribution snapshots of the aforementioned test case group. Mach number figures (see Figure 4.32) are for better visualization of how radial flow rate expands proceeding from case #3 to case # 9; whereas, temperature figures (see Figure 4.33) are for picturizing the enhancing impact area of the increasing radial mass flow. For both mentioned figures, pyrogen igniter nozzle design configuration ejecting 20% radial mass flow rate is at the top, 50% is in the middle and 75% is at the bottom.

In Figure 4.32, as the radial mass flow rate increases from 20% to 80% the radial jets grow in speed and magnitude while the axial flow shrinks. In Figure 4.33, it can be observed that as this radial flow rate rises, the heated areas (to approximately 3500 K) almost cover entire domain of head-end of the SRM propellant. Therefore, it can be concluded that, the increase in the radial mass flow rate favors a short ignition transient time interval. Again, the further disscussion about this subject is made in Section 4.4 and the concluding remarks of this comparison regarding the ignition transient phenomena is presented there.

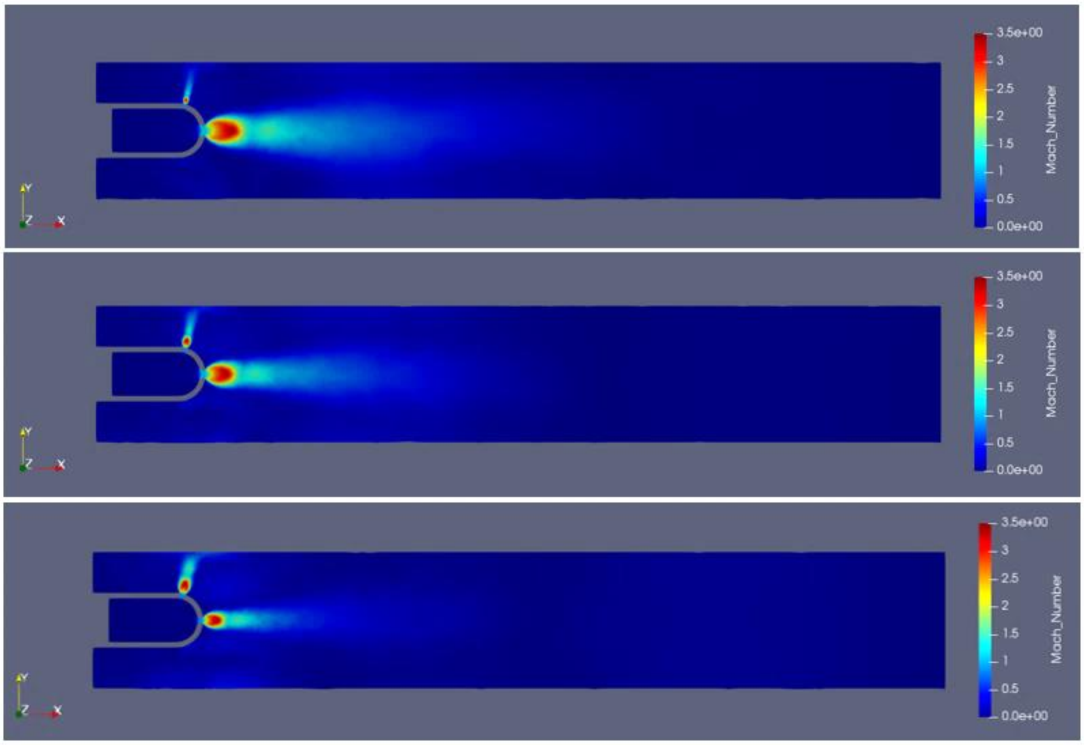


(a)

(b)

(c)

Figure 4.32. Comparison of Mach number behavior on the propellant surface of the SRM for Test Group 3 (20% radial mass flow rate (a), 50% (b) and 80% (c)) having 75° of radial nozzle angle

(a)

(b)

(c)

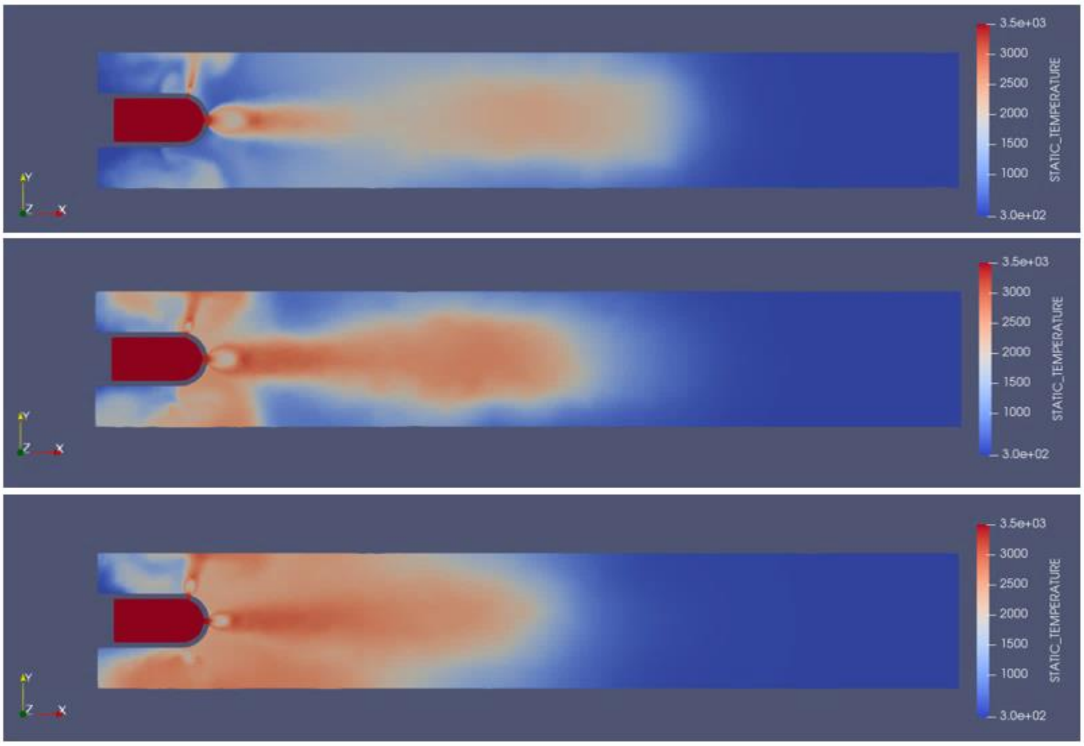


Figure 4.33. Comparison of temperature behavior on the propellant surface of the SRM for Test Group 3 (20% radial mass flow rate (a), 50% (b) and 80% (c)) having 75° of radial nozzle angle

## 4.4. Discussion

The aim of this study is to determine the dominant parameters in the nozzle design of a pyrogen igniter operating inside a bigger SRM system, from ignition transient point of view. As mentioned in Section 1 - Figure 1.3, ignition transient in solid rocket motors are divided into three parts: induction, flame spreading and the chamber filling phases. In this particular work, a pyrogen igniter having fixed geometrical and ballistic features and variable nozzle parameters is tested. The variable parameters are radial nozzle angle, radial nozzle number and the radial mass flow rate it ejects into SRM. For this test, a full factorial experiment approach is selected and 27 cases are formed. All of the parameter combinations are tested via a 'fully coupled compressible gas flow' solver and their particular pressure, Mach number and temperature behavior is analyzed a the 20$^{th}$ millisecond of test results. Here, 20 milliseconds seem like a small number; however, ignition transient of very large solid rocket motor system occur merely in this little period of time. The phenomena are also very unstable; therefore, hard to analyze.

The mentioned time instance (20 milliseconds) is generally in the induction phase of any SRM. Induction phase starts with delivering of the ignition signal and ends when the first tiny spot self-ignites in the SRM propellant surface. This self-ignition is the outcome of heating and pressurizing. Thus, in this work, the more temperature and pressure a test case has in the SRM, the better it is in terms of ignition transient because it shortens the induction period to its best.

After modelling, meshing and solving the cases, first of all the pressure distribution inside the longitudinal axis of the SRM is analyzed (see Figure 4.20). However, for all cases this distribution envelops a very tight area in the graphs, all of the pressure plots have very close mean pressure values and the change between any point of any two arbitrary plots do not exceed 10-20 kPa. These outcomes are not suitable for a comparison. That's why, pressurization at the surface of the propellant SRM gained more importance. The places where pyrogen jets hit exhibit varying distribution; although, remaining parts same similar behavior happened when analyzing the longitudinal axis (see Figure 4.21). Temperature values and illustrations are also in the same basis with the pressure plots, supporting the argument that has been made.

After examining the results of the study, it has been found out that all these parameters (radial nozzle angle, number and mass flow rate) are important parameters in the nozzle design of a pyrogen igniter. They affect the pressurization of the SRM surface influentially and they are surely not redundant from ignition transient point of view.

The first parameter that has been analyzed as a variable was the radial nozzle angle of the pyrogen igniter and its effect when changed. It has revealed that when the radial nozzle angle increase, the pressure on the SRM propellant surface increases.

Therefore, in order to shorten the induction time and obtain a efficient ignition transient, using pyrogen igniter with high radial angles is advised.

The second parameter that has been analyzed was the radial nozzle number and its impact on pressurization. It seems that increasing the radial nozzle number divides the radial flow and makes it inefficient. Therefore, for a better ignition transient performance, using radial nozzles but keeping their number as much as possible is advised.

The third and the last parameter that has been analyzed was the radial mass flow rate. This was achieved by manipulating the radius of the nozzles. Since radial mass flow has directly proportional relationship with radial nozzle radius, increasing the radius of radial nozzle means increasing radial mass flow ejected out of the pyrogen; as well as, decreasing the axial flow. After the analysis, it has been concluded that increasing the radial mass flow rate enhances the pressure at the SRM propellant surface; that's why, in order to achieve shorter ignition transient time, using more radial flow is advised.

The maximum pressure outcomes that has been seen on the propellant surface of the SRM is put into General Full Factorial Design experiment with the test matrix including all combinations of the aforementioned parameters and the following results has been obtained in Minitab 19. There are three factors (radial nozzle angle, number and mass flow rate) each having three levels without any replicates.

The individual effect of each parameter on the pressurization of the SRM system can be investigated separately in Figure 4.34. The results of the Full Factorial DOE analysis are in concordance with the comments that have been made. As it seen in Figure 4.34, increasing the radial nozzle angle and radial mass flow rate favors the pressurization; thus, shorter ignition transient time. Radial nozzle angle has more aggressive behavior than radial flow rate by the way, as it covers more range in the pressure plot. On the other hand, increasing the radial nozzle number has adverse effects on pressurization.

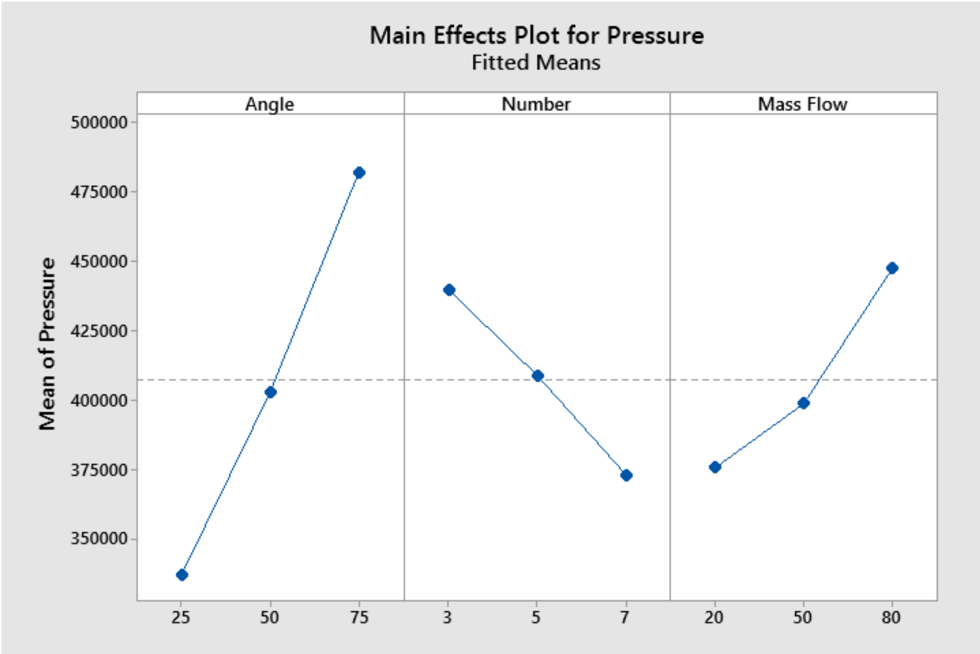


Figure 4.34. Main effect plots for each factor

From these findings, it can be concluded that a test case having more radial nozzle angle with more radial mass flow and less radial nozzle number should be the best option in this thesis work in terms of pressurization of the surface of the grand SRM propellant. The test case having these virtues is the case #7, having 75° of radial nozzle angle, 80% radial mass flow rate and 3 radial nozzles. Therefore, this test case should be the optimum choice.

The combined interaction effects of dual parameters on the pressurization of the SRM system can be investigated in Figure 4.34. When the plot on the top (combined radial nozzle angle and number effects) is analyzed, the maximum pressure result is obtained when the radial nozzle angle is increases, but also when then the radial nozzle decreases. In the lowest angle value (25°) all cases show similar pressure behavior. When the angle starts to rise, pressure values starts to increase too. This increase is more apparent when the nozzle number is decreased. In middle range (50°), cases having five radial nozzles have approximately 25 kPa more pressure than the ones having seven nozzles, in the average. What's more, cases having three radial nozzles have 75 kPa more pressure value than cases having five nozzles. The rise in the comparison value 200%. As the angle grows more (75°), between the cases having five and seven radial nozzles, the pressure difference jumps to 100 kPa, more than 400% relative the comparison made with middle range results. Furthermore, between the cases having three and five nozzles, the pressure gap decreases 50%, and between the cases having three and seven radial nozzles, the pressure difference remains the same as approached from 50° to 75° of radial nozzle angle. Therefore, it is concluded that radial nozzle angle and number certainly show inversely proportional relationship in terms of pressurization.

When the plot in the middle (combined radial nozzle angle and mass flow rate effects) is analyzed, the maximum pressure result is obtained when both the radial nozzle angle and mass flow rate increase. In low and middle radial nozzle angle ranges, cases having low mass flow rate unfavored for there exists approximately 50 kPa difference between 20% radial mass flow rate cases compared to 50% and 80% ones. However, as the angle reaches to its maximum value the trend changes. Compared to middle angle ranges, the pressure difference drops 400% in the value (from 50 kPa to 10 kPa) between the cases having 20% and 50% radial mass flow rate. Between the cases having 50% and 80% flow rate this difference skyrockets, as it increases from 5 kPa to 100 kPa, exhibiting approximately 2000% rise. Moreover, the pressure gap widens from 50 kPa to 200 kPa between the cases having 20% and 80% radial mass flow rate, increasing 300% as the radial nozzle rises. Thus, the results exhibit that radial nozzle angle and mass flow rate have certain directly proportional relationship in terms of pressurization.

When the top and the middle plots -having same radial nozzle angles- are analyzed together, it seems decreasing nozzle number becomes more dominant factor rather than increasing mass flow rate in the middle range, in terms of pressurization. However, this effect wears of as the angle rises more and the dominance levels of these factors become similar in the high range of nozzle angles.

When the plot at the bottom (combined radial nozzle number and mass flow rate effects) is analyzed, the minimum pressure values are obtained when the radial nozzle number increases and the mass flow rate decreases. In the low range configurations (three radial nozzles) the pressure difference between having 20% and 50% radial mass flow rate is merely 5 kPa; whereas, the same difference between 50% and 80% flow rates is 100 kPa and 105 kPa between 20% and 80% flow rates. As approaching to middle range configurations (five radial nozzles) the gap between 20% and 50% radial mass flow rate configurations widens from 5 kPa to 50 kPa; whereas, the it shrinks from 100 kPa to 25 kPa between 50% and 80% cases. The difference between 20% and 80% configurations roughly remain the same. In the high range configurations (seven radial nozzles) the average pressure difference shrinks 50% compared to middle range results for all situations. It is apparent that radial nozzle and mass flow rate has inversely proportional relationship in terms of pressurization.

In this point a question may rise regarding the fact that the best case (in terms of pressurizing the propellant surface of the grand SRM) has the largest radial nozzle angle and mass flow rate and the least number of nozzles. What happens when these parameters are expanded? For example, what happens when the radial nozzle angle is increase to 80° rather than 75°? The answer is obvious that the pressurization will increase since the jet flow is more directed to the propellant surface. However, there are two things that should be considered in this point. First, taking geometrical constraints into account that will provide a feasible and manufacturable design. Second and the more important one is that, the aim of work carried out in this thesis is to scan the design space regarding the combinations of the nozzle parameters. Rather than concluding that the nozzle design having the maximum angle or mass flow rate and the minimum radial nozzle number parameters are the best options for a pyrogen nozzle, the approach to the subject at the end should be like this: if the ignition transient phase of a grand SRM is longer than predicted and this causes some issues, adjusting the nozzle parameters (for example only increasing the radial nozzle angle by some amount) could fix or at least heal the problem.

Furthermore, since the induction phase ends when the first ignited hot spot is observed on the propellant surface and the time duration of the dealt cases in this work remain in the induction phase, comparing the pressure values is appropriate. Once the ignition starts, flame spreading phase starts and ends in an extremely fast fashion. Therefore, the more pressurized scenario, even in the smallest area of the propellant surface of the grand SRM, has the advantage in terms of shortening the ignition transient.

On the other hand, the highest-pressure value observed in the outcomes of this work on the propellant surface of the grand SRM is approximately 700 kPa (and that's in the best case). Although this the highest value, this pressurization is not critical from the mechanical endurance point of view of the propellant of the grand SRM. The propellant will not deform or crack under these pressure conditions and will maintain is structural integrity until ignition. As seen in Figure 1.7, these type composite propellants including polymers as binders can withstand more than 6 or 7 MPa of chamber pressure during the grand SRM operation. Thus, the pressurization effect due to existence of pyrogen jets are not critical for the propellant in terms of mechanical strength.

To conclude, it is shown that all three factors that have been examined are dominant and important factors in the pressurization of the SRM system and play key roles. Radial nozzle angle and mass flow rate parameters favor shorter ignition transients time span; and on the contrary, radial nozzle number exhibits adverse effect on it.

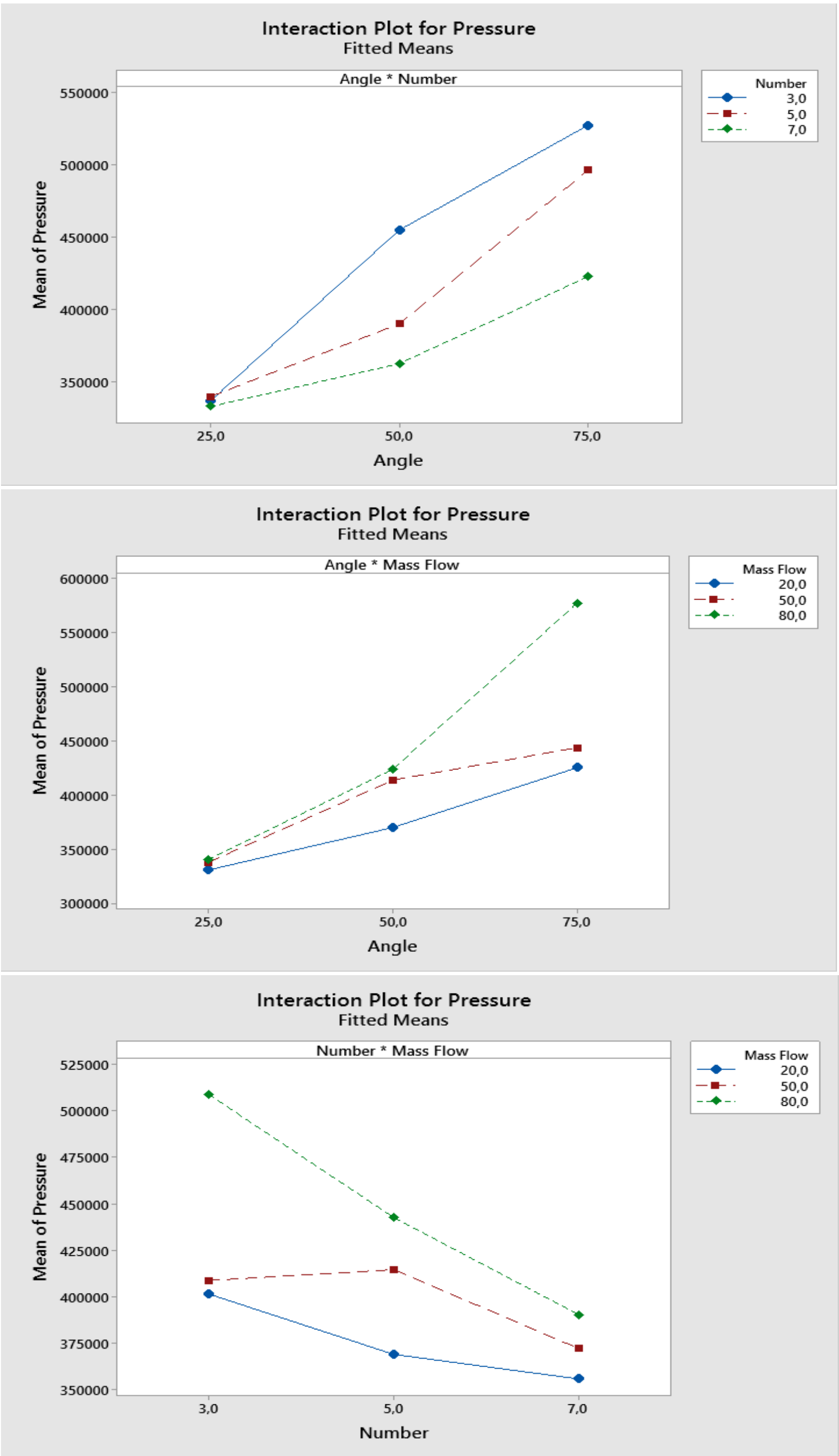


(a)

(b)

(c)

Figure 4.35. Interaction effect plots for each dual factor: angle-number (a), angle-mass flow (b) and number-mass flow (c)

## 4.5. Extreme Cases

Two test cases, which are not part of the test matrix shown in Table 3.2 are also analyzed in this thesis work. They are additional test cases having solely axial or radial mass flow rate. These cases are called extreme cases, for the previously solved cases all having both axial or radial mass flows ejected out of the pyrogen igniter into the SRM chamber. The motivation behind the analysis these cases had been explained in Section 3.4.

These test cases have the same geometric and ballistic features with the previous ones except their nozzle configurations, as seen in Figure 3.12. Since the nozzle exit area is the same in all cases and its value is 1500 mm$^2$, fully axial case includes a pyrogen igniter having one axial nozzle with nozzle radius of 21.85 mm. Fully radial case is selected to have only 5 radial nozzles making 50° with the longitudinal axis of the SRM (which is the middle selection in the test matrix shown in Table 3.2). The radius of one the radial nozzles is therefore 9.77 mm.

Again, possessing the similar virtues, the simulation time of these cases are 20 milliseconds. The pressure, Mach number and static temperature distributions of these cases at the 20$^{th}$ millisecond of solution are illustrated in Figure 4.36 and in Figure 4.37, respectively.

As seen in Figure 4.36, pressure and Mach number behavior of the fully axial case is similar to the cases having 20° of radial nozzle angle and 20% radial mass flow rate, which are close configurations to this extreme case. The flow ejected out of the pyrogen igniter experiences are shock followed by a rarefaction and these phenomena repeat until the pressure and the speed of the flow reaches to the same level with the gas that has been already in the grand SRM chamber. The pressure becomes 600 kPa at it peak value and the temperature reaches to 3000 K in the longitudinal axis of the SRM. In the surface of the propellant of the SRM, nearly no pressurization effect is observed; the pressure is distributed more or less evenly with the remaining surfaces of the SRM and the temperature only reaches to 2000 K. As it will become much clearer in the discussion of comparison, these merits are very unfavorable in terms of ignition transient compared to other cases.

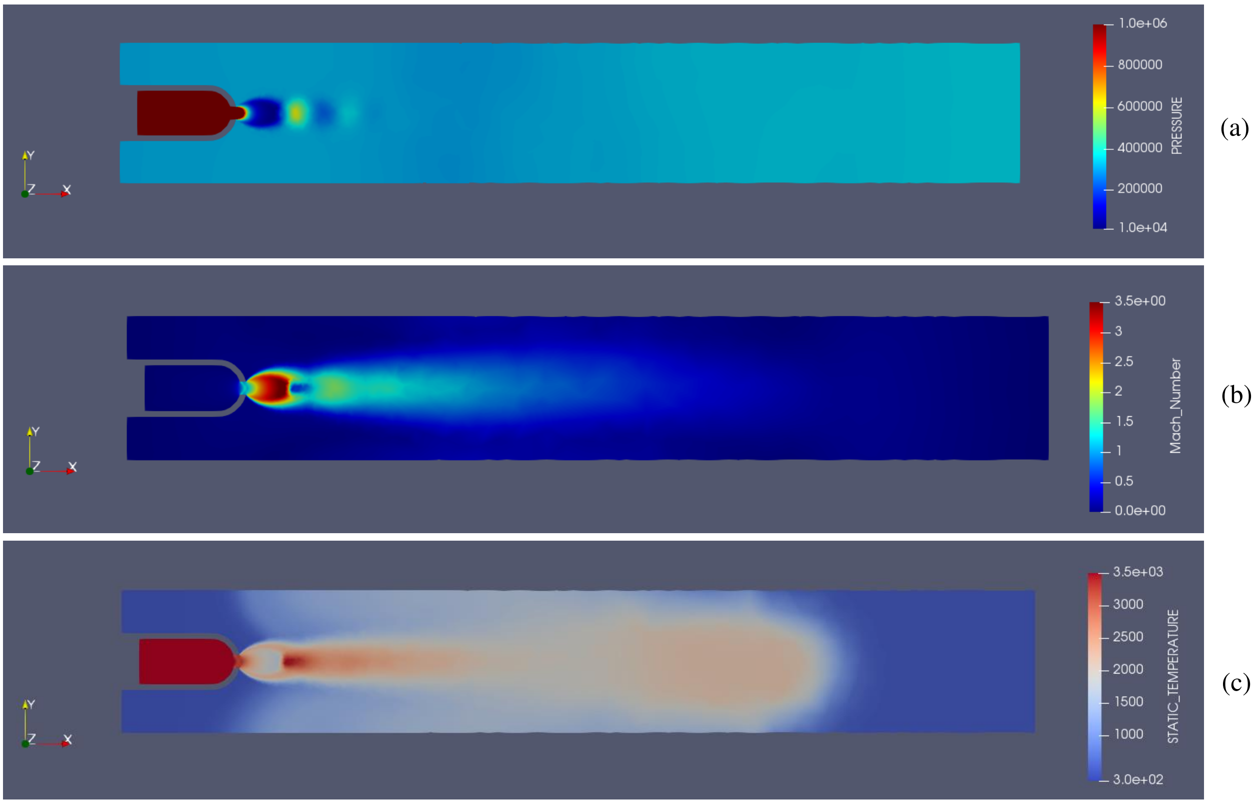


Figure 4.36. Pressure (a), Mach number (b) and static temperature (c) distribution of the test case ejecting only axial mass flow

A different story lies in the visuals of the fully radial case, which can be observed in Figure 4.37. No remarkable pressurization, heating or acceleration of the flow velocity effects can be seen in the longitudinal axis of the SRM at the 20$^{th}$ millisecond of the simulation, since there exists no axial nozzle in this configuration. However, even in these circumstances, as it will be clear in the comparison of the cases, mean pressure values of full axial and full radial cases are not excessively different in the longitudinal axis. What’s more, on the propellant surface of the SRM, fully radial case reaches to

600 kPa and 3500 K, which creates the difference between the extreme cases in terms of ignition transient.

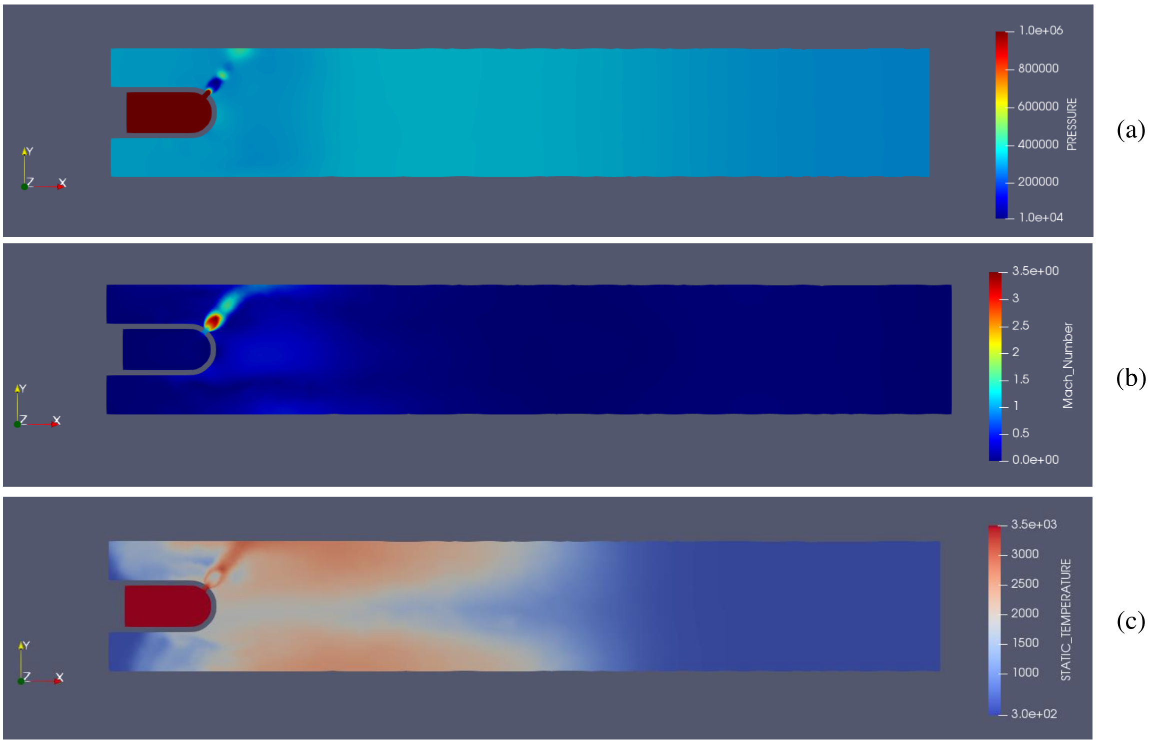


Figure 4.37. Pressure (a), Mach number (b) and static temperature (c) distributions of the test case ejecting only radial mass flow

In Figure 4.38, the pressure behavior of the extreme cases; as well as the optimum cases, in the longitudinal axis and on the surface of the propellant of the SRM is shown. The best case chosen as the result of the Full Factorial DOE, the case #7, having 75° of radial nozzle angle, 80% radial mass flow rate and 3 radial nozzles is one of the optimum cases. The other optimum case is the best case among the configurations having 50° of radial nozzle angle. Remember, the results of the experiment tell that decreasing the radial nozzle number and increasing the radial mass flow favors the ignition transient. Therefore, this second optimum case has also 80%

radial mass flow rate and 3 radial nozzles but 50° for the comparison with the fully radial case having same angle of radial nozzles.

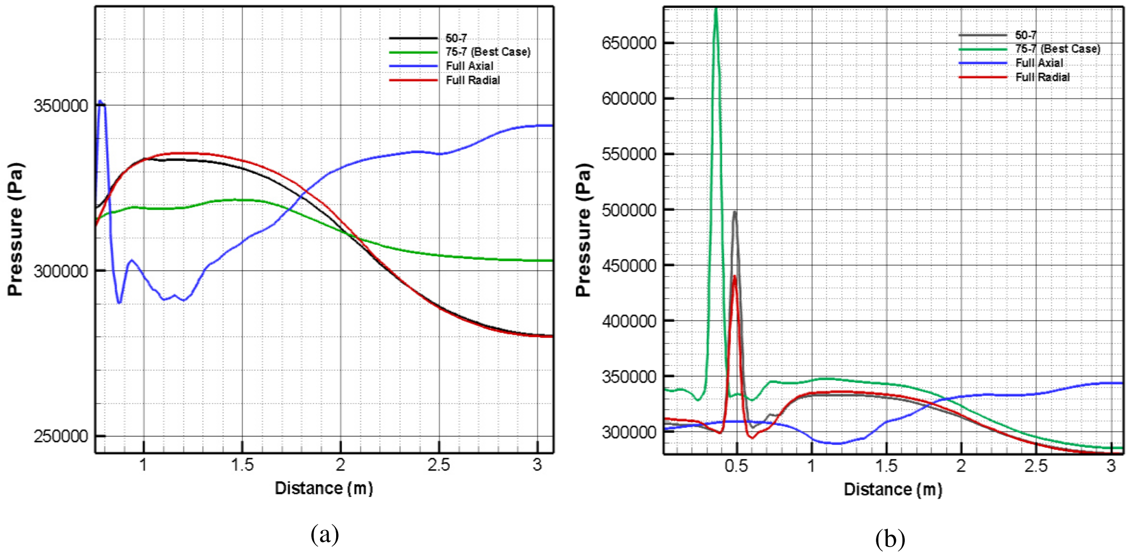


Figure 4.38. Comparison of the pressure behavior of optimum and extreme cases: in the longitudinal axis of the SRM (a) on the propellant surface of the SRM (b)

As it can be clearly observed in the pressure plots of the cases in the longitudinal axis of the SRM in the left portion of Figure 4.38, the cases much or less have the similar mean pressure (310-320 kPa) and the pressure variation between the cases is merely 30-40 kPa for any two points having the same distance.

However, when the pressure plots on the propellant surface is investigated, the difference become observable and meaningful. Having similar mean pressure values in the longitudinal axis, fully radial case surpasses the fully axial one by means of pressurization because on the propellant surface, there is a 150 kPa of difference where its jets hit to. The pressure value of the remaining portions is again similar; therefore, it can be comfortably concluded that fully radial case is more favorable than fully axial case in terms of ignition transient. On the other hand, since nozzle angle is a decisive parameter in pressurization, fully radial case is less favorable compared to the best case of the DOE, since there exist almost a 250 kPa difference of pressure where the igniter jets hit when other regions are close to each other. Also, fully radial case is not the favorite case among the cases having 50° of radial nozzle angle, since the best case of 50° DOE configurations have three radial nozzles rather than five which concentrates the radial flow onto the SRM propellant in more efficient manner; thus, having 60 kPa more pressure on the propellant surface where the jets hit as seen in Figure 4.38.

The last comparison can be made between the best case of the DOE and the fully axial case. In the longitudinal axis they have similar mean pressure value, but on the propellant surface the local difference becomes more than 350 kPa, which is the largest value in a comparison so far in this work.

Therefore, in this study, it can be concluded that extreme cases are inadequate in terms of ignition transient since they have weak pressurization merits compared to other configurations that have been tested. Especially, designing a pyrogen igniter ejecting solely axial mass flow into the SRM chamber is one of the actions that should strongly be avoided.

# CHAPTER 5

# CONCLUSIONS

## 5.1. Summary of the Thesis Work

In this thesis work, the effects of various nozzle design parameters of a pyrogen igniter on the ignition transient of the large-scale SRM system is investigated.

A pyrogen igniter is both a SRM and an igniter that is utilized in large-scale SRM systems where pyrotechnic materials are unable to supply sustainable and reliable ignition. Since there is an extra element is added to ignition chain with the existence of a pyrogen igniter, the ignition transient phase (which consist of three substages called induction, flame spreading and the combustion chamber filling) of a SRM elongates. A pyrogen having sufficient pressurization effect can shorten this elongated time in an effective manner. The focus point of this work is to catch this faster pressurization effect with optimized pyrogen nozzle design.

Therefore, first of all, the pyrogen igniters that are manufactured and fired in several countries (USA, Italy, India, etc.) and their nozzle structures are analyzed. It has been concluded that most of these igniters have varying radial nozzle numbers, radial mass flow rates that is ejected into their own grand SRMs and radial nozzle angles. Thus, with this motivation, an optimization process is carried out via a design of experiment approach in order to determine the importance of these parameters on the ignition sequence of the SRM and select the most feasible design of the nozzle of a pyrogen igniter.

In order to carry out this process, 3D simulations are made regarding pyrogen firing inside a grand SRM chamber. These simulations are made by ‘fully coupled compressible solver for turbulent perfect gas flows’ developed by Kalpaklı [19]. Since the investigated part of the ignition transient phenomena occurs in the first milliseconds of the motor start-up before the nozzle plug of the grand SRM bursts; that is, in a closed volume, when the acoustic effects are dominant, this solver is suitable for this investigation. The hot jets coming out from the pyrogen igniter and filling the grand SRM volume are examples of compressible fluid flow and the 3D feature of the solver helps to visualize the phenomena in an effective manner.

Then, a test geometry with fixed initial and boundary conditions is modelled. These conditions are both in geometric and ballistic aspects. After that, a test matrix is constructed with respect to varying design parameters of the nozzle of a pyrogen igniter. These parameters are the radial nozzle angle, radial nozzle number and the radial mass flow rate ejected from the pyrogen igniter. Also, two extreme cases, with having solely axial and radial flows are also modelled for deeper investigation.

After pointing out the meshing that is used in the simulation do not affect the outcomes, simulations have been started and their outcomes in terms of pressure, Mach number and temperature are reported and compared in a detailed manner. Lastly, the optimization process is made according to these varying nozzle parameters and the best nozzle design is selected.

### 5.2. Concluding Remarks

According to the data obtained from the simulations, the following deductions are made by the comparison of the test cases:

- In terms of decreasing the ignition transient time duration, a pyrogen igniter having superior pressurization effect on the grand SRM is favorable.

- With same fixed ballistic and geometric initial and boundary conditions, the pressurization effects of pyrogen igniters with different nozzle designs are compared. For a meaningful analysis, the pressurization on the propellant surface of the grand SRM by the effect of pyrogen igniter should be compared rather than the pressurization in the longitudinal axis of that SRM.

- All of the investigated parameters (radial nozzle angle, number and mass flow rate) seem to be important and dominant in the pressurization of the SRM and its ignition transient, since the standalone effects of these parameters create pressure peaks on the surface of the propellant of the grand SRM.

- Increasing radial angle of the nozzle of a pyrogen igniter increases the pressure on the propellant surface of the SRM; therefore, radial angle rise favors the ignition transient.

- Increasing radial number of the nozzle of a pyrogen igniter decreases the pressure on the propellant surface of the SRM; therefore, radial number decrease favors the ignition transient.

- Increasing radial mass flow rate coming out of the nozzles of a pyrogen igniter increases the pressure on the propellant surface of the SRM; therefore, radial mass flow rate increase favors the ignition transient.

- Extreme designs, especially the one having full axial mass flow rate, should be avoided. A pyrogen igniter having full radial mass flow has developable design features, in terms of ignition transient; therefore, should not be selected.

The above-mentioned deductions are the practical conclusions that are derived from this thesis work with the help of 3D simulations. This information could be beneficial for improving the ignition transient behavior of solid rocket motors. It could also be used in the improvement of design process of pyrotechnic igniters. Furthermore, it might give an insight to compressible fluid flow problems involved in a closed volume.

As mentioned in Section 1.5. the aim of this work is to investigate the effect of nozzle parameters of a pyrogen igniter on the ignition transient; whereas, its motivation is the lack of references related to the design concept of pyrogen igniters. This work is carried out in order to have at least a small idea while designing a pyrogen igniter and predict its ballistic performance in a meaningful and feasible manner before manufacturing stages. The outcomes are expected to influence the opinions of the investigators and readers on the ignition transient and pyrogen igniter concepts in solid rocket motor physics.

### 5.3. Suggestions for Future Work

In this thesis work, the effects of three design parameters -radial nozzle angle, number and the radial mass flow rate- of a pyrogen igniter nozzle on the ignition transient phenomena is discussed. Their relationship with the pressurization the a larger SRM system, as well as each other is analyzed. Furthermore, extreme cases (both having full axial and full radial flows) are investigated and the results are reported. Indeed, in order to expand the study, following subjects can be considered to be studied:

- Investigation of the similar subject with the inclusion of Aluminum (Al) in the products of exhaust jets leaving the pyrogen igniter and hitting to the propellant surface of the SRM: Aluminum is a highly energetic material that are used in the SRM propellants. With its combustion product $Al_2O_3$, it can increase the pressure inside the SRM in an effective manner. However, in SRM ignitions agglomeration phenomena is also observed which is the merging of $Al_2O_3$ and unburned Al particles and piling up in the nozzle regions [25]. If the nozzle radius gets smaller in degree, the consequences of this agglomeration might be observed as the clogging of the nozzle exits; which in turn, if its degree is too much, possibly leading to burst of the pyrogen and the failure of the SRM operation. Therefore, it would be an interesting subject to find out the optimum axial and radial nozzle design configurations of a pyrogen igniter ejecting aluminized products, in terms of the best pressurization and the safe operation manners.

- Validating the results of the solver and simulations that have been made with the data obtained from actual static firing of a SRM system utilizing a pyrogen igniter: As it is extremely costly to prepare a test set up or produce a pyrogen igniter and a SRM solely for this purpose, the pressure data in the SRM combustion chamber obtained from past experiences could be useful here. To achieve this aim, the design of the same pyrogen igniter used in the static firing or flight mission with its own wall and boundary conditions (both geometrically and ballistically) should be modelled and the simulations must be carried out. The pressure data gained from the SRM operation and the solver could be compared and the result might be interpreted. Then, instead of only proving the correctness of the solver hypothetically, actual firing results obtained will guide the investigators and innovative arguments could be voiced.
- The solver used in this thesis work has no capability of solving heat transfer and/or pyrolysis equations. With the addition and verification of these capabilities, the solver can cover the whole ignition transient stages (induction, flame spreading and chamber filling) of a SRM. Therefore, adjusting the solver with the mentioned equations will make it an excellent tool that deals with an extremely difficult transient phenomenon.
- Number of levels in factors can be increased in order to scan a more expanded design space while regarding geometric and manufacturing restrictions also.

Of course, there could be more possible future work regarding this particular thesis work, as it is analyzed and studied on deeply. One of the aims of this work is also to open new doors regarding the subject for the investigators and the readers

## REFERENCES


[1] Sutton, G.P., Biblarz O. 2001. Rocket Propulsion Elements, 7th edn., Canada: John Wiley & Sons, Inc

[2] Serraglia, F. 2008. 'Vega Launcher', VEGA Integrated Project Team ESA - ESRIN, pp. 12,20,25.

[3] Zaghi, S. 2008. SRM Igniter Jet Simulation”, Multidimensional Unsteady Gasdynamics, Scuola di Ingegneria Aerospaziale Sapienza, Università di Roma Via Eudossiana 16, 00184 Rome, Italy: Sapienza, Università di Roma.

[4] Price, E. W., Bradley Jr, H. H., Dehority, G. L., and Ibiricu, M. M., 1966. 'Theory of ignition of solid propellants', AIAA Journal, 4:1153-1181.

[5] Vari, E., Palamidessi, F., 1987. 'Ariane 4 Strap-on-Booster, Higher Performance for a Better Launcher', AIAA 87-2080, pp. 1-7.

[6] Bolieau, C., W.,Baker, J., Folkman S., 1987. 'Space Shuttle SRM Ignition System', AIAA 78-987, pp. 2-8.

[7] Richards, M.C., Laubacher, B.A., 1989. RSRM-3 (360L003) Final Report Ballistics / Mass Properties Final Report, Utah: Morton Thiokol. Inc, Aerospace Group, Space Operations.

[8] Kessler, S., Carson, D., 1979. 'Development of an Advanced Motor for the Third Stage of the Scout Launch Vehicle', AIAA 79-1294, pp. 5.

[9] Santilli, M., Fontana, A., 1994. 'ARIANE 5 MPS Igniter Subsystem – Design Approach and Development Phase Results', AIAA 94-3065, pp. 2-12.

[10] Trapani, C., Anglone, M., Scoccimaro, D., Paglia, F., Cospite, L., Betti, F., Leofanti, L., Bonnet, M. 2010. 'Dynamic at Ignition of the Vega Zefiro 9 SRM at the Firing Test Bench: Phenomenological Explanation and Numerical Reconstruction', Space Propulsion 2010, pp. 2-8.

[11] Favini, B., Di Giacinto, M., Attili, A. 2007. 'Internal Ballistic and Dynamics of VEGA Launcher Solid Rocket Motors during Ignition Transient: Firing Test Predictions and Post Firing Analysis', AIAA 2007-5814, pp. 2.

[12] Brauers, B., Goorden, B., Angelone, M., Gautronneau, E., Vita, G. 2009. 'Qualification and Production of the VEGA Solid Rocket Motor Igniters', AIAA 2009-5322, pp. 2-12.

[13] Welland, W.H.M., Brauers, B.M.J., Vermeulen, E.J. (n.d.) 'Future Igniter Technologies', Aerospace Propulsion Products, pp. 2-4.

[14] Serraglia, F. 2003. Modeling and Numerical Simulation of Ignition Transient of Large Solid Rocket Motors, Italy: Università degli Studi di Roma “La Sapienza” Scuola di Ingegneria Aerospaziale.

[15] Di Giacinto, M., Cavallini, E. (2007) 'Grain Design in SRM Internal Ballistic & Performances', pp. 4-19.

[16] King P.C., 'Consumable Pyrogen Igniter', The United States of America as represented by the Secretary of Navy. Pub. No: US 3,392,673. 1968

[17] Heier W.C., Lucy H., 'Molded Composite Pyrogen Igniter for Rocket Motors', The United States of America as represented by the Administrator of the National Aeronautics and Space Administration, Washington, DC., 1978. Pub No: 4,080,901. 1978

[18] Smith J.O.,Vetter R.F.,Sieg G.F., 'Pyrogen Igniter', The United States of America as represented by the Secretary of Navy. Pub. No: US 4,557,197. 1985

[19] Chandradathan, S.M. 2017. 'Challenges in Manufacturing Large Solid Boosters', Chemical Rocket Propulsion, pp. 879-880.

[20] Kalpaklı, B. 2013. Numerical Modeling of General Compressible Multi-Phase Flows, The Graduate School of Natural and Applied Sciences of Middle East Technical University: Middle East Technical University.

[21] Mason, W.H. 2018. Configuration Aerodynamics, Blacksburg, VA: Virginia Tech.

[22] Gordon, S., McBride, B.J. 1976. Computer program for calculation of complex chemical equilibrium compositions rocket performance incident and reflected shocks, and Chapman-Jouguet detonations, Nasa: U.S. Department of Commerce National Technical Information Service, Springfield, va. 22161.

[23] Rigas, F. and Sklavounos S. (2005) 'Experimentally Validated 3-D Simulation of Shock Waves Generated by Dense Explosives in Confined Complex Geometries', Journal of Hazardous Materials, A121(23–30), pp. 1-8.

[24] SPAC Consulting, 2013. 'Chapter 5-Philosophy of Design of Experiment Notes', Design of Experiment Training, pp. 11-17.

[25] Orlandi, O., Godfroy, F., Holstein, A., Larrieu, S., Yiao, M., Cesco, N. and Robert, E. (2016) 'A Specific Aspect of Aluminium Combustion on SRM Instabilities', Space Propulsion 2016, SP2016_3125204, pp. 3-4.